University of Ljubljana

Faculty of Electrical Engineering

Darko Šekuljica

Using the Moon as a calibrated noise source to measure the G/T figure-of-merit of an X-band satellite receiving station with a large antenna 200...400 wavelengths in diameter

Master's thesis

Mentor: prof. dr. Matjaž Vidmar

Ljubljana, 2017

Univerza v Ljubljani

Fakulteta za elektrotehniko

Darko Šekuljica

Uporaba Lune kot umerjenega šumnega vira za meritev razmerja G/T satelitske sprejemne postaje v pasu X z veliko anteno premera 200...400 valovnih dolžin

Magistrsko delo

Mentor: prof. dr. Matjaž Vidmar

Ljubljana, 2017

Acknowledgments

I would like to express my gratitude to my mentor, prof. dr. Matjaž Vidmar, for his availability, valuable practical advices and constructive critics during the making of this thesis.

I would also like to thank my supervisors, dr. Stefano Badessi and dr. Massimiliano Ferrante, for their guidance, unconditional support, advices and all technical and scientific help while working as an International Research Fellow at the European Space Agency.

Finally, I would like to thank all my friends, my loving family and my girlfriend for their support during my studies.

Contents

List of Figures

List of Tables

Symbols

In this thesis following denotements and units were used:

Denotement		**Unit**	
Name	Symbol	Name	Symbol
frequency	f	Hertz	Hz
bandwidth	B	Hertz	Hz
wavelength	λ	meter	m
Boltzmann's constant	k_B		$\mathrm{m^2\,kg\,s^{-2}\,K^{-1}}$
Planck's constant	h		$\mathrm{m^2\,kg\,s^{-1}}$
electric power	P	Watt	W
equivalent isotropically radiated power	$EIRP$	Watt	W
directivity	D		dimensionless
gain	G		dimensionless
free space path loss	$FSPL$		dimensionless
temperature	T	Kelvin	K
gain to system noise temperature ratio	G/T		$\mathrm{K^{-1}}$
half power beamwidth	θ_{HPBW}	degree	$^\circ$
Moon's angular diameter	θ_{Moon}	degree	$^\circ$
solid angle	Ω	steradians	sr
edge taper	T_e	decibel	dB
brightness distribution	$B(\theta, \phi)$		$\mathrm{W\,m^{-2}\,sr^{-1}\,Hz^{-1}}$
flux	S		$\mathrm{W\,m^{-2}\,Hz^{-1}}$

Table 1: Denotements and symbols

Abstract

This Master's thesis describes a study intended to consolidate an efficient G/T antenna quality factor measurement method for X-band, large aperture, parabolic antenna systems, that are in constant operation as it happens for antennas used for the reception of Low Earth Orbiting (LEO) satellites, and have small allotments of available time for performing the measurement. Standing on ESA requirements on acquisition services, these types of antenna systems need at least one G/T quality factor measurement per year in order to check whether the ground station still meets the specifications for the specific service. The measurement procedure described in this thesis uses a direct approach where the G/T ratio is directly measured.

Analysis of the available RF sources and their flux densities showed that the most appropriate RF source for direct G/T measurement, for the antennas and frequencies of interest to ESA in the frame of the Earth Observation activities, is the Moon. Moon's radiation can be taken as a stable black-body radiation and may be represented as uniform brightness disk, with dependence of the average brightness temperature, lunar phase, and on the lunar angular diameter as seen from the antenna site at the time of measurement.

Because the Moon's angular size is wider than the antenna half power beamwidth, a throughout analysis of extended source size correction factor approximation methods was performed and finally, a novel best-fit correction factor method was calculated in a dependence to feed's edge taper.

As final verification of the procedure, a set of G/T measurements were per-

formed on an operational X-band large aperture Cassegrain antenna used for receiving LEO orbit satellite data. The settings of the different instruments used for the measurement were subject of discussion and final selection was done on the basis of ensuring the maximal measurement stability with the minimal measurement error.

Major result of the study is that measurements of G/T factor carried out with our direct method using the Moon, well agree with those obtained by using a star (Cassiopeia A) as a source and those obtained with pattern simulation and estimation using MATLAB code, with deviations within 0.35dB.

As additional result of the study, it turned out that vendor provided values for extended source correction factor are often too optimistic while the Gaussian pattern method in dependence of edge taper is proposed. Given that the complexity of the direct method for the large aperture parabolic antenna measurements is much smaller than when measuring separately the gain and system noise temperature, ESA has consolidated the method described in this thesis as the standard approach for the G/T measurement of X-band antennas used for the acquisition of Earth Observation satellites.

Key words: G/T, quality factor, figure of merit, direct measurement method, Moon, antennas, X-band, satellite communication.

Razširjen povzetek

Namen te magistrske naloge je bil potrditi učinkovitost merilne metode G/T faktorja za kakovost pri paraboličnih antenskih sistemih X frekvenčnega pasu, z veliko zaslonko, ki so v stalnemu obratovanju kot so na primer antene, ki sprejemajo signal z nizko tirničnih satelitov (ang. Low Earth Orbit - LEO) in imajo kratke pavze med prehodi satelitov. Glede na zahteve evropske vesoljske agencije (ang. European Space Agency - ESA), potrebujejo omenjeni antenski sistemi vsaj eno meritev G/T faktorja letno, za preverjanje, ali zemeljska postaja še vedno ustreza zahtevam storitve.

Meritev opisana v tej študiji je bila izvedena z direktno metodo ocene G/T razmerja. Ta metoda omogoča oceno G/T razmerja pomočjo dveh meritev, in sicer meritev moči šuma ko je antena usmerjena v RF vir (P_1 [W]), in meritev moči šuma, ko je antena usmerjena v hladno nebo na isti elevaciji (P_2 [W]). Direktna metoda ocene G/T faktorja v enotah [K^{-1}] je podana z enačbo:

$$\frac{G}{T} = \frac{8\pi \cdot k_B \cdot (\frac{P_1}{P_2} - 1)}{\lambda^2 \cdot S} \cdot K_1 \cdot K_2 \ .$$

V zgornji enačbi k_B predstavlja Boltzmann-ovo konstanto, K_1 korekcijski faktor zaradi atmosferskega slabljenja, K_2 korekcijski faktor zaradi razširjene velikosti vira, λ valovno dolžino v metrih in S gostoto pretoka RF vira v [$\mathrm{W\,m^{-2}\,Hz^{-1}}$].

Analiza obstoječih RF virov in njihove gostote pretokov je pokazala, da je za antene in frekvence, ki zanimajo ESA v okviru aktivnosti opazovanja Zemlje (ang. Earth Observation - EO), Luna najboljši RF vir za direktno metodo merjenja G/T faktorja. Lunino sevanje lahko vzamemo kot stabilno sevanje črnega telesa,

ki je predstavljeno kot disk z enakomerno osvetlitvijo in je odvisno od povprečne temperature osvetlitve (ang. brightness temperature), Lunine mene in Luninega kotnega premera glede na lokacijo antene v času izvajanja meritve.

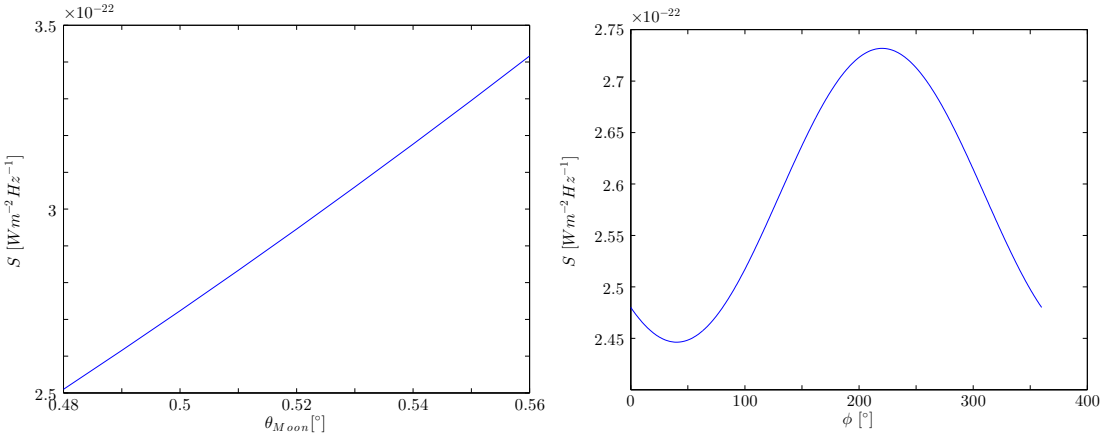

(a) (b)

Slika 1: Lunina gostota pretoka S v odvisnosti od (a) kotnega premera in (b) Lunine mene

Zaradi ožjega glavnega snopa antene od zornega kota Lune je bila izvedena celovita analiza metod približkov korekcijskega faktorja zaradi razširjene velikosti vira (ang. extended source size correction factor), K_2, in razvita nova najbolj prilegajoča metoda za izračun približka korekcijskega faktorja v odvisnosti od robnega slabljenja osvetlitve žarilca T_e dB (ang. edge taper). Približek korekcijskega faktorja K_2 je podan z enačbo:

$$K_2 = \frac{\ln(2) \cdot \left(\frac{\theta_{Moon}}{\theta_{HPBW}}\right)^2}{1 - e^{-\ln(2) \cdot \left(\frac{\theta_{Moon}}{\theta_{HPBW}}\right)^2}} \ ,$$

kjer θ_{Moon} [°] predstavlja kotni premer Lune in θ_{HPBW} [°] kot med točkah kjer sevalni diagram pade na polovico moči (ang. Half Power Beam Width). Kot θ_{HPBW} je odvisen od valovne dolžine, premera največjega reflektorja ter faktorja k:

$$\theta_{HPBW} = k \cdot \frac{\lambda}{d} \ .$$

Faktor k je faktor širine glavnega snopa antene (ang. beamwidth factor). Formula za izračun k faktorja je produkt najboljšega prileganja krivulje na številne rezultate K_2 korekcijskega faktorja različnih anten. Rezultati K_2 faktorja so bili izračunani s pomočjo numerične integracije nad sevalnimi diagrami številnih anten simuliranih v programski opremi GRASP. Antene smo načrtovali in simulirali z različnimi premeri reflektorjev in različnimi robnimi slabljenji žarilca. Faktor širine glavnega snopa antene je podan v odvisnosti od robnega slabljenja osvetlitve žarilca:

$$k = 58.96(1 + 0.0107 \cdot T_e) \ .$$

Za zadnje preverjanje postopka smo izvedli niz G/T meritev na Cassegrain anteni z veliko zaslonko v X frekvenčnemu pasu, ki se uporablja za sprejemanje LEO satelitskih podatkov. Nastavitve uporabljenih posameznih instrumentov so bile predmet razprave in na koncu je bila izbrana kombinacija, ki omogoča največjo možno stabilnost meritve ob najmanjši možni merilni napaki. Predlagana nastavitev spektralnega analizatorja je tako bila:

1. Središnja frekvenca: Vmesna frekvenca (običajno 750 MHz)
2. Frekvenčni razpon: 0 Hz
3. dB/razdelek: 1
4. RBW: 100 kHz
5. VBW: 10 Hz
6. Marker: ON
7. Čas brisanja: 100 ms
8. Povprečenje: 10.

Glavni rezultat študije je bil, da se meritev G/T faktorja izvedena z predlagano direktno metodo, ki uporablja Luno kot RF vir, zelo dobro ujema z metodo, ki uporablja kot vir zvezdo (Cassiopeia A), in oceno G/T faktorja s pomočjo MATLAB simulacije. Pri merjenju G/T faktorja, z uporabo K_2 metode opisane v tej magistrski nalogi in Lune kot RF vira smo dobili rezultat $[G/T]_{\mathrm{dB}} = 36.49$ dB. Z uporabo zvezde kot RF vira in iste direktne metode smo dobili rezultat

$[G/T]_{\mathrm{dB}} = 36.81$ dB. Pri oceni G/T faktorja s pomočjo MATLAB kode podane v Dodatku B pa smo dobili rezultat $[G/T]_{\mathrm{dB}} = 36.43$ dB. Ujemanje $[G/T]_{\mathrm{dB}}$ rezultatov različnih metod je bilo znotraj 0.35dB.

Dodaten rezultat študije je bil, da so vrednosti podane s strani proizvajalcev anten, za korekcijski faktor zaradi razširjene velikosti vira, pogosto preoptimistične in je zato predlagana uporaba izvedene metode, ki uporablja Gaussov sevalni diagram s faktorjem širine glavnega snopa antene v odvisnosti od robnega slabljenja osvetlitve žarilca. Slika 2 prikazuje primer opaznega odstopanja K_2 vrednosti podane s strani proizvajalca antene v polinomski obliki.

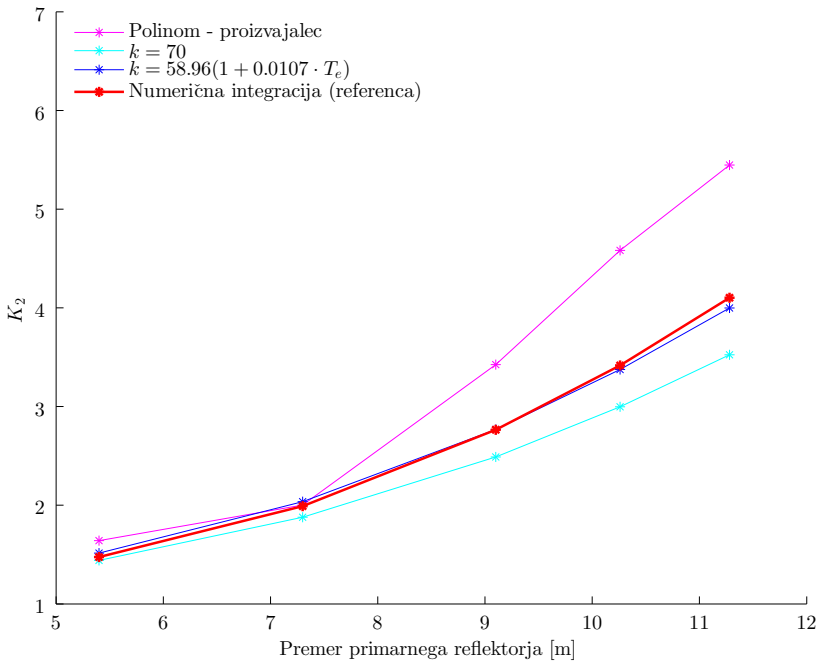

Slika 2: Primerjava metod približkov K_2 faktorja, za Cassegrain anteno z $T_e = -10dB$, in Luno z $\theta_{Moon} = 0.50°$

Glede na to, da je merjenje z direktno metodo za parabolične antene z veliko zaslonko mnogo manj kompleksno od ločenega merjenja dobitka antene in odgovarjajoče šume temperature sistema, je ESA potrdila metodo opisano v tej študiji kot standarden pristop merjenja G/T faktorja za antene v X frekvenčnem pasu, ki se uporabljajo za sprejem signala od zemeljskih opazovalnih satelitov.

Ključne besede: G/T, faktor kakovosti, direktna metoda meritve, Luna, antene, frekvenčni pas X, satelitske komunikacije.

1 Introduction

As satellite data rate in practical applications is constantly increasing, it must be ensured that the transmission process from the satellite to the Earth ground station is maintained error-free. Given the limited resources on board of satellites, the ground station must be carefully designed in a way that the received satellite signal level always remains higher than the noise level, regardless of the weather conditions and satellite position. To ensure that the ground station antenna is fulfilling the requirement, it is necessary to correctly specify its quality factor G/T - the antenna gain to system noise temperature ratio.

The reason why G/T is an important parameter is that G/T factor together with satellite's Equivalent Isotropically Radiated Power (EIRP), determines the resulting input Signal to Noise ratio of the satellite-to-ground communication system. Hence, it is strictly related to the system performance such as the output signal-to-noise ratio of an analog system or the bit error rate of a digital system, and provides an upper bound to reliable information transfer rate through the system.

Ground stations receiving the non-geostationary orbit satellite data are equipped with tracking automation and are constantly operational, sometimes with just a few minutes pause in between satellite passes. These ground station antennas usually perform full rotations in azimuth and elevation angles, are exposed to wind, precipitations and material stretching due to thermal and gravity effects. All this effects can cause antenna dish distortions and hence, degradations in antenna gain and performance. Therefore, at ESA it has been decided to perform

the G/T quality factor measurements at least once per year, in order to ensure that the selected antenna maintains the required performance.

For operational ground station antennas, the indirect method of measuring the antenna's quality factor G/T by measuring the antenna gain and system noise temperature separately, is very time consuming and mostly not practical as it requires a long unavailability of the system to measure each single component.

The direct methods of G/T measurement, presented in this thesis, allow simple, fast, highly accurate and efficient method of G/T quality factor estimation, as accurate as measuring the gain and system noise temperature separately and calculating its ratio. In this approach, neither gain nor system noise temperature are explicitly measured, and the measurement depends mostly on the accurate flux determination from a radio frequency (RF) source.

The main advantage of direct methods is the relative ease of its measurement procedure, which allows less time consuming verifications than using an indirect approach method. This point is of great importance when the ground station is used to perform frequent acquisitions and minimal allotment of time is available to perform the measurement. Even though that the calibration of some RF sources is a process at least as difficult as indirect approach of quality factor measurement, once that the RF source is calibrated it is possible to accurately and easily measure the G/T quality factor of any number of ground stations.

The most appropriate RF source for X-band G/T measurement would be transmitting satellite in the same frequency range. However, only a small number of non-military, commercial satellites (if any) with calibrated EIRP and operating in the X-band frequencies of interest are available. The military satellites, on the other hand, are operating on the lower frequencies, usually not usable with commercial down-converters.

This work includes the survey and analysis of the possible direct measurement methods with the available RF sources flux densities. Stars, the Moon and the Sun have been considered as alternative sources. Considered the most stable

and strong-enough radio source with very accurate estimation of flux density considering uniform brightness disk, the Moon was selected as proposed radio source.

Methods for Moon's flux density estimation has been carefully reviewed. In principle Moon radiation can be assimilated to a black-body radiation of a uniform brightness disk.

However, on the contrary of stars, Moon's angular diameter is wider than the large aperture parabolic antenna's half-power beamwidth (θ_{HPBW}) operating in X-band, and therefore must be considered as an extended source. The extended-source size correction factor was examined, tested and analysed using the existing estimation equations, and then compared to the calculated correction factor values using the simulated radiation patterns of realistic antennas. Using antenna simulated patterns, a best-fit approximation method of extended source size correction factor was achieved and given in polynomial form. Antenna design and simulations have been performed using GRASP, a very accurate antenna analysis software developed by TICRA, which uses Physical Optics and different scattering models to compute the far field values in a prescribed grid of points.

Using the antenna pattern a method to simulate the antenna noise temperature and G/T has been implemented using MATLAB code. The program is provided in the appendix and provides an estimation of the G/T also considering weather conditions, external temperature, antenna elevation, and receiver noise temperature.

Following the selected method using the Moon as external source, the G/T of a real antenna was measured. The detailed test procedure was subject of a detailed analysis. The proposed settings for the instruments involved have been traded-off and selected in order to provide the best compromise between stability and measurement error. Optimal settings were identified and given in the last chapter along with the measurement results. These measurements were performed on one operational X-band Cassegrain antenna used for receiving LEO

orbit satellite data which is located at the e-GEOS station in Matera.

2 Satellite to Earth Transmission Link Balance

Satellite communication has two main components: the space segment which is satellite itself and the ground segment. Ground segment consists of RF terminal including the antenna, the baseband and control equipment, and the signal processing unit [2]. In downlink, the transmission link efficiency is dependent on many parameters of the link, like the effective isotropically radiated power ($EIRP$), the distance between satellite and the ground station, the receiving antenna gain, the transmitting and receiving antenna pointing accuracy, the atmospheric attenuation, the additional transmitting and receiving system losses and finally the receiving system noise temperature. Also, the effects of noise generated by terrestrial and cosmic environment in which the ground station antenna is immersed must be taken into the account.

The link efficiency is commonly expressed with the signal-to-noise ratio (SNR), capacity and the link budget $\frac{C}{N_0}$, whereas the receiving antenna sensitivity is expressed as gain-over-noise-temperature ratio $\frac{G}{T_{sys}}$.

2.1 Noise and Noise Temperature

The noise is an unavoidable disturbance contribution which overlaps with the transmission of a signal that carries information and degrades the signal characteristics [3]. The thermal noise is macroscopic effect due to thermal agitation

usually of the free electrons, and is proportional to the temperature. The thermal noise present in the transmission system, however, comes from numerous sources that can be grouped into two main categories: internal sources, i.e. sources that produce noise inside of the receiving system circuits and external sources that produce noise in outer space. Noise power P_n expressed in Watts is given as:

$$P_n = k_B \cdot T \cdot B \ , \tag{2.1}$$

where k_B is Boltzmann constant with value $k_B = 1.38064852 \cdot 10^{-23}[\mathrm{m^2\,kg\,s^{-2}\,K^{-1}}]$, T[K] is the elements temperature and B[Hz] is the bandwidth. It must be noted that temperature T does not represent the physical temperature of the element but the equivalent temperature that produces the same mean noise power like the element does. The noise power, for example, on the Earth's surface, under the mean ambient temperature of $T = 290$K yields approximately $[P_n]_{dB} = 174\mathrm{dB\,Hz^{-1}}$.

2.2 Friis - Transmission Equation

Friis transmission equation is one of the most fundamental equations in antenna theory. It is used to calculate the received power expressed in Watts from one antenna when a known amount of power is transmitted from another antenna under idealized conditions. The Friis transmission equation is given as:

$$P_R = P_T \cdot G_T \cdot G_a \cdot (\frac{\lambda}{4\pi r})^2 \ , \tag{2.2}$$

where P_R, P_T are received and transmitted power expressed in Watts [W], and G_a, G_T are received and transmitted antenna gains in linear scale.

Last term of the Equation (2.2) describes the free space path loss. However, in non-idealized conditions, additional attenuations of the signal have to be taken in the consideration.

2.3 Attenuation and Losses in Satellite Communications

Attenuations in the satellite communications come from various sources conditioned by physical laws and mechanical inaccuracies. Further, attenuations can be divided in three major groups: the free space attenuation which introduces the highest amount of attenuation, the atmospheric attenuation, and the antenna losses consisting of pointing inaccuracy and polarisation mismatch losses.

2.3.1 Free Space Path Loss

Free space path loss (*FSPL*) is the loss in signal strength of an electromagnetic wave between two isotropic radiators that is consequence of the line-of-sight path through the free space, usually air, with no obstacles nearby to cause diffraction or reflection. FSPL depends on the signal wavelength λ[m] , and the distance between antennas r[m]:

$$FSPL = (\frac{4\pi r}{\lambda})^2. \tag{2.3}$$

2.3.2 Atmospheric Effects on Earth-Space Radio Propagation

Atmospheric attenuation is highly dependent on the frequency and the elevation angle, as well as on the current weather conditions, and consist of gaseous attenuation, rain and cloud attenuation and scintillations. In the X-band the attenuation due to atmospheric gases is almost negligible comparing to higher frequencies and can be very-well calculated by the approximations given in [4]. Approximations are derived from the flat-earth model.

The attenuations by rain will be neglected in this thesis, as the rain introduces high attenuations and is strongly recommended not to perform measurements during rainy weather or rainy clouds.

2.3.2.1 Attenuation due to atmospheric gases

Attenuation by the atmospheric gases [4] is entirely caused by absorption and depends mainly on frequency, elevation angle, water vapour density and altitude above sea level. Typically the maximum attenuation due to atmospheric gases occurs during the season of maximum rainfall.

Refractive index of the atmosphere decreases with the increasing height above the surface, therefore the radio waves traveling through the atmosphere encounter lower values of the refractive index and according to the Snell's law bend towards the region with higher refractive index (Figure 2.1). This phenomenon is especially important for the elevation angles lower than 5°. Approximation equations given in following are very good estimates for the X-band and the elevation angles $\theta > 5°$. Attenuation for the elevation angles $\theta \leq 5°$ can be further estimated using just the zenith attenuation [5]. For altitudes higher than 10 km, and in cases where higher accuracy is required, the line-by-line calculation should be used [4].

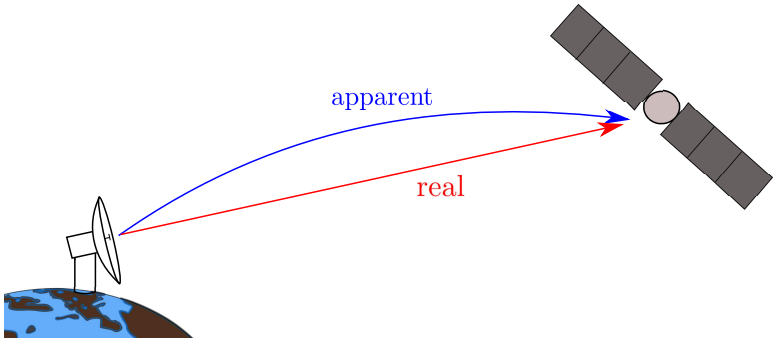

Figure 2.1: Real and apparent direction to the satellite due to ray bending

To estimate the gaseous attenuation four factors are needed: the specific attenuations of oxygen γ_o[dB km^{-1}] and water vapour γ_w[dB km^{-1}], and the equivalent height values in kilometres (h_o and h_w [km]) to obtain zenith attenuation. The concept of equivalent height is based on the assumption of an exponential atmosphere specified by a scale height to describe the decay in density with al-

titude. It must be noted that water vapour distributions in the real atmosphere may differ from the exponential assumption with corresponding changes in equal heights.

For dry air, the attenuation due to oxygen, is dependent on the mean surface ambient temperature $t\,[^{\circ}\mathrm{C}]$, the total air pressure $P[\mathrm{hPa}]$, and the frequency expressed in GHz (f_{GHz}):

$$\gamma_o = \left(\frac{7.2 \cdot {r_t}^{2.8}}{{f_{\mathrm{GHz}}}^2 + 0.34 \cdot {r_p}^2 {r_t}^{1.6}} + \frac{0.62 \cdot \epsilon_3}{(54 - f_{\mathrm{GHz}})^{(1.16 \cdot \epsilon_1)} + 0.83 \cdot \epsilon_2}\right) {f_{\mathrm{GHz}}}^2 {r_p}^2 \cdot 10^{-3} \ , \tag{2.4}$$

where,

$$\epsilon_1 = {r_p}^{0.0717} {r_t}^{-1.8132} e^{0.0156(1-r_p)-1.6515(1-r_t)}$$
$$\epsilon_2 = {r_p}^{0.5146} {r_t}^{-4.6368} e^{-0.1921(1-r_p)-5.7416(1-r_t)}$$
$$\epsilon_3 = {r_p}^{0.3414} {r_t}^{-6.5851} e^{0.2130(1-r_p)-8.5854(1-r_t)}$$

$$r_p = \frac{P}{1013}$$
$$r_t = \frac{288}{273 + t}$$

To be able to estimate the total attenuation due to oxygen, the equivalent height value is given as:

$$h_o = \frac{6.1}{1 + 0.17 \cdot {r_p}^{-1.1}} (1 + t_1 + t_2 + t_3) \ , \tag{2.5}$$

where,

$$t_1 = \frac{4.64}{1 + 0.066 \cdot {r_p}^{-2.3}} e^{-\left(\frac{f_{\mathrm{GHz}} - 59.7}{2.87 + 12.4 \cdot e^{-7.9 \cdot r_p}}\right)^2}$$

$$t_2 = \frac{0.14 \cdot e^{2.12 \cdot r_p}}{(f_{\mathrm{GHz}} - 118.75)^2 + 0.031 \cdot e^{2.2 \cdot r_p}}$$

$$t_3 = \frac{0.0114}{1 + 0.014 \cdot {r_p}^{(-2.6)}} f_{\mathrm{GHz}} \frac{-0.0247 + 0.0001 f_{\mathrm{GHz}} + 1.61 \cdot 10^{-6} {f_{\mathrm{GHz}}}^2}{1 - 0.0169 f_{\mathrm{GHz}} + 4.1 \cdot 10^{-5} {f_{\mathrm{GHz}}}^2 + 3.2 \cdot 10^{-7} {f_{\mathrm{GHz}}}^3}$$

Water vapour specific attenuation, in addition to temperature $t\,[^\circ\mathrm{C}]$, pressure P[hPa] and frequency in GHz (f_{GHz}), considers also the relative humidity expressed in $H[\%]$. Specific attenuation with its helping factors is given:

$$\begin{aligned}\gamma_w =\{&\frac{3.98\eta_1 e^{2.23(1-r_t)}}{(f_{\mathrm{GHz}}-22.235)^2+9.42{\eta_1}^2}g(f_{\mathrm{GHz}},22)+\frac{11.96\eta_1 e^{0.7(1-r_t)}}{(f_{\mathrm{GHz}}-183.31)^2+11.14{\eta_1}^2}+\\&\frac{0.081\eta_1 e^{6.44(1-r_t)}}{(f_{\mathrm{GHz}}-321.226)^2+6.29{\eta_1}^2}+\frac{3.66\eta_1 e^{1.6(1-r_t)}}{(f_{\mathrm{GHz}}-325.153)^2+9.22{\eta_1}^2}+\\&\frac{25.37\eta_1 e^{1.09(1-r_t)}}{(f_{\mathrm{GHz}}-380)^2}+\frac{17.4\eta_1 e^{1.46(1-r_t)}}{(f_{\mathrm{GHz}}-448)^2}+\frac{844.6\eta_1 e^{0.17(1-r_t)}}{(f_{\mathrm{GHz}}-557)^2}g(f_{\mathrm{GHz}},557)+\\&\frac{290\eta_1 e^{0.41(1-r_t)}}{(f_{\mathrm{GHz}}-752)^2}g(f_{\mathrm{GHz}},752)+\\&\frac{8.3328\cdot 10^4\cdot\eta_2\cdot e^{0.99(1-r_t)}}{(f_{\mathrm{GHz}}-1780)^2}g(f_{\mathrm{GHz}},1780)\}{f_{\mathrm{GHz}}}^2{r_t}^{2.5}\rho\cdot 10^{-4}\ ,\end{aligned} \tag{2.6}$$

where,

$$\begin{aligned}\rho&=\frac{216.7}{t+273.7}\frac{H}{100}\{1+10^{-4}(7.2+P(0.0032+5.9\cdot 10^{-7}t^2))\}\cdot 6.1121e^{(\frac{(18.678-\frac{t}{234.5})\cdot t}{t+257.14})}\\ \eta_1&=0.955r_p{r_t}^{0.68}+0.006\rho\\ \eta_2&=0.735r_p{r_t}^{0.5}+0.0353{r_t}^4\rho\\ g(f_{\mathrm{GHz}},f_i)&=1+(\frac{f_{\mathrm{GHz}}-f_i}{f_{\mathrm{GHz}}+f_i})^2\ .\end{aligned} \tag{2.7}$$

Finally the equivalent height of the atmosphere for the water vapour is given with following equation:

$$\begin{aligned}h_w=1.66(1+&\frac{1.39\sigma_w}{(f_{\mathrm{GHz}}-22.235)^2+2.56\sigma_w}+\frac{3.37\sigma_w}{(f_{\mathrm{GHz}}-183.31)^2+4.69\sigma_w}+\\&\frac{1.58\sigma_w}{(f_{\mathrm{GHz}}-325.1)^2+2.89\sigma_w})\ ,\\ \sigma_w&=\frac{1.013}{1+e^{-8.6(r_p{}^{-0.57})}}\ .\end{aligned} \tag{2.8}$$

Total zenith attenuation caused by the gaseous absorption in the atmosphere expressed in decibels A_G[dB] can now be defined with the above approximated values:

$$A_G(90^\circ)=A_o(90^\circ)+A_w(90^\circ)=h_o\gamma_o+h_w\gamma_w\ . \tag{2.9}$$

In case when the ground station is situated on the location above the mean sea level h_1[km], the oxygen, h_o, and water vapour, h_w, heights have to be corrected, as well as the distribution of water vapour in the atmosphere ρ used in the (2.6):

$$\begin{aligned} h_o{}' &= h_o \cdot e^{\frac{-h_1}{h_o}} \\ h_w{}' &= h_w \cdot e^{\frac{-h_1}{h_w}} \\ \rho' &= \rho \cdot e^{\frac{-h_1}{2}} \end{aligned} \tag{2.10}$$

where ρ' is the value corresponding to altitude h_1 of the station in question, and the equivalent height of water vapour density is assumed as $h_w = 2$[km] [6].

Gaseous atmospheric attenuation for the elevation angles $90° \geq \theta > 5°$ can be simply estimated multiplying the zenith attenuation with the cosecant function $csec(\theta)$ [4]. Therefore it is possible to write:

$$A_G(\theta) = \frac{A_o(90°) + A_w(90°)}{\sin(\theta)} \ . \tag{2.11}$$

However, in order to estimate the total gaseous atmospheric attenuation for the elevation angles $\theta < 5°$, correction for the ray bending considering the curvature of the Earth has to be taken into the account. The corrected attenuation depending also on the effective radius of the Earth (4/3 Earth radius) $R = 8497$[km] is given in [5], in logarithmic scale (A_G[dB]), by the equation:

$$A_G(\theta) = \frac{2 \cdot A_o}{\sqrt{\sin(\theta)^2 + \frac{2h_o}{R}} + \sin(\theta)} + \frac{2 \cdot A_w}{\sqrt{\sin(\theta)^2 + \frac{2h_w}{R}} + \sin(\theta)} \ . \tag{2.12}$$

Total, dry air and water-vapour zenith attenuation from sea level, with surface pressure $P = 1013$ hPa, surface temperature $t = 15°$C and surface water vapour density $\rho = 7.5\ \mathrm{g\,m^{-3}}$ is presented in the Figure 2.2.

2.3.2.2 Attenuation due to Clouds

Attenuation through clouds, A_C[dB], is due to propagating through the small water droplets in size of few tens of millimetres, hence in order of X-band wavelength

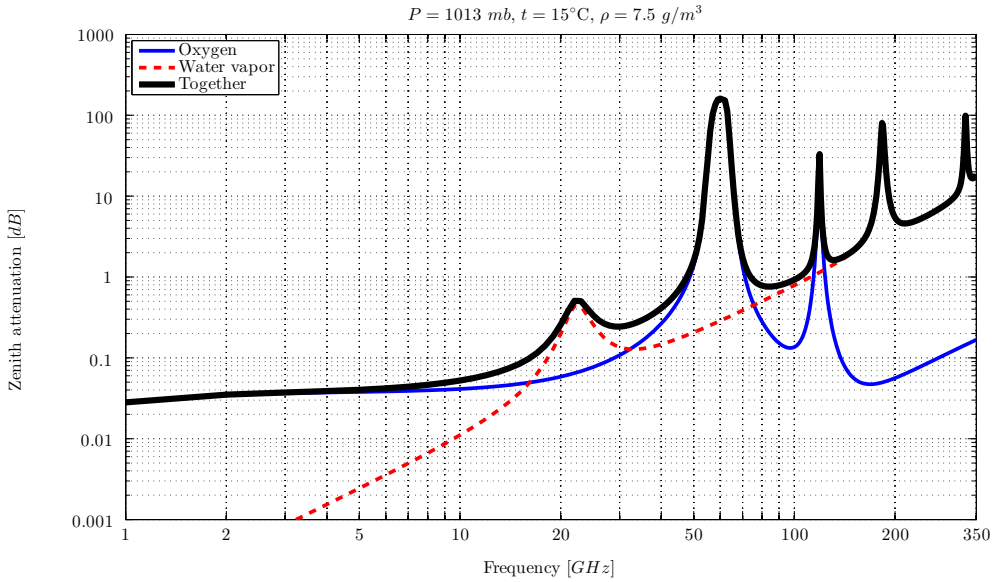

Figure 2.2: Total dry air and water vapour zenith attenuation at sea level

size. The detailed explanation and procedure to calculate attenuation due to clouds is given in [7]. When total columnar content of liquid water $L_{red}[\mathrm{kg\,m^{-2}}]$ for a given location reduced to a temperature of 0° is known, it is possible to estimate the total attenuation due to clouds given as:

$$A_C = \frac{L_{red} K_l}{\sin(\theta)} \ . \tag{2.13}$$

where θ is the elevation and K_l is a factor calculated from a mathematical model based on Rayleigh scattering [7].

2.3.2.3 Tropospheric scintillation

Scintillation [5] describes the condition of rapid fluctuations of the signal parameters of a radiowave caused by time dependent irregularities in the transmission path. Signal parameters affected include amplitude, phase, angle of arrival, and polarization. Scintillation effects can be produced in both the ionosphere and in the troposphere. Electron density irregularities occuring in the ionosphere can affect frequencies up to about 6 GHz, while refractive index irregularities occur-

ring in the troposphere cause scintillation effects in the frequency bands above about 3 GHz. Tropospheric scintillation is typically produced by refractive index fluctuations in the first few kilometers of altitude and is caused by high humidity gradients and temperature inversion layers. The effects are seasonally dependent, vary day-to-day, and vary with the local climate.

The scintillation attenuation A_S[dB] calculation is also divided in two parts according to the antenna elevation, and its estimate can be obtained by [8].

2.3.2.4 Total Atmospheric Attenuation

Gaseous atmospheric attenuation expressions summarized in this chapter are extracted from [4], while the cloud and scintillation attenuation expressions are extracted from [7] and [8] respectively. Extracted equations are adapted for the G/T measurement procedure for the X-band.

Finally total atmospheric attenuation for the X-band [8], A_T[dB], can be expressed in logarithmic scale and combines the effects of gaseous attenuation, precipitation attenuation and scintillation attenuation in following way:

$$A_T = A_G + \sqrt{{A_C}^2 + {A_S}^2} \ . \tag{2.14}$$

2.4 Antenna losses

The most significant antenna losses are polarization mismatch and pointing inaccuracy. Polarization mismatch can be due to the use of improper antenna polarization, and because of the satellite rotation and Faraday rotation. Inaccuracy of antenna pointing can be divided on the inaccuracy due to satellite antenna pointing the fixed direction not necessarily in our antenna direction, and due to ground station antenna miss-pointing.

The second type of misalignment is the antenna pointing loss and it is usually quite small yielding less than 1[dB]. Also, the ground station misalignment loss

is not calculated but is estimated using the statistical data observed in several ground stations.

2.5 Link Budget

The link budget is the way of quantifying the link performance. The performance of any communication link depends on the quality of the equipment being used, as on the medium and weather conditions we don't have influence [9]. In the satellite communications, link budget is defined with carrier to noise ratio C/N_0, representing a measure of the received carrier strength relative to the strength of the received noise (2.15). That ratio limits the link capacity and defines the threshold of successful link for given modulation [10]:

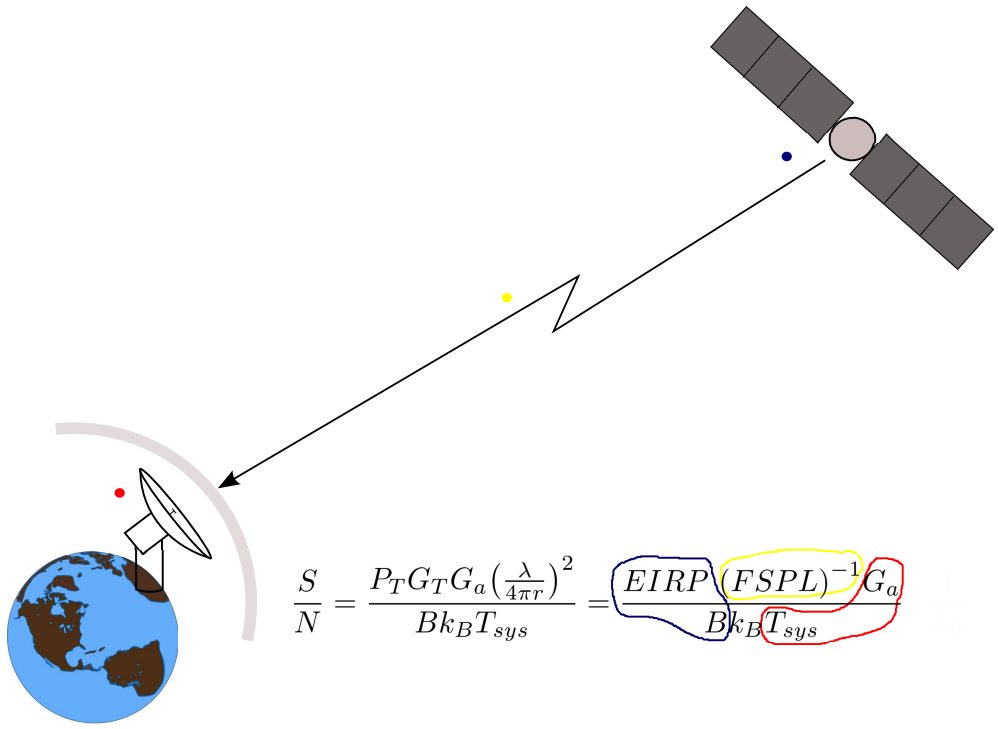

Figure 2.3: Satellite to Earth transmission path

$$\frac{C}{N_0} = \frac{P_c}{P_n} = \frac{P_T G_T G_a \left(\frac{\lambda}{4\pi r}\right)^2}{B k_B T_{sys}} = \frac{EIRP \cdot FSPL^{-1} \cdot G_a}{B \cdot k_B \cdot T_{sys}} \tag{2.15}$$

Observing the Equation (2.15) explained in the Figure 2.3, it can be seen that the link budget depends on the satellite $EIRP$[W], attenuation in the free space propagation $FSPL$, Boltzmann's constant k_B[W s K^{-1}], operational bandwidth B[Hz], and finally of the antenna gain and system noise temperature ratio G_a/T_{sys}[K^{-1}].

The G_a/T_{sys} parameter is the only parameter we can adjust in our satellite communication link planning and design, and is dependent only on the ground station. Therefore, the mentioned ground segment depended parameters can be described as the ground segment station quality factor. The quality factor G_a/T_{sys}, or otherwise specified as a figure of merit, will be in following specified as G/T. Usually, the G/T value is also given in the logarithmic form expressed in [dB K^{-1}]:

$$\frac{G}{T}[dB/K] = 10 \cdot \log_{10}(\frac{G}{T}) \ . \tag{2.16}$$

The difference in logarithmic scale between the required power to noise ratio and the receive power to noise ratio at the receiver is specified as the link margin [2]. Link margin must be positive and maximised, to prevent that the signal, during unpredictable situation, becomes undetectable. Link margin is given by:

$$LM = \frac{(\frac{C}{N_0})_{received}}{(\frac{C}{N_0})_{required}} \ . \tag{2.17}$$

3 Ground Station Satellite Receivers

Ground station receiving system can be divided in three major segments: The RF terminal including the antenna, baseband and control equipment, and signal processing unit. Signal processing unit vary with satellite communication applications and will not be discussed in this thesis.

Baseband equipment performs the modulation-demodulation function along with the baseband processing and interfacing with the terrestrial tail or network. Control equipment is a complex system used for the antenna pointing by controlling the azimuth, elevation and polarization motors. Besides the manual antenna pointing control, antenna control unit device (ACU) usually provides sophisticated methods for satellite tracking. To perform satellite tracking, ACU takes as an input two reference signals, from which estimates in what direction the antenna has to be shifted. Input signals that ACU uses for satellite tracking are different mode signals in order to obtain the sum and difference radiation pattern [11]. Typically, for circularly polarized signal, TE_{11} mode is used to obtain the sum pattern, while for the difference pattern the TM_{01} mode is used. In order to receive both desired modes, a multi-mode feed system is designed to receive both modes and then effectively separate the modes using the mode filters, like resonant rings and waveguide system. Both modes, after the separation, are amplified, down-converted and guided to the ACU. Antenna control unit then combines both modes in a way that the maximum ratio between the sum and difference pattern is obtained, looking for the minimum of TM_{01} mode. That provides the information of how much the antenna needs to be moved. The

direction of movement, it is defined by the phase between TE_{11} and TM_{01} mode.

In following, the RF terminal and the large aperture parabolic antennas will be discussed separately. An example of an large aperture ground station with Cassegrain geometry, operating in X-band, with a reflector diameter size $d = 10$ m is shown in Figure 3.1.

Figure 3.1: Example of X-band ground station antenna with $d = 10$ m

3.1 RF terminal

The RF terminal of an receiving ground station consists of low noise amplifier (LNA), couplers, switches, attenuators, splitters, and up and down converters. All the electronic equipment in the terminal is mostly connected with the waveguides, or sometimes with the high-quality high-frequency cables.

The reason why the mentioned electronic parts are situated directly behind the antenna is that the LNA has to be connected as close as possible to the antenna output terminal, to minimize the signal loss and amplifications of the undesired noisy signals. The signal is carried from the feed to the LNA through the waveguides which introduce losses and noise to the signal. In the downlink, after the LNA, amplified signal is carried to the down converter which has to be set for a desired frequency. Converted signal is then carried from the RF terminal to the antenna baseband and control equipment.

However, in the RF terminal block, usually, there are more than one LNAs and more than one down converter, where waveguides switchers and splitters take their role in signal directing. Also, if the infrastructure provides it, there is a separated LNA used for automated tracking.

Schematic of simplified receiving ground station RF terminal block diagram is presented in Figure 3.2.

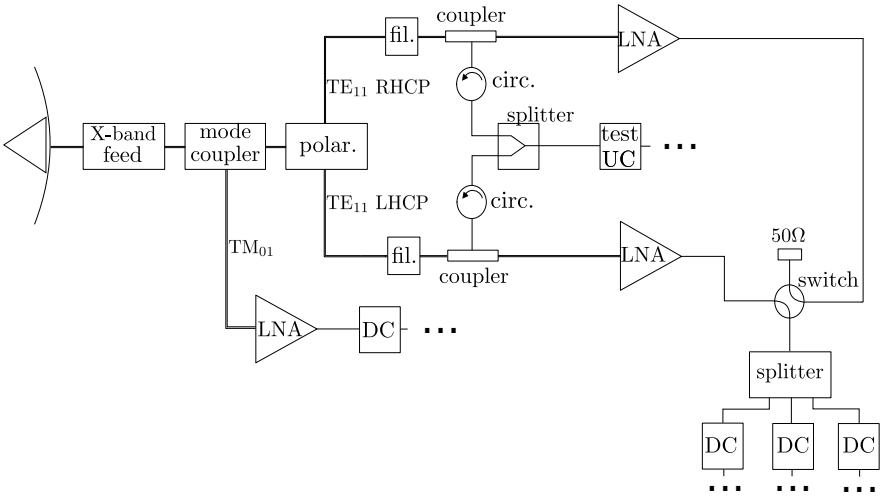

Figure 3.2: Example of RF terminal block diagram including the antenna of receiving ground station

3.1.1 Low Noise Amplifier

The low noise amplifier is the most important part of the downlink chain after the antenna. It is used to amplify the received signal, which is in order of picowatts, to much higher power values without significantly degrading its signal to noise ratio. In large ground segment systems, LNA gain can be in range of 40 - 60[dB].

Also, being the first electronic segment in the downlink chain, it contributes the most to the receiver noise temperature, which implies the necessity of keeping the noise temperature of LNA at the lowest possible levels, consequently having the large impact on the LNA price.

Important factor which describes the best the efficiency of an LNA is the noise factor which is tightly connected to the LNA noise temperature, and can be relatively simply measured.

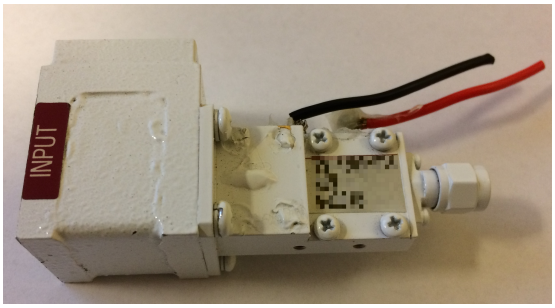

Figure 3.3: Example of low noise figure and high gain LNA

To sum up, LNA combines a low noise figure, high gain, and a stability without oscillation over entire useful frequency range.

3.1.2 Down converter

The down converter is used to convert the signal at receiving band frequency to a lower frequency typically around few hundred MHz. It is composed of a direct digital synthesizer, a low-pass filter, and a downsampler. Good down converters have the possibility of manually selecting the frequency of interest, from which

the conversion has to be made.

3.2 Large Aperture Reflector Antenna

To obtain a high G/T antenna quality factor, it is necessary to select the antenna with high antenna gain, which is proportional to the antenna directivity. Both antenna directivity D, and gain G are given with following equations [12]:

$$D = \frac{4\pi |F(\theta,\phi)_{max}|^2}{\int_0^{2\pi}\int_0^{\pi} |F(\theta,\phi)|^2 \sin(\theta)\, d\theta\, d\phi} \ , \tag{3.1}$$

$$G = \eta_0 \cdot D \ . \tag{3.2}$$

where $|F(\theta,\phi)|^2$ is the angular distribution of the radiated energy or antenna radiation pattern, and η_0 is the antenna radiation efficiency.

The antenna gain is proportionally related to the antenna aperture, implying that for the higher antenna gains, larger antenna apertures are needed. Large apertures can be obtain using the antenna arrays or reflectors, where the latter ones are far more simpler using a simple feed and a free space as its feed network.

Observing just the X-band ground stations, and in order to satisfy high gain needs, different types of parabolic reflector antennas are used.

3.2.1 Parabolic reflector antennas

Parabolic reflector antennas have the biggest percentage among the used receiving antennas in the X-band for satellite communication purposes. The rough division can be made on the front-fed parabolic reflector antennas, and the dual-reflector antennas like Cassegrain and Gregorian.

3.2.1.1 Front-Fed parabolic reflector antennas

First of the parabolic antennas is front-fed parabolic antenna [13] which can be divided to symmetric and offset front-fed antenna types. Front-fed antennas have

low focal distance to reflector diameter ratio (f/d), and the feed is positioned in the reflector's focus. Parabolic geometry is used so that rays emanating from the focus of the reflector are transformed into plane waves.

The antenna aperture, as one of the most important parameters of parabolic reflectors, is given with the described f/d ratio. The focal point of the front-fed parabolic reflector is given as:

$$f = \frac{d^2}{16h} \ , \tag{3.3}$$

where d is reflector diameter and h is the reflector depth both expressed in meters.

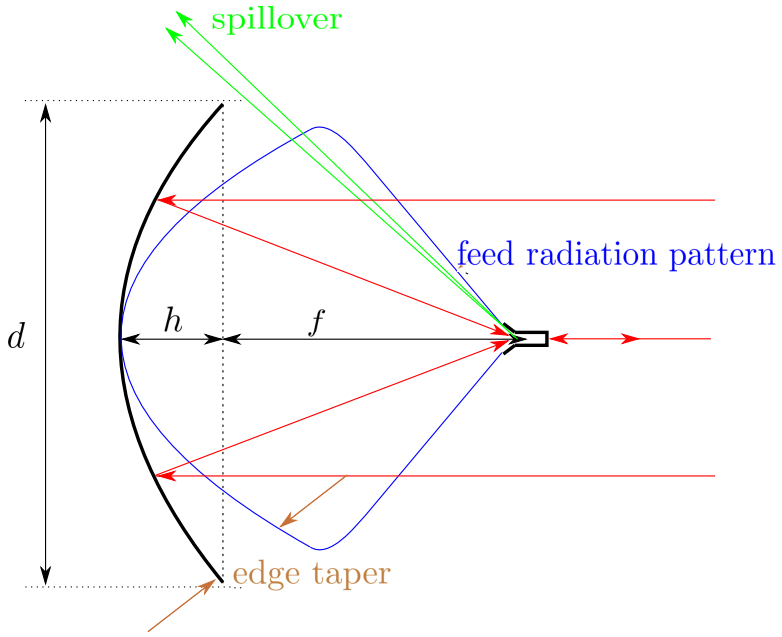

Figure 3.4: Symmetric front-fed parabolic reflector antenna

Symmetric front-fed antenna feed's phase center is located in the reflector's focal point, in front of the antenna on its axis. From the Figure 3.4 it can be observed that the feed is producing electromagnetic (EM) *shadow* on the reflector by blocking a small part of the EM blockage with its size. In order to keep the blockage effect in acceptable amounts, the rule of thumb for the reflector diameter size is $d > 5\lambda$. Symmetric front-fed antenna requires smaller feed dimension and has larger illumination angle α. Also, the f/d ratio is typically between 0.3 and

0.4. Because of parabolic geometry, the distance between feed and the vertex is smaller than the distance between feed and the reflector edge, introducing the illumination losses dependent on the feed's radiation pattern.

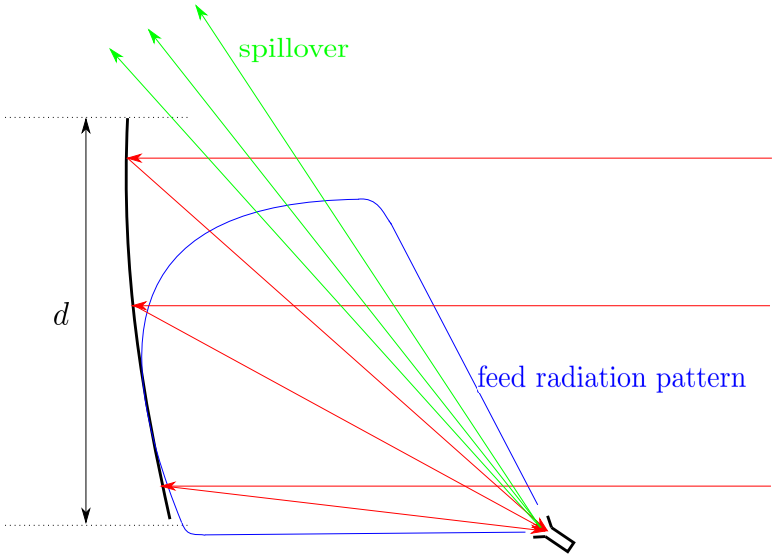

Figure 3.5: Offset front-fed parabolic reflector antenna

Offset parabolic reflector (Figure 3.5) is made from an offset cut of formed parabola, has the larger feed size and smaller illumination angle α. Focal point is located outside the illumination of the reflector and it doesn't introduce the blockage loss. However, the spillover in offset antennas is larger, augmenting the antenna noise temperature T_{ant}. Aperture of the offset parabolic antenna f/d is typically between 0.6 and 0.7.

A primary advantages of front-fed reflector antennas is the ease of coupling the receivers, high gain, full manageability and simple change of working bandwidth by changing the feed at the focus. However, a front-fed antennas have some additional disadvantages as poor image forming quality due to lower f/d ratios, and large spillover of the feed *looking* at the ground and hence picking up the undesired thermal radiation considered as noise.

3.2.1.2 Dual-reflector antennas

The most represented antenna type in the large aperture satellite receiving antennas, in order to obtain higher gain and lower antenna noise temperature, are dual-reflector antennas. From dual-reflector antennas, the most commonly used is Cassegrain antenna, followed by the Gregorian antenna type.

Dual reflector antenna consist of main reflector and the secondary reflector, where one focal point of secondary reflector matches the focal point of main reflector, and the second focal point of secondary reflector is positioned at the feed's phase center [13]. Secondary reflector, with its diameter usually larger than $0.1 \cdot d$ and struts holding it, introduces larger effect of aperture blockage resulting in higher undesired sidelobe level and slightly lower axial gain. For both dual reflector types it is possible to calculate the equivalent front-fed parabolic reflector, always keeping in mind that the original aperture blockage effect must not be neglected.

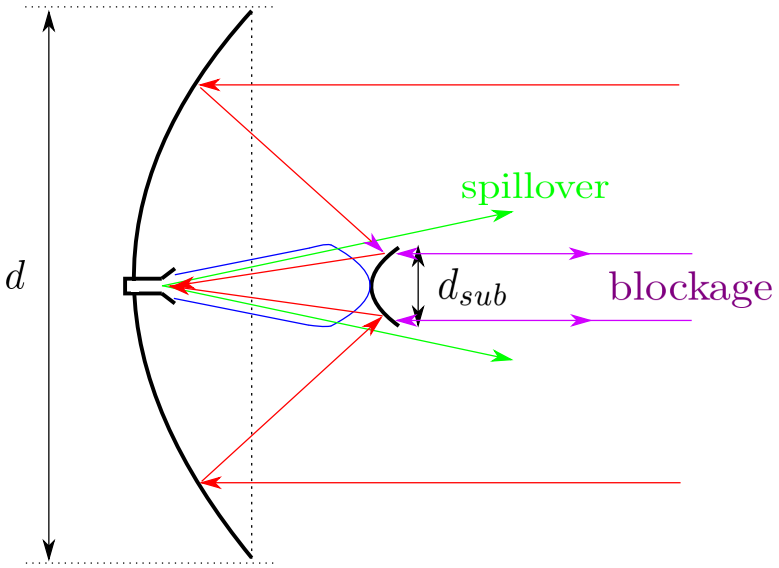

Figure 3.6: Cassegrain antenna

Cassegrain antenna is shown in Figure 3.6, consists of main reflector with parabolic symmetrical cut, and the secondary reflector with hyperbolic geome-

try. The secondary reflector edge curvature increases the diffraction and reduces the control of the field incident on the main reflector, but by shaping or small adjustments of the Cassegrain secondary reflector it is possible to increase overall efficiency.

One of the main advantages of Cassegrain antenna is that the feed is oriented towards the secondary reflector and its spillover illuminates the cold sky instead of the Earth having as a consequence significantly lower antenna noise temperature T_{ant}, and hence, higher G/T ratio.

Some of the electrical characteristics of the Cassegrain antenna can be simulated with the equivalent front-fed parabolic antenna, using the equations given in [13]. Equivalent front-fed parabola usage is very good for the approximations of the amplitude taper and the small angle beam scan of initial Cassegrain antenna. The equivalent front-fed parabolic antenna has the same reflector diameter size as the Cassegrain's primary reflector diameter, with a different reflector depth. Feed used in the equivalent parabola approximation is the same feed used in the Cassegrain configuration. Usually typical aperture parameter of the equivalent front-fed parabola is $f/d = 1.6$.

3.2.2 Antenna modelling and analysis

In this thesis, I have used GRASP reflector antenna modelling software made by TICRA [14] for the antenna modelling, simulation of radiation patterns, and understanding of various effects on antenna radiation pattern like blockage, spillover, change of reflector diameters and edge tapering, for large aperture X-band antennas. In modelling and analysis, the Gaussian feed pattern was used in lack of additional real-feed specifications. Gaussian feed provides a beam with a Gaussian taper, with edge tapering of desired value. The integral of the radiation pattern over the sphere is normalized to 4π.

The electromagnetic wave propagation and hence, the radiation pattern was obtained using the Physical Optics method (PO) in combination with Physi-

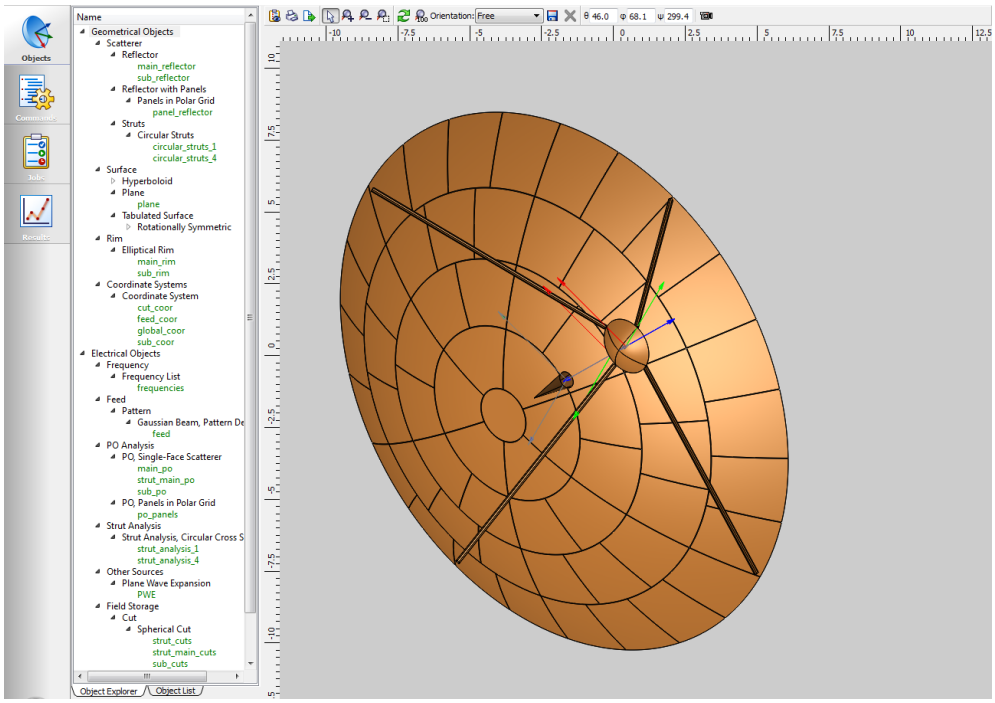

Figure 3.7: Example of $d = 11m$ X-band Cassegrain antenna model

cal Theory of Diffraction (PTD) providing efficient approximations of Maxwell's equations.

PO is a short-wavelength approximation commonly used in electrical engineering using ray optics to estimate the field on a surface and then integrating that field over the surface to calculate the transmitted or scattered field. Physical optics gives an approximation of the induced currents on a scatterer derived from scattering by an infinite planar surface, and is valid for the perfectly conducting scatterers which are large in terms of wavelengths. Then the radiation integral of the surface is calculated by numerical integration with high accuracy. If the scatterer is not ideal, it is possible to provide its coefficients in tabulated form.

However, the special behaviour of the currents close to the edge of the scatterer is not modelled by the PO. Therefore, the Physical Theory of Diffraction (PTD) approximates the difference between the PO currents and the exact induced currents, by considering the induced currents on an infinite perfectly conducting half

plane illuminated by a plane wave.

Nevertheless, the most recommended and accurate method, in case it is available, is Method-of-Moments (MoM) [15], a numerical computational method of solving linear partial differential equations which have been formulated as integral equations requiring only the boundary values.

The use of antenna modelling and analysis becomes of significant importance, for the large aperture antennas, where entire radiation pattern can not be measured for the full solid angle of 4π, in order to estimate the sidelobe and backlobe effect and influence on the antenna noise temperature.

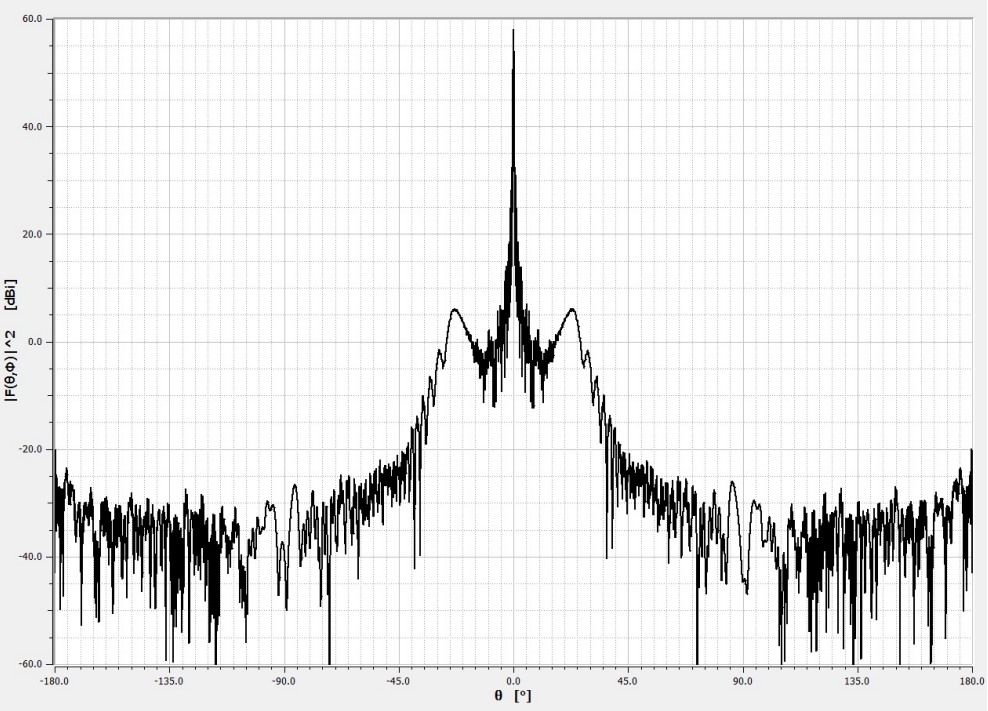

Figure 3.8: Example of one simulated X-band Cassegrain antenna radiation pattern cut

Figure 3.8 shows entire cut of simulated radiation pattern of an non-optimized Cassegrain antenna in X-band, with main reflector diameter of $d = 11$m, using PO + PTD method, and considering the blockage effect and spillover, produced in GRASP.

3.2.3 Antenna noise temperature

In addition to desired signal, antenna picks up the noisy signals from the surrounding, as are sky, atmosphere, ground or other natural or man-made noise sources. This noise sources are coming from the different directions and are weighted according to the antenna radiation pattern. This way, the weighted average noise power is obtained at the output antenna terminals, and is strongly dependent on the antenna elevation from the horizon plane. To provide an insight, if the antenna is pointing the zenith, it will still pick up the noisy signals from the ground through its side lobes.

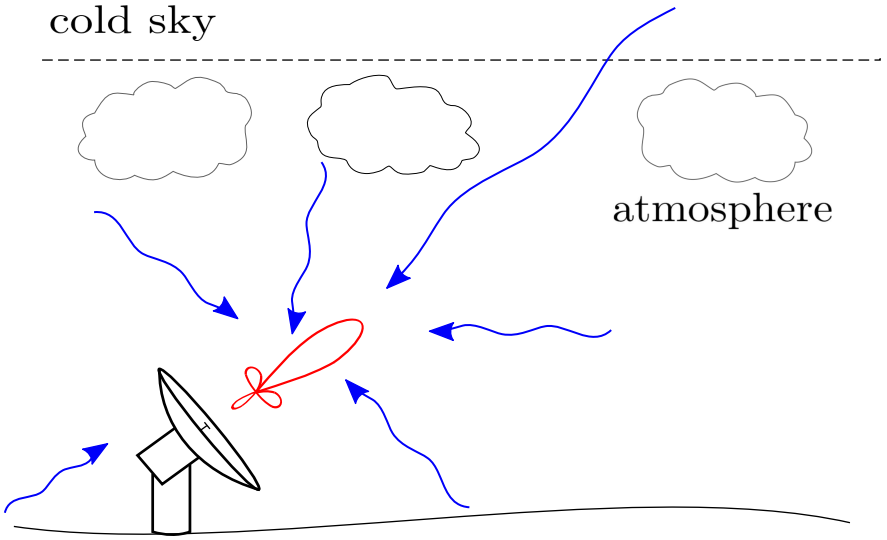

Figure 3.9: Antenna collects noise with entire radiation pattern

For a specific direction in space characterized with azimuth and elevation (θ, ϕ), a noise source is dependent on the effective noise temperature or brightness temperature in that direction $T(\theta, \phi)$. The antenna temperature T_{ant}, for elevation of interest, is given as the average over all sources (average over all directions) weighted by the radiation pattern of the antenna [16]:

$$T_{ant} = \frac{\int_0^{2\pi} \int_0^{\pi} T(\theta, \phi) D(\theta, \phi) \sin(\theta)\, d\theta\, d\phi}{\int_0^{2\pi} \int_0^{\pi} D(\theta, \phi) \sin(\theta)\, d\theta\, d\phi}\,, \tag{3.4}$$

where $D(\theta, \phi)$ is the antenna directivity. However, it is more convenient to express

the antenna noise temperature with the normalized radiation pattern $g(\theta, \phi)$ [17]:

$$g(\theta,\phi) = \frac{D(\theta,\phi)}{D(\theta,\phi)_{max}} = \frac{G(\theta,\phi)}{G(\theta,\phi)_{max}} = \frac{|F(\theta,\phi)|^2}{|F(\theta,\phi)|^2{}_{max}} \ . \tag{3.5}$$

Hence, the antenna noise temperature can be written:

$$T_{ant} = \frac{\int_0^{2\pi}\int_0^{\pi} T(\theta,\phi)g(\theta,\phi)\sin(\theta)\,d\theta\,d\phi}{\int_0^{2\pi}\int_0^{\pi} g(\theta,\phi)\sin(\theta)\,d\theta\,d\phi} \ . \tag{3.6}$$

3.3 System noise temperature

In the satellite communication systems, it is common to define the system noise temperature T_{sys}[K] (3.7) combined of the antenna noise temperature T_{ant}, and the receiver noise temperature T_{rec}:

$$T_{sys} = T_{ant} + T_{rec} \ . \tag{3.7}$$

System noise temperature does not represent a physical temperature of the antenna or the receiver. It represents the equivalent system temperature, at which the simple resistor would produce the same amount of noise power. The temperature is always expressed in Kelvins [K]. Figure 3.10 represents the block scheme of antenna and receiver, also marking the reference point of system noise temperature measurement.

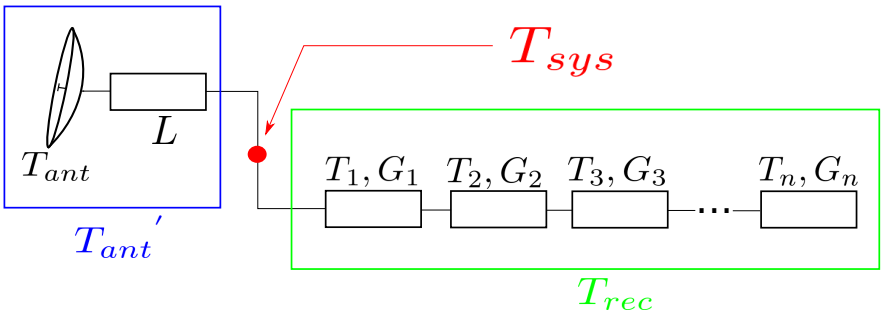

Figure 3.10: Reference point of system noise temperature

Receiver considers all the downlink cascade from the antenna output to the measurement end terminal. Receiver noise is primarily thermal noise due to thermal motion of free electrons and has the Gaussian distribution.

All downlink cascade elements, passive or active, introduce some gain or losses to the signal level. Each element can be described with its equivalent element temperature or its noise factor. Noise factor F is a measure of degradation of the signal to noise ratio on the element input and signal to noise ratio on the element output. The connection between noise temperature T and noise factor F is expressed as:

$$F = 1 + \left(\frac{T}{T_0}\right) \ , \tag{3.8}$$

where $T_0 = 290\text{K}$ is the surface average temperature.

The most important element in the cascade is the first element because his noise contribution is added to the cascade noise in its entirety, while the following elements are diminished by the product of previous element gains. Cascade is shown on the right side of Figure 3.10 and its noise temperature is given by:

$$T_{cascade} = T_1 + \frac{T_2}{G_1} + \frac{T_3}{G_1 \cdot G_2} + \cdots + \frac{T_n}{G_1 \cdot G_2 \cdot G_3 \cdots G_{n-1}} \ , \tag{3.9}$$

where the numbers represents the index of the element looking from the antenna output terminal towards the measurement end terminal, and G represents the indexed element gain. It must be noted that gains are not expressed in decibels, and that losses can be expressed as ${G_i}^{-1}$.

Observing the Figure 3.10, and selected measurement point, it can be seen that the antenna's ohmic losses and waveguide losses have to be adequately added to the antenna noise temperature value, also following the cascade equation:

$${T_{ant}}' = \frac{T_{ant}}{L} + \frac{T_0}{L}\left(L - 1\right) \ , \tag{3.10}$$

where L is the product of antenna feed losses and filter, waveguide and switch losses in linear scale, and $T_0 = 290\text{K}$ is the average surface temperature.

Finally it is possible to express the system noise temperature T_{sys} for given measurement point on Figure 3.10:

$$T_{sys} = \frac{T_{ant}}{L} + \frac{T_0}{L}\left(L - 1\right) + T_{rec} \ , \tag{3.11}$$

where T_{sys}[K] is the system noise temperature, T_{ant}[K] is antenna noise temperature, T_0[K] is average surface temperature (usually $T_0 = 290$K), and L are antenna ohmic losses combined and given in linear scale.

4 Adequate Astronomical Radio Frequency Source Analysis

Astronomical radio sources are objects in the outer space that emit strong radio frequency waves, coming from a wide variety of sources. There are two different families of sources: galactic sources, concentrated towards the galactic plane and extragalactic sources distributed more or less uniformly in space. The unresolved, spatially continuous radiation belongs to the galactic component. In addition, there is the 2.7K thermal background radiation which is cosmological in origin [18]. Further division is based on the source spectral characteristics where two source types are distinguished: type with the roughly constant flux density with increasing frequency and the type that is more intense at lower frequencies. Some of the most intense sources are of the second type as are Cassiopeia A, Taurus A etc. As it can be seen from the Figure 4.1, Orion, Moon and Sun have increasing flux density with increasing frequency which is identified with objects well known from the optical range of the spectrum. On the ordinate axis of Figure 4.1, the flux density (S) is expressed in Jansky's which equals $1Jy = 10^{-26}\ \mathrm{W\,m^{-2}\,Hz^{-1}}$.

The most used and most powerful RF sources in the skies, beside artificial satellites, are the Sun, the Moon and the radio stars Cassiopeia A and Taurus A. In order to use the astronomical RF sources to calculate the G/T quality factor, it is necessary to know the source's flux density and its angular diameter size.

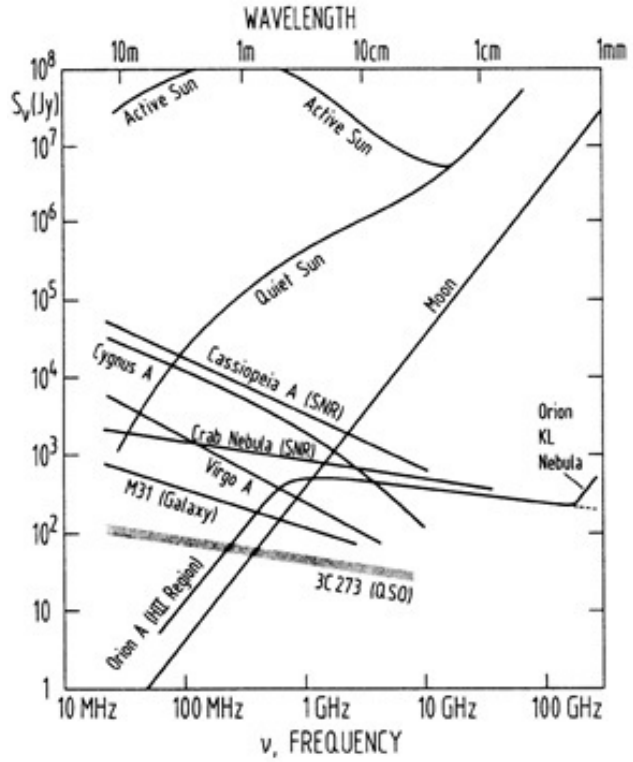

Figure 4.1: The spectral distributions of various radio sources [1]

4.1 Black-body radiation

Radiation of some sources like Moon and cold sky can be represented as a black-body radiation, depending on the black-body physical temperature. Black-body physical temperature does not represent the temperature distribution of the source, but the temperature on which the black-body produces the same amount of noise as the source of interest.

Black-body radiation is described by the Planck's law (4.1), providing the brightness distribution, $B(f,T)[\mathrm{W\,m^{-2}\,sr^{-1}\,Hz^{-1}}]$, of electromagnetic radiation emitted by a black-body in thermal equilibrium at a given temperature T[K] and frequency f[Hz]:

$$B(f,T) = \frac{2hf^3}{{c_0}^2} \cdot \frac{1}{e^{\frac{hf}{k_B T}} - 1} \ , \tag{4.1}$$

where k_B is a Boltzmann constant and h is Planck constant expressed as:

$$\begin{aligned} k_B = &\quad 1.38064852 \cdot 10^{-23} \quad [\mathrm{m^2\,kg\,s^{-2}\,K^{-1}}] \\ h = &\quad 6.62607004 \cdot 10^{-34} \quad [\mathrm{m^2\,kg\,s^{-1}}] \end{aligned} \tag{4.2}$$

However, in the X-band frequencies the photon energy ($h \cdot f$) is negligible being significantly lower than thermal energy ($k_B \cdot T$). Therefore, the radiation of the black-body, brightness distribution, can be efficiently approximated with the Rayleigh-Jeans law [16]:

$$B(f, T) = \frac{2f^2 k_B T(\theta, \phi)}{{c_0}^2} \ , \tag{4.3}$$

where f is frequency in [Hz], k_B is Boltzmann constant given in (4.2), c_0 is speed of light in $[\mathrm{m\,s^{-1}}]$, and $T(\theta, \phi)$ is the black-body temperature in [K] dependent on the (θ, ϕ) direction of the radiation.

The flux density of the source radiation, $S[\mathrm{W\,m^{-2}\,Hz^{-1}}]$, is calculated integrating the brightness distribution over the source's solid angle (4.4), and appropriately correcting according to the source and receiver polarization. For example, if the source is randomly polarized, like Moon, just half of the radiated energy is intercepted by single polarized antenna, and the flux density calculation must be corrected by a factor of 0.5.

$$S = \int_0^{2\pi} \int_0^{\pi} B(\theta, \phi) \sin(\theta)\, d\theta\, d\phi \ . \tag{4.4}$$

In most cases it is possible to approximate the source as the uniform brightness disk, with a constant brightness temperature $T(\theta, \phi) = T_{source}[\mathrm{K}]$ with almost negligible errors [19, 20]. The uniform brightness disk flux density is given with following expression:

$$S = \frac{2f^2 k_B T_{source}}{{c_0}^2} \Omega_{source} \ , \tag{4.5}$$

where Ω_{source} represents the source's solid angle given in steradians [sr].

The distance between the receiving antenna and the black-body is, in this scenario, included in angular distances and measures used to address the Earth-Moon geometry.

4.2 The Sun

The Sun is the strongest astronomical radio source observed from Earth, but is the subject to large and unpredictable variation with time, mostly due to Sun storms and bursts.

The solar flux densities, $S_{Sun}[\mathrm{W\,m^{-2}\,Hz^{-1}}]$, are measured on specific frequencies from several observatory locations at different times. The measurement frequencies are: 0.245, 0.410, 0.610, 1.415, 2.695, 2.800, 4.995, 8.800 and 15.400 GHz. The solar flux density for the frequency of interest in X-band is determined by interpolation of flux measurements made on a daily basis in between $f_1 = 4.995\mathrm{GHz}$ and $f_2 = 8.800\mathrm{GHz}$ [21]:

$$S_{Sun} = 10^4 \left(\frac{S_{f_1}}{S_{f_2}}\right)^{\alpha_1} S_{f_2} \cdot 10^{-26} \ , \tag{4.6}$$

where S_{f_1} and S_{f_2} are solar flux values, expressed in $[\mathrm{W\,m^{-2}\,Hz^{-1}}]$, at frequencies f_1 and f_2, obtained from the radio observatories, and α_1 factor is given as:

$$\alpha_1 = \frac{\log_{10}\left(\frac{f_{\mathrm{GHz}}}{f_2}\right)}{\log_{10}\left(\frac{f_1}{f_2}\right)} \ , \tag{4.7}$$

where f_{GHz} is a frequency of interest given in [GHz].

Measured solar flux densities are available on the web page of National Oceanic and Atmospheric Administration (NOAA) at [22]. For example, the observatory of interest in Italy, and for this thesis, is San Vito dei Normanni, Brindisi.

When Sun is used as a uniform brightness disk, the equivalent solar disk angular diameter $\theta_{Sun}\,[^\circ]$ is given with a dependence of frequency expressed in GHz [23]:

$$\theta_{Sun} = 0.533 \cdot 10^{\frac{1}{\alpha_2}} \ , \tag{4.8}$$

where,

$$\alpha_2 = \frac{{f_{\mathrm{GHz}}}^4}{1818} - \frac{{f_{\mathrm{GHz}}}^3}{23.348} + 1.22{f_{\mathrm{GHz}}}^2 - 2.66 f_{\mathrm{GHz}} + 11.43 \ . \tag{4.9}$$

4.3 Radio Stars

In the northern hemisphere, the most appropriate discrete radio sources for G/T quality factor measurements are Cassiopeia A and Taurus A, while Orion and Omega are similarly appropriate for the measurements with ground stations located in the southern hemisphere [24].

Because the angular diameters of the radio stars are much smaller than the X-band typical large aperture antenna HPBWs, radio stars can be considered point-like sources. Using the radio star as an RF source in direct G/T measurements, the error introduced using the correction factors is minimized.

However, the brightness of radio stars is much lower than those of the Sun or the Moon. For the X-band antennas with reflector diameter size smaller than $20m$, using the direct G/T measurement method with radio stars introduces significant uncertainties. Uncertainties and hence, possible errors in the calculation, are due to very small ratio between the received noise power while pointing the radio star, and received noise power while pointing the cold sky at the same elevation - the measurement of significant influence in the direct G/T measurement method.

Table 4.1 gives values of the flux-density of the radio stars indicated, where the frequency is given between 1 and 20 GHz:

Table 4.1: Radio source flux densities

Radio source	Flux density at f_{GHz}	Units
Cassiopeia A	$S_{Cas} = 10^{[5.745-0.770\cdot\log_{10}(1000\cdot f_{\mathrm{GHz}})]} \cdot 10^{-26}$	$\mathrm{W\,m^{-2}\,Hz^{-1}}$
Taurus A	$S_{Tau} = 10^{[3.794-0.278\cdot\log_{10}(1000\cdot f_{\mathrm{GHz}})]} \cdot 10^{-26}$	$\mathrm{W\,m^{-2}\,Hz^{-1}}$
Orion	$S_{Ori} = 10^{[3.317-0.204\cdot\log_{10}(1000\cdot f_{\mathrm{GHz}})]} \cdot 10^{-26}$	$\mathrm{W\,m^{-2}\,Hz^{-1}}$
Omega	$S_{Ome} = 10^{[4.056-0.378\cdot\log_{10}(1000\cdot f_{\mathrm{GHz}})]} \cdot 10^{-26}$	$\mathrm{W\,m^{-2}\,Hz^{-1}}$

Using the Cassiopeia A as RF source, the flux density value must be multiplied by a decay factor $K_{Casdecay}$ to compensate for its fading rate at the X-band

frequency range [25, 26]:

$$K_{Casdecay} = 1 - \frac{0.97 - 0.3\log_{10}(f_{\mathrm{GHz}})}{100} \cdot \tau \ , \tag{4.10}$$

where τ represents the number of years elapsed since January 1$^{\mathrm{st}}$ 1980 (ex. 7$^{\mathrm{th}}$ April 2016 = 36.26503). Also, $K_{Taudecay} = K_{Oridecay} = K_{Omedecay} = 1$.

4.4 The Moon

The Moon's radiation is indirect, it re-radiates the solar energy, and can be modelled as the black-body radiation, which temperature changes with lunar phases and Earth-Moon geometry. The flux density of the Moon S_{Moon}, considered a black-body radiation (4.11), can be efficiently represented as a uniform brightness disk with dependance on the Moon's solid angle changing with distance, and the average brightness temperature of the Moon $\overline{T_{Moon}}$, introducing minimal errors [19, 20].

$$S_{Moon} = \frac{2f^2 k_B \overline{T_{Moon}}}{{c_0}^2} \Omega_{Moon} \ , \tag{4.11}$$

where S_{Moon} is a flux density given in [W m^{-2} Hz^{-1}], k_B is the Boltzmann constant given in (4.2), $\overline{T_{Moon}}$ is Moon's average brightness temperature given in [K], f is frequency in [Hz] and Ω_{Moon} is Moon's solid angle in [sr].

The solid angle can be given in the dependence of the Moon's angular diameter θ_{Moon} expressed in degrees [°], using the following approximation formula:

$$\Omega_{Moon} \doteq \frac{\pi^3}{4 \cdot 180^2} \cdot {\theta_{Moon}}^2 \ . \tag{4.12}$$

Hence, the Moon's flux density S_{Moon}, can be written with the extended expression, depending on the frequency in [Hz] (f), average brightness temperature in [K] ($\overline{T_{Moon}}$) and angular diameter in degrees (θ_{Moon}):

$$S_{Moon} = \frac{2k_B\pi^3}{4 \cdot 180^2 {c_0}^2} \cdot f^2 \cdot \overline{T_{Moon}} \cdot {\theta_{Moon}}^2 \ . \tag{4.13}$$

Average brightness temperature $\overline{T_{Moon}}$, is the function of frequency, lunar phase and solar mean anomaly. Approximation of the average brightness temperature is given by [19, 20] in dependence of the frequency, lunar phase angle, and the phase lag, without taking into the consideration the yearly variation in the solar irradiation at the lunar surface due to the Earth's eccentric orbit, and also neglecting higher brightness temperature harmonics:

$$\overline{T_{Moon}} = \overline{T_0}\left[1 - \frac{\overline{T_1}}{\overline{T_0}}\cos(\phi - \psi)\right] \ , \tag{4.14}$$

where $\overline{T_0}$ is the constant brightness temperature term expressed in [K], $\overline{T_1}$ is the first harmonic of the brightness temperature in [K], ϕ is the lunar phase angle in degrees and ψ is the phase lag in degrees. In case that the lunar phase angle ϕ is in decreasing cycle, value of $\phi^{'} = 360° - \phi$ must be used in calculation of Equation (4.14). Neglecting the higher harmonics introduce the error less than 0.18% [19]. Therefore, the Equation (4.14) is written as :

$$\overline{T_{Moon}} = \overline{T_0}\left[1 - \frac{\overline{T_1}}{\overline{T_0}}\cos(\phi - \psi)\right] \pm 0.18\% \ . \tag{4.15}$$

The values $\overline{T_0}$[K], $\overline{T_1}$[K], ψ [°] and the ratio $\frac{\overline{T_1}}{\overline{T_0}}$, were determined from accurate radio measurements at a few frequencies and extrapolated in between [27, 28]. The interpolation equations for estimation of selected parameters are:

$$\begin{aligned} \overline{T_0} &= 207.7 + \frac{24.43}{f_{\mathrm{GHz}}} \\ \frac{\overline{T_1}}{\overline{T_0}} &= 0.004212 \cdot {f_{\mathrm{GHz}}}^{1.224} \\ \psi &= \frac{43.83}{1 + 0.0109 \cdot f_{\mathrm{GHz}}} \ , \end{aligned} \tag{4.16}$$

where f_{GHz} is the frequency of interest expressed in [GHz]. Each of the interpolation equations has its own uncertainty which will be presented in following section.

The lunar angular diameter θ_{Moon} and lunar phase angle ϕ in degrees, are functions of the current orbital positions of the Earth, Moon and Sun, and are

provided by NASA on the web page [29]. Figure 4.2 shows the proposed settings for obtaining necessary data, for selected time span and observer location.

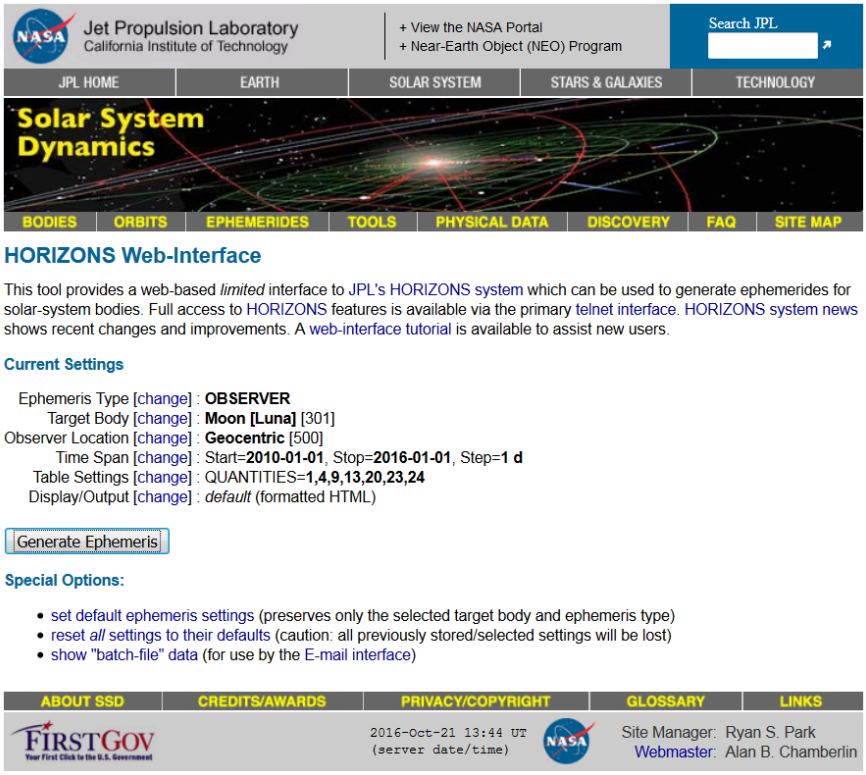

Figure 4.2: Proposed settings for Moon's astronomical information

The lunar flux density S_{Moon} in dependence of lunar phase angle, for fixed frequency $f = 8.1775$ GHz and fixed angular diameter $\theta_{Moon} = 0.5°$ is shown on the Figure 4.3. On the other hand, Figure 4.4 shows the lunar flux density change with its angular diameter variation, for fixed frequency $f = 8.1775$ GHz and fixed lunar phase $\phi = 240°$.

4.5 Uncertainties and proposed radio source

The overall G/T measurement uncertainty is calculated as the linear sum of the uncertainties, expressed in dB, estimated for flux density S and the ratio of received noise power while pointing the radio source and while pointing the cold

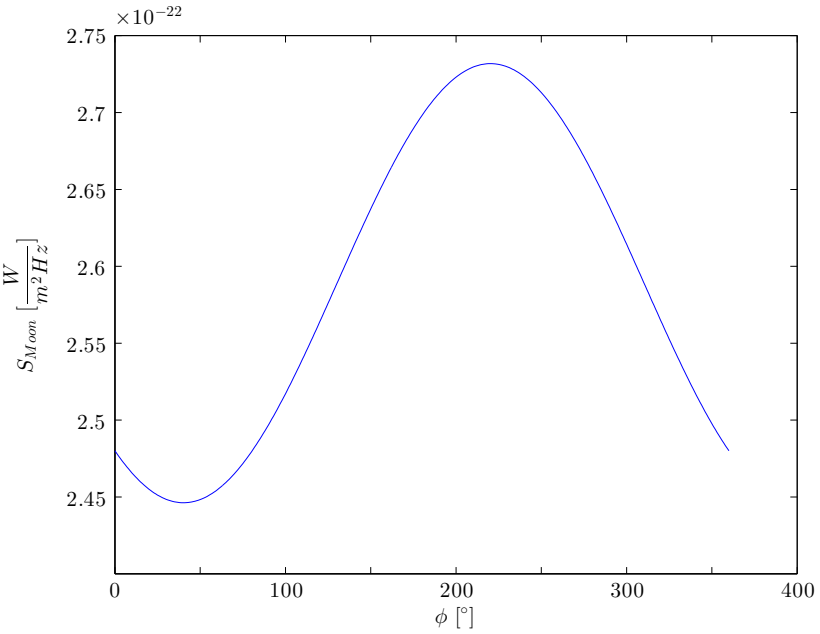

Figure 4.3: Lunar flux density change with phase angle

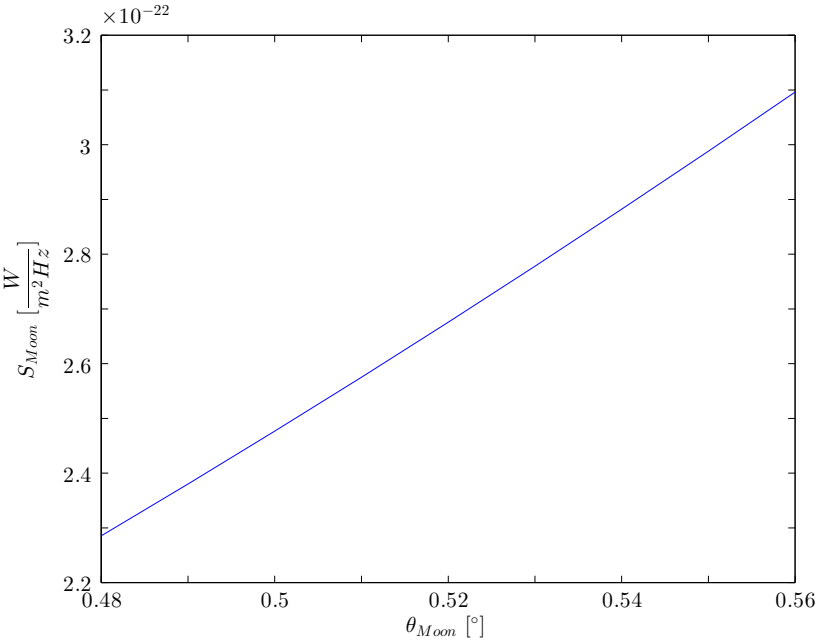

Figure 4.4: Lunar flux density change with angular diameter

sky at the same elevation (Y-factor) [19, 30].

The following Table 4.2 reports the above mentioned values of uncertainty, expressed in [dB]. Values in the table represent the G/T uncertainty due to S and Y-factor uncertainties, not their uncertainties itself.

Table 4.2: $\frac{G}{T}$ influencing uncertainties [dB]

	Moon	Sun[1]	Cassiopeia A	Taurus A
S	0.33 dB	0.3 dB	0.05 dB	0.05 dB
Y-factor	0.1 dB	0.1 dB	1 dB	1 dB
$(G/T)_{dB}$	0.43 dB	0.4 dB	1.1 dB	1.1 dB

From Table 4.2, the uncertainty in the G/T measurement is lower when using Sun and Moon as source and higher with stars, due to Y-factor contribution. As already mentioned, in this analysis the uncertainty in Sun measurements due to bursts is not included, because it is not easily computable. To avoid Sun burst influence a quite large number of measurement is required and a careful evaluation of the results is necessary, in order to check that measurement are not influenced by Sun bursts.

The Moon as source is very stable. The flux density is much lower than the Sun, but the expected Y-factor is still in the order of dB and can be easily measured with available instruments. A few number of measurements can be sufficient to get a small Y-factor uncertainty. For small G/T ratios, the error in the Y factor measurement becomes predominant, whereas for larger G/T ratios or large antenna gains, the error in beam correction prevails. Therefore, the accuracy requirement on the G/T ratio measurement sets the limitation on the applicability of the Moon as calibration source for the very high and the very low G/T ratios [31].

Radio stars are very stable, but G/T measurement using radio stars is affected

[1]The potential Sun burst problems, if the Sun is used, are not considered in the table, because Sun burst contribution is not easily computable.

by a quite high uncertainty due to the Y-factor contribution, as explained in section 4.2. It can be very difficult to get lower Y-factor uncertainty without the advanced measurement instrumentation. Furthermore the expected Y-factor is very small, in the order of tenth of dB and measurements can be heavily influenced by other factors like meteorological conditions.

Considering all these factors, the Moon is the proposed source for an accurate G/T measurement, with low uncertainty and good stability.

5 Gain over System Noise Temperature Quality Factor G/T

The gain over system noise temperature ratio G/T is a quality factor, also labelled figure of merit used to indicate the ground station sensitivity in a satellite communication system [30]. Higher the ratio, more efficient is the ground station in receiving a weak satellite signal. However, the G/T ratio must always be above the required value to ensure the quality link and service in every weather condition. The measure of the sensitivity qualifies an antenna whether it is good enough for establishing desired communication link.

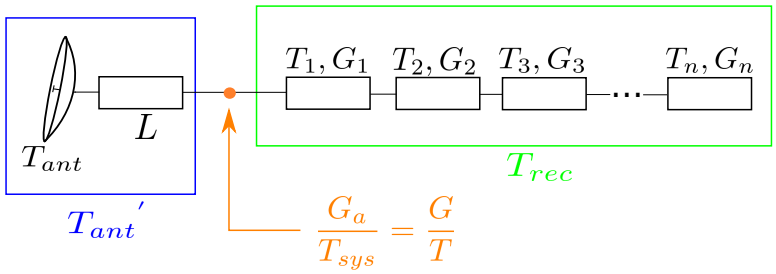

Figure 5.1: Point where G/T factor is defined

Quality factor measure depends on the internal noise produced in ground station elements, and also on the effects of noise generated in the entire environment, terrestrial and cosmic, in which the receiving ground station antenna is immersed. Figure 5.1 shows the components of the ground station and the point where the G/T factor is defined. Usually, the quality factor is referred to antenna port, even-though it should yield the same result on each point of measurement. Also,

from Figure 5.1 can be seen the dependants of G/T ratio on the environmental noise in form of the antenna noise temperature.

There are two approaches of G/T factor measurements, namely indirect and direct approach. In the indirect approach, the G and T factors are measured separately and their ratio is calculated. In the direct approach, however, neither G nor T are explicitly measured, instead to obtain the quality factor, the measurement of the ratio of two noise powers from two defined sources at some point in the intermediate frequency (IF) section of the ground station is performed.

In order to calculate the gain G for the indirect method, or to calculate the noise power ratio required in direct method, it is necessary to work with well-defined noise sources considered as transmitters. The sources, however, have to be in the antenna's far field determined by the Fraunhoffer's distance, which for the large aperture reflector antennas in X-band results always more than two kilometres. The large distances of the far field makes it impossible to obtain the laboratory measurements and very hard to obtain terrestrial measurements with distant antenna set as a source because of terrain, high multipath and various man-made or natural noises. Therefore, the optimal source must be found in the skies. However, chosen source for quality factor measurement must be frequently visible, with negligible flux density variations on specific frequency, and of course with sufficiently high flux density so the received signal is satisfactorily higher than the noise level (at least 1 dB). The most appropriate sources in the sky are geostationary satellites and RF sources like Sun, Moon and radio stars.

5.1 Indirect calculation method

Indirect G/T ratio calculation method involves the separate calculations of antenna peak gain and the system temperature [32]. While the antenna gain is usually known, or can be relatively easy calculated, the system noise temperature calculation is rather complicated. Receiver noise temperature can be calculated

using the later described methods, but the antenna noise temperature integral calculation is often just roughly estimated following the ITU-R curves [33]. Gain, however, can be changed during the time due to dish deformations, and in case of indirect method it has to be checked regularly.

If large aperture antennas are used, the test ranges using the transmitting antenna and one additional already calibrated antenna is not practical due to large distances (far field) and the transmitting antenna tower heights required to maintain an acceptable test environment. In that case, a use of extra-terrestrial RF source is needed, and the direct G/T calculation method is recommended. In case of small aperture antennas, not covered in this thesis, the gain transfer measurement method can be used [32].

The most common way of indirect method measurement for the large aperture antennas, is using the geostationary satellite to estimate the antenna gain, and separately measuring the noise temperature of the receiver.

5.1.1 Receiver noise temperature

Receiver noise temperature is usually calculated in two different ways: using the noise figure meter or using the Y-factor method.

The noise figure meter in the most cases is the most accurate way to measure the noise figure of the receiver. However, a noise figure meter has limitations and the analysers have certain frequency limits. This method also requires a very expensive equipment, mostly due to noise head for high frequencies.

Y-factor method, involve more measurements and calculations which but under certain conditions happen to be more convenient and sometimes more accurate. Performing the Y-factor method, the received noise power is measured, coming from two different black-body radiations. Difference between black-body source temperatures must be high, as the increasing Y-factor means lower uncertainty in measurements. Y-factor is given with following equation, where received

noise powers P_1 and P_2 are expressed in Watts:

$$Y = \frac{P_1}{P_2} = \frac{k_B(T_1 + T_{rec})B}{k_B(T_2 + T_{rec})B} = \frac{T_1 + T_{rec}}{T_2 + T_{rec}} \ , \tag{5.1}$$

where values T_1 and T_2 represent the source noise temperatures, or if measured with antenna, the antenna noise temperature pointing at the source, usually estimated at the brightness temperature of the source of interest. k_B is Boltzmann's constant, and B is bandwidth in [Hz] From the Y-factor Equation (5.1), the receiver noise temperature yields:

$$T_{rec} = \frac{T_1 - YT_2}{Y - 1} \ . \tag{5.2}$$

However, in order to avoid and minimize measurement uncertainties, it is necessary to express the final receiver noise temperature as a mean value of several performed measurements.

In case of calculating the Y-factor using the antenna instead of noise sources, the final result of receiver noise temperature has to be corrected for the noise that was added by the antenna's ohmic losses with its efficiency η. Antenna with efficiency $\eta < 1$ can be approximated as the antenna with efficiency $\eta = 1$ and a following attenuator with the attenuation $a = \eta$. Also, a very good noise sources on different temperatures are electromagnetic absorber for the given frequency with temperature equal to ambient temperature (usually $T = 290$K), and the cold sky at the high antenna elevation (around $T = 10$K for the X-band).

Another, more recommended solution, to measure receiver noise temperature, instead of using antenna, involves the measurement using the hot-cold noise source, with provision to change its temperature by means of a heater/cooler arrangement that can use liquid nitrogen, $T = 77$K or liquid helium, $T = 4$K.

5.1.2 Antenna noise temperature

Antenna noise temperature T_{ant}[K] contributes to the system noise temperature and is given with the Equation (3.6) and repeated below. Calculation of the

antenna noise temperature is a complex task as it involves the integration over the full solid angle of the antenna radiation pattern weighted with the apparent brightness temperatures at given directions. Apparent brightness temperatures surrounding the antenna varies with the frequency, antenna elevation, and the weather (atmosphere attenuation).

$$T_{ant} = \frac{\int_0^{2\pi}\int_0^{\pi} T(\theta,\phi)g(\theta,\phi)\sin(\theta)\,d\theta\,d\phi}{\int_0^{2\pi}\int_0^{\pi} g(\theta,\phi)\sin(\theta)\,d\theta\,d\phi}\ .$$

In ordinary ground station systems, the antenna noise temperature contribution to the system noise temperature is much smaller than the receiver noise temperature contribution, and it can be easily estimated using the antenna noise temperature curves presented in [33]. However, in advanced, professional, cooled receiver systems, the receiver noise temperature is significantly smaller and is comparable to the antenna noise temperature. Hence, becomes important to estimate antenna noise temperature more efficiently.

5.1.2.1 MATLAB antenna noise temperature estimation

To estimate antenna noise temperature a full radiation pattern is needed. For the circular polarization antennas that are rotationally symmetric, one radiation pattern cut is sufficient. Otherwise full radiation pattern with sampling $\Delta\theta = \Delta\phi = \frac{\lambda}{4}$ or denser is recommended. When calculating the radiation pattern it is proposed to interpolate the dense pattern points using the cubic interpolation and to represent the radiation pattern in the Theta-Phi (θ,ϕ) grid format. Theta-Phi grid format allows representation of whole solid angle of the antenna radiation pattern (4π). In this grid the unit vector to the field point is given by $\vec{r} = (\sin\theta\cos\phi, \sin\theta\sin\phi, \cos\theta)$ in the Cartesian coordinate system. Linear polarized large aperture antenna radiation pattern in Theta-Phi grid is shown on Figure 5.2: The noise power received by a receiving station antenna is due to the

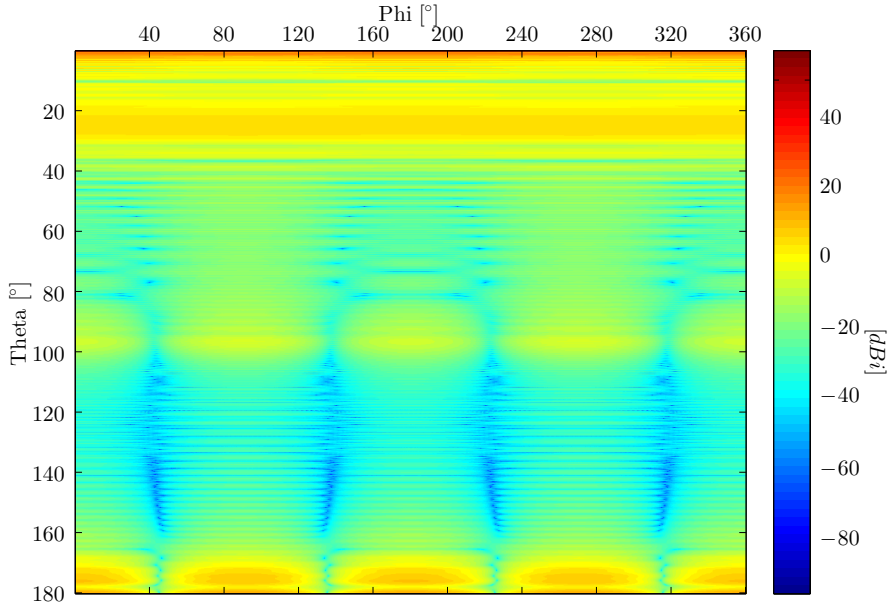

Figure 5.2: Linear polarized large aperture antenna gain pattern in dBi

emission at the given frequency of various sources surrounding the antenna, usually expressed in terms of the source's brightness temperature, also called noise temperature. The brightness temperature of the source is not it's physical temperature, but it can be approximated as a physical temperature of the blackbody (perfect absorber) emitting the same power in given band as the selected source. Therefore, the brightness temperature is the background temperature in a certain direction, and it is independent of the receiver noise temperature or antenna gain. In following the surrounding brightness temperatures will be divided in the two categories, the Earth brightness temperature and the sky brightness temperature [34].

To derive a brightness temperature expression, one can start with radiative transfer theory. Radiative transfer theory describes the intensity of radiation propagating in the media, like atmosphere, that absorb, emit and scatter radiation in terms of thermal radiation. The scattering, for the simplification will be neglected in further calculations. The brightness temperature equation derived

from [35, 36], and taking into the consideration Rayleigh-Jeans approximation of Planck's law, as well as the assumption of homogeneous isothermal atmosphere, is given as:

$$T_B = T_{cosm} e^{-\tau_\nu(\infty)} + T_{mpt} \int_0^{s_0} k_a \cdot e^{-k_a \cdot s}\, ds \ , \tag{5.3}$$

where T_{cosm}[K] is the cosmic background brightness temperature, T_{mpt}[K] is the physical temperature of the medium, k_a is the atmospheric absorption coefficient dependent on the elevation angle, and s represents the distance from the antenna. The first term in the above equation $T_{cosm} e^{-\tau_\nu(\infty)}$ at the X-band reduces to T_{cosm}. Cosmic background brightness temperature, for the X-band yields about 3K.

Related to the Equation (5.3), there is a relation between the atmospheric attenuation A[dB] due to gaseous effects and the atmospheric opacity τ_0 expressed in Neper, given as:

$$\tau_0 = k_a s_0 = \frac{A[\text{dB}]}{4.34} \ . \tag{5.4}$$

Also, it is possible to express the linear loss factor L due to the atmospheric absorption:

$$L = e^{\tau_0} = e^{k_a s_0} = e^{\frac{A[\text{dB}]}{4.34}} = 10^{\frac{A[\text{dB}]}{10}} \ . \tag{5.5}$$

Proceeding with the integration of the Equation (5.3) the following equation is obtained [34]:

$$T_B = T_{mpt} - \frac{T_{mpt} - T_{cosm}}{L} \ , \tag{5.6}$$

where the T_{mpt}[K] is the mean ambient temperature that ranges from about 260K to about 280K on Earth, but the best practice is to work with a value of $T_{mpt} =$ 270K.

Atmospheric attenuation in decibels, and hence, the linear loss factor for different elevation angles are given with the equations for estimated atmospheric attenuation in chapter (2.3.2).

Brightness temperature of the Earth, T_{Bearth}, depends upon the surface physi-

cal temperature T_{earth} and emissivity ϵ_{earth} with following relation [37]:

$$T_{Bearth} = \epsilon_{earth} \cdot T_{earth} \ . \tag{5.7}$$

Given relationship is an approximation of the Planck's radiation law for small frequencies, Rayleigh-Jean's approximation. The physical temperature T depends on the incident energy from the Sun and the thermal properties of the soil surface. Emissivity ϵ_{earth} and brightness temperature T_{Bearth} depend on the geometrical and dielectric properties of the surface. Dielectric properties, however, are connected to the soil moisture content and are affected by the evapotranspiration, rain and height above the sea level. Emissivity ranges from 0 to 1, and in the X-band for the most natural surfaces can be taken as $\epsilon_{earth} = 0.93$.

Up to this point, the method of sky brightness temperatures and Earth brightness temperatures, depending on elevation angle measured from horizon has been given. However, in order to generate the brightness temperature matrix containing the brightness temperatures from different directions surrounding the antenna, it is necessary to transform the coordinate reference system from East-North-Up reference system to antenna reference coordinate system. This transformation was done using the spherical law of cosines, used for solving spherical triangles, presented in Figure 5.3 and given with the Equation (5.8) [38].

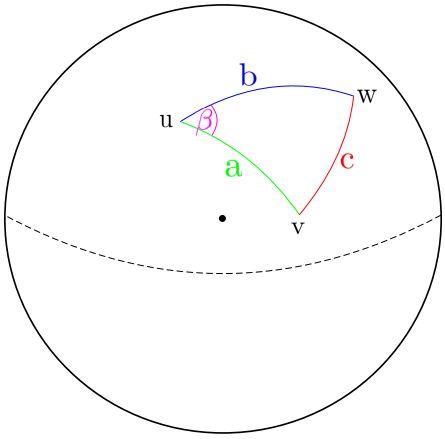

Figure 5.3: Spherical triangle solved by the law of cosines

$$\cos(c) = \cos(a)\cos(b) + \sin(a)\sin(b)\cos(\beta) \ . \tag{5.8}$$

Spherical law of cosines adjusted for the coordinate transformation needed is shown in Figure 5.4. Colours marking the spherical triangle edges and angle, are the same shown in Figure 5.3. Theta (marked green), and Phi (marked magenta), are the antenna radiation pattern reference coordinates, and the Corr value (marked red) is the corrected value of the elevation angle in degrees that needs to be used in the calculation of the atmospheric attenuation, or in determining whether the antenna radiation pattern coordinates are pointing the ground. Black dot in the center is marking the antenna position.

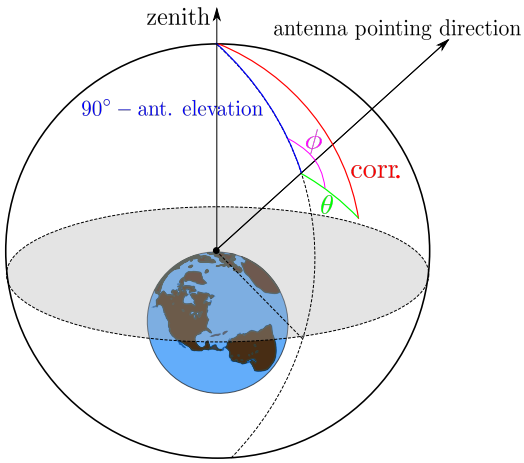

Figure 5.4: Spherical triangle adjusted for the needed coordinate reference transformation

Following equation explaining Figure 5.3 is given as:

$$\cos(corr) = \cos(\theta)\cos(90 - elevation) + \sin(\theta)\sin(90 - elevation)\cos(\phi) \ . \quad (5.9)$$

The calculated brightness temperatures coming from directions surrounding the antenna, with the same sampling as the antenna radiation pattern, is given in Theta-Phi grid and shown in Figure 5.5 for the antenna elevation of 30° measured from horizon. Hence, the surrounding brightness temperature matrix is given in the same coordinate system reference as the radiation pattern (the antenna reference system), with $\theta = 0$ describing the direction of antenna pointing.

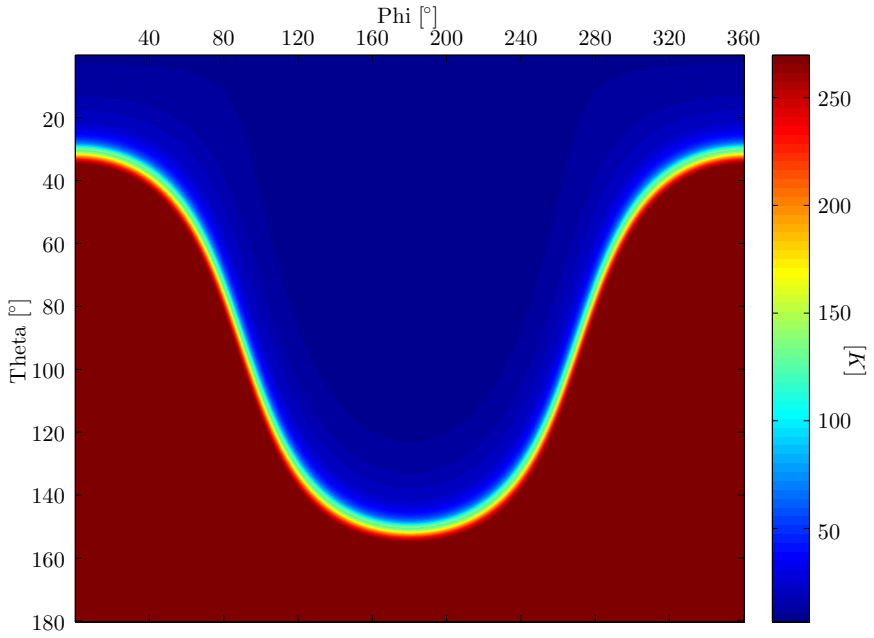

Figure 5.5: Surrounding brightness temperatures [K] for 30° antenna elevation

Having obtained the full antenna radiation pattern and the brightness temperatures for all directions of the full solid angle surrounding the antenna, it is possible to estimate the antenna noise temperature given with the Equation (3.6), where surrounding brightness temperatures and antenna radiation pattern are given in matrix form and are labelled $M_{brightness}$ and $M_{pattern}$ respectively. To adequately address the area of the integration on the sphere, the area matrix M_{area} dependent on the sampling density was calculated and presented in Figure 5.6. Hence, colorbar explaining Figure 5.6 does not contain exact numeric values, because they are sampling dependant, but it points to maximal and minimal area values representation.

Finally the antenna noise temperature estimation following the Equation (3.6), can be given as:

$$T_{ant} = \frac{\sum_{i=1}^{n}\sum_{j=1}^{m} M_{brightness} \odot M_{pattern} \odot M_{area}}{\sum_{i=1}^{n}\sum_{j=1}^{m} M_{pattern} \odot M_{area}} \,, \tag{5.10}$$

where n and m represent number of matrix columns and rows respectively, and

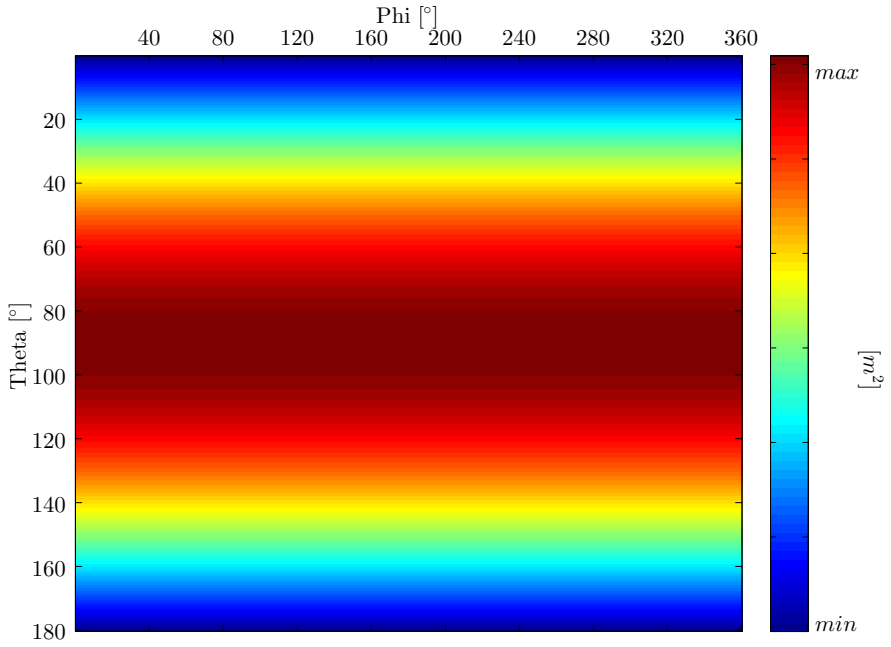

Figure 5.6: Integration area matrix

$\odot$ sign stands for the element-wise matrix multiplication.

Antenna noise temperature MATLAB code is provided in the Appendix B, at the end of the document.

5.2 Direct calculation method

The main advantage of the direct method is that G/T factor can be accurately measured using a simple measurement procedure, which allows more frequent and less time consuming measurements than using the indirect approach. That advantage is very important if the ground station is in constant operation, or if the minimal time span is available to perform the measurements, like it is the case with ground stations that communicate with satellites in LEO orbit.

5.2.1 Direct method equation

Direct method for G/T calculation requires measurements of two different, but very well known and defined, signal sources. Hence, measurements are obtained reading the received noise power first pointing the Moon, P_{Moon}[W], and then pointing the cold sky, P_{sky}[W] [39]:

$$P_{sky} = k_B T_{ant} + k_B T_{rec} = k_B T_{sys} \ , \tag{5.11}$$

$$P_{Moon} = \underbrace{k_B T_{ant}{}' + k_B T_{rec}}_{\sim k_B T_{sys}} + \frac{1}{2} \int_0^{2\pi} \int_0^{\frac{\theta_{Moon}}{2}} B(\theta,\phi) A_{eff}(\theta,\phi) \sin(\theta)\, d\theta\, d\phi \ , \tag{5.12}$$

where k_B is Boltzmann constant, T_{ant}, T_{rec} and T_{sys} are antenna, receiver and system noise temperature respectively, $T_{ant}{}'$ is antenna noise temperature contribution from the radiation pattern angles not looking at the Moon, B [W m^{-2} sr^{-1} Hz^{-1}] is Moon's brightness distribution and A_{eff}[m^2] is antenna's effective aperture. Factor of 1/2 is a correction for polarisation mismatch, since the Moon is randomly polarised. θ_{Moon} is the Moon's angular diameter in degrees, over which the integration is performed.

Next, to derive the direct method equation, it is necessary to express the Y-factor with measured noise powers. Y-factor is given by the Equation (5.1), and is expanded below:

$$Y = \frac{P_1}{P_2} = \frac{P_{Moon}}{P_{sky}} = \frac{k_B(\sim T_{sys}) + \frac{1}{2} \int_0^{2\pi} \int_0^{\frac{\theta_{Moon}}{2}} B(\theta,\phi) A_{eff}(\theta,\phi) \sin(\theta)\, d\theta\, d\phi}{k_B T_{sys}} \ . \tag{5.13}$$

In order to extract G/T ratio from the Equation (5.13) following helping equations are needed:

$$A_{eff}(\theta,\phi) = \frac{(\lambda)^2}{4\pi} G(\theta,\phi) \ , \text{ and}$$

$$g(\theta,\phi) = \frac{A_{eff}(\theta,\phi)}{A_{eff}(\theta,\phi)|_{max}} = \frac{G(\theta,\phi)}{G(\theta,\phi)|_{max}} = \frac{G(\theta,\phi)}{G_{max}} \ . \tag{5.14}$$

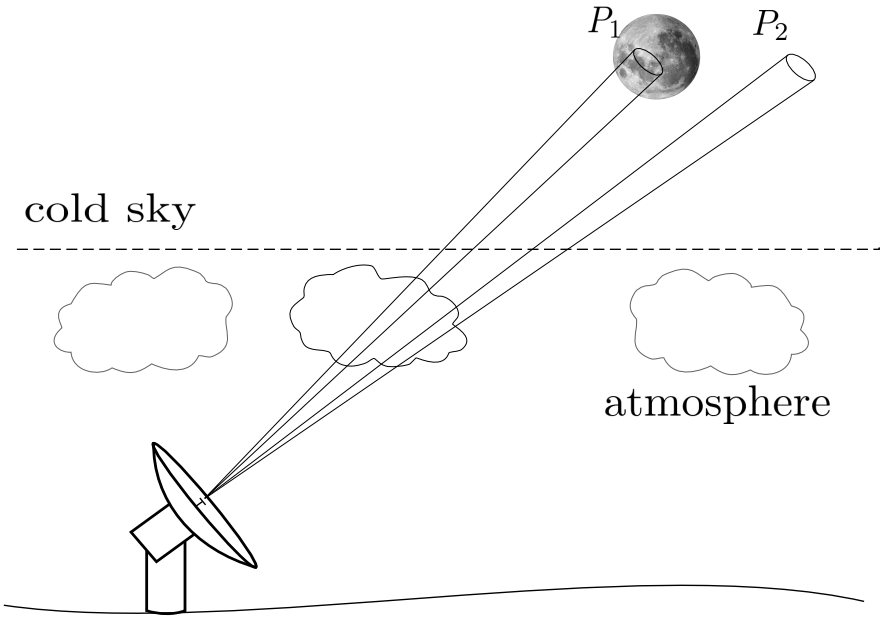

Figure 5.7: Measurement includes receiver noise power readings from two sources

The above helping equations express the relation between antenna effective aperture A_{eff} and the antenna gain G. Also they provide the normalized radiation pattern expression. The radiation pattern is normalized in a way that the maximum pattern value yields unity.

The Y-factor now becomes:

$$Y = 1 + \frac{\lambda^2 \cdot G_{max} \cdot \int_0^{2\pi} \int_0^{\frac{\theta_{Moon}}{2}} B(\theta,\phi) g(\theta,\phi) \sin(\theta)\, d\theta\, d\phi}{8\pi \cdot k_B \cdot T_{sys}} \,. \tag{5.15}$$

Hence, it is now possible to express the G/T equation as:

$$\frac{G}{T} = \frac{8\pi \cdot k_B \cdot (Y-1)}{\lambda^2 \int_0^{2\pi} \int_0^{\frac{\theta_{Moon}}{2}} B(\theta,\phi) g(\theta,\phi) \sin(\theta)\, d\theta\, d\phi} \,. \tag{5.16}$$

The value of the integral expression in the Equation (5.16) represents the Moon's flux density per beam section, while the more desired option would be to express G/T ratio with total Moon's flux density expressed in Equation (4.11). Therefore, the relation between Moon's flux density per beam section, S_b, and total flux

density, S, is given by:

$$S_b = \frac{1}{2} \int_0^{2\pi} \int_0^{\frac{\theta_{Moon}}{2}} B(\theta, \phi) g(\theta, \phi) \sin(\theta)\, d\theta\, d\phi \ ,$$

$$S = \frac{1}{2} \int_0^{2\pi} \int_0^{\frac{\theta_{Moon}}{2}} B(\theta, \phi) \sin(\theta)\, d\theta\, d\phi \ , \text{ and}$$

$$S = S_b \cdot K_2 \ . \tag{5.17}$$

The direct method G/T ratio equation can now be given in both extended and shortened version, where K_2 stands for the extended source size correction factor:

$$\frac{G}{T} = \frac{8\pi \cdot k_B \cdot (Y-1)}{\lambda^2 \int_0^{2\pi} \int_0^{\frac{\theta_{Moon}}{2}} B(\theta, \phi) \sin(\theta)\, d\theta\, d\phi} \cdot \frac{\int_0^{2\pi} \int_0^{\frac{\theta_{Moon}}{2}} B(\theta, \phi) \sin(\theta)\, d\theta\, d\phi}{\int_0^{2\pi} \int_0^{\frac{\theta_{Moon}}{2}} B(\theta, \phi) g(\theta, \phi) \sin(\theta)\, d\theta\, d\phi} \ ,$$

$$\frac{G}{T} = \frac{8\pi \cdot k_B \cdot (Y-1)}{\lambda^2 \cdot S} \cdot K_2 \ . \tag{5.18}$$

Finally, to address also the effect of the atmospheric attenuation, the above direct method equation has to be additionally corrected. The correction is calculated using the atmospheric attenuation equations given in [2.3.2] in linear form, and will further be labelled as K_1. Therefore, the final direct method G/T equation using the Moon as an RF source, expressed in [K^{-1}], can be written as:

$$\frac{G}{T} = \frac{8\pi \cdot k_B \cdot (Y-1)}{\lambda^2 \cdot S} \cdot K_1 \cdot K_2 \ . \tag{5.19}$$

The source polarization correction factor K_3 is neglected for measurements with Moon as RF source. However, it must be taken into account if the radio source for the measurements is geostationary satellite or partially polarized radio star.

5.2.1.1 Elevation angle adjustment

Direct measurement of ground station G/T using extra-terrestrial RF sources typically occurs at an elevation angle that differs from the minimum elevation angle considered in the G/T specification. The following sections will present a method of adjusting the measured $G/T(\theta_i)$ values to allow proper comparison with the specified G/T quality factor.

G/T values can be adjusted by noting that the variation of G/T with elevation angle is equal to the variation of the cold sky noise power (assuming constant antenna gain). The G/T ratio at two elevation angles is labelled $G/T(\theta_i)$ for the measurement obtained value at incidence elevation angle, and $G/T(\theta_0)$ for the corrected value to the minimum elevation angle.

$$\frac{\frac{G}{T}(\theta_i)}{\frac{G}{T}(\theta_0)} = \frac{\frac{G}{T_{sys}(\theta_i)}}{\frac{G}{T_{sys}(\theta_0)}} \ , \tag{5.20}$$

where G is the antenna gain given in linear scale, and T_{sys} is the system noise temperature in [K]. Since G is the same for all antenna elevation angles, and considering noise power Equation (2.1), previous ratio becomes:

$$\frac{\frac{G}{T}(\theta_i)}{\frac{G}{T}(\theta_0)} = \frac{T_{sys}(\theta_0)}{T_{sys}(\theta_i)} = \frac{P_n(\theta_0)}{P_n(\theta_i)} \ . \tag{5.21}$$

Therefore, the quality factor at minimum elevation angle $\frac{G}{T}(\theta_0)$, can now be written both in linear and logarithmic scale as follows:

$$\frac{G}{T}(\theta_0) = \frac{G}{T}(\theta_i) \cdot \frac{P_n(\theta_i)}{P_n(\theta_0)} \ ,$$

$$\left[\frac{G}{T}(\theta_0)\right]_{dB} = \left[\frac{G}{T}(\theta_i)\right]_{dB} + [P_n(\theta_i)]_{dB} - [P_n(\theta_0)]_{dB} \ , \tag{5.22}$$

where $P_n(\theta_i)$ and $P_n(\theta_0)$ are noise powers expressed in [W] measured pointing incidence angle and minimum elevation angle respectively.

The ratio of $P_n(\theta_i)$ and $P_n(\theta_0)$ can be labelled as ΔCEL and can be expressed both in linear and logarithmic scale, yielding a shortened expression for G/T

quality factor in decibels:

$$\Delta CEL = \frac{P_n(\theta_i)}{P_n(\theta_0)}$$

$$[\Delta CEL]_{dB} = [P_n(\theta_i)]_{dB} - [P_n(\theta_0)]_{dB} \tag{5.23}$$

$$\left[\frac{G}{T}(\theta_0)\right]_{dB} = \left[\frac{G}{T}(\theta_i)\right]_{dB} + [\Delta CEL]_{dB} \ .$$

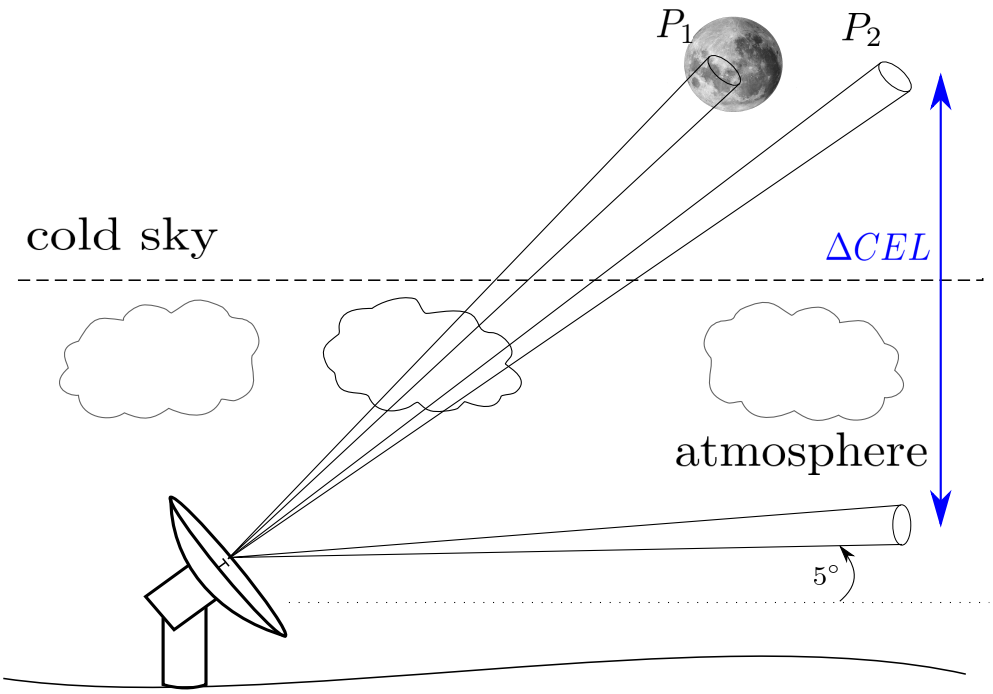

Figure 5.8: Measurement for elevation angle adjustment

5.2.1.2 Extended source correction factor (definition and analysis)

Extended radio source is considered the source whose angular size exceeds one fifth of the antenna HPBW. When the radio source exceeds one fifth of the antenna's HPBW, the antenna radiation pattern is averaged within the solid spatial angle subtended to the source, resulting with the measured antenna noise power smaller than what would be expected for the antenna's effective collecting area and the aperture illumination [40].

Therefore it is required to correct the measurement by the extended source size correction factor K_2 to account for the convolution of the extended radio source angular size, angular source brightness distribution and the shape of the antenna's far-field radiation pattern. Extended source size K_2 is given by the equation:

$$K_2 = \frac{\int_0^{2\pi} \int_0^{\frac{\theta_{Moon}}{2}} B(\theta,\phi)\sin(\theta)\,d\theta\,d\phi}{\int_0^{2\pi} \int_0^{\frac{\theta_{Moon}}{2}} B(\theta,\phi)g(\theta,\phi)\sin(\theta)\,d\theta\,d\phi}\ . \tag{5.24}$$

If the source angular size is smaller than one fifth of antenna's HPBW, the radiation pattern across the source is almost everywhere equal to unity, consequently setting the extended source size correction factor to unity value, $K_2 \doteq 1$.

The calculation of Equation (5.24) can be performed considering a uniform brightness distribution for the Moon [19], following the section (4.4), for a range of values of the source disc diameter and using the validated antenna beam shape (Figure 5.9). The extended source size correction factor for the sources represented with the equivalent uniform brightness disc, labelled as $K_{2uniform}$, is given by [21]:

$$K_{2uniform} = \frac{\int_0^{2\pi} \int_0^{\frac{\theta_{Moon}}{2}} \sin(\theta)\,d\theta\,d\phi}{\int_0^{2\pi} \int_0^{\frac{\theta_{Moon}}{2}} g(\theta,\phi)\sin(\theta)\,d\theta\,d\phi}\ . \tag{5.25}$$

The above equation implies that antenna's radiation pattern must be obtained for the correction factor calculation.

However, if the source angular size does not exceed for much the main beam full width, or if the angular source size and antenna's θ_{HPBW} ratio is less than 3, it is possible to obtain a good approximation of the normalized antenna radiation pattern using the normalized Gaussian far-field radiation pattern adjustment, g_{Gauss}, depending on the antenna's real θ_{HPBW}, and hence determine the K_2 approximated value. The normalized Gaussian approximation of radiation pat-

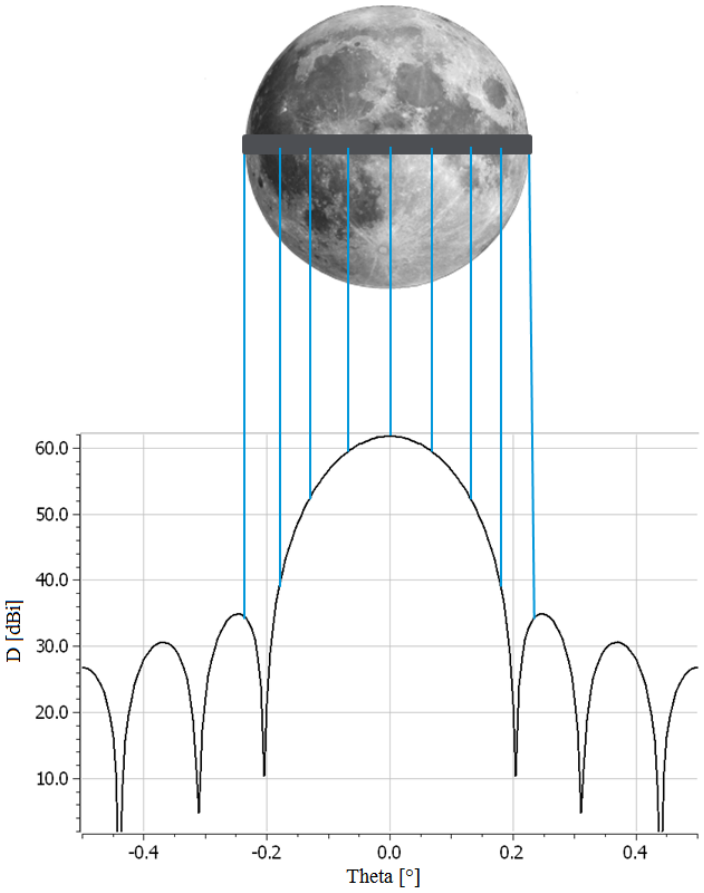

Figure 5.9: Moon as a uniform brightness disk

tern is given by [41], where θ_{HPBW} is the value of antenna's HPBW expressed in degrees:

$$g_{Gauss}(\theta, \phi) = e^{-\ln(2)\cdot\left(\frac{2\cdot\theta}{\theta_{HPBW}}\right)^2} . \tag{5.26}$$

Having expressed the approximation of the radiation pattern, and assuming $sin(\theta) \approx \theta$ for small angles, it is possible to perform the integrations and estimate the K_2 correction factor value (Appendix A):

$$K_{2uniform_{Gauss}} = \frac{\ln(2)\cdot\left(\frac{\theta_{Moon}}{\theta_{HPBW}}\right)^2}{1 - e^{-\ln(2)\cdot\left(\frac{\theta_{Moon}}{\theta_{HPBW}}\right)^2}} , \tag{5.27}$$

where θ_{Moon} represents the value of the Moon's angular diameter.

The approximated K_2 correction factor Equation (5.27) depends on the Moon's angular diameter θ_{Moon} and the antenna's HPBW θ_{HPBW}. While the

Moon's angular diameter can be easily obtained on [29], the antenna's θ_{HPBW} has to be properly measured or estimated.

The estimation of $\theta_{HPBW}[^\circ]$ is based on the following equation [42]:

$$\theta_{HPBW} = k \cdot \frac{\lambda}{d} \ , \tag{5.28}$$

where λ is wavelength, d is the antenna reflector diameter and k is beamwidth factor that depends on the antenna illumination and edge-taper, usually given by the antenna vendor. Beamwidth factor definition k vary in different literatures, like $k = 70$ in [43], and $k = 65$ in [44].

However, beamwidth factor has to be dependent on the edge-taper and can not be approximated with a constant value. For that purpose, using the GRASP(TICRA) software, numerous radiation patterns for different antenna reflector diameters and edge-tapers in range (5dB - 25dB) were calculated, and the corresponding θ_{HPBW} values were extracted. From that point, the best polynomial function fit to the θ_{HPBW} values was interpolated, and the minimal beamwidth factor k was normed to the value of $k = 58.96$. That value corresponds to the uniform illumination pattern. The obtained best fit for calculating the beamwidth factor is given bellow:

$$k = 58.96(1 + 0.0107 \cdot T_e) \ , \tag{5.29}$$

where T_e represents the absolute value of the edge taper given in decibels.

Extended source size correction factor K_2 is usually also provided by the vendor in form of polynomial best fit for the specific antenna reflector sizes. Polynomial K_2 approximation is usually given in dependence on frequency, f_{GHz}, and Moon's angular diameter, θ_{Moon}, as:

$$\begin{aligned} K_{2uniform_{poly}} =& a_0 \cdot \theta_{Moon} \cdot {f_{\mathrm{GHz}}}^2 + a_1 \cdot {f_{\mathrm{GHz}}}^3 + a_2 \cdot {f_{\mathrm{GHz}}}^2 + \\ & a_3 \cdot f_{\mathrm{GHz}} + a_4 \cdot \theta_{Moon} \cdot f_{\mathrm{GHz}} + \\ & a_5 \cdot {\theta_{Moon}}^2 \cdot f_{\mathrm{GHz}} + a_6 + \\ & a_7 \cdot \theta_{Moon} + a_8 \cdot {\theta_{Moon}}^2 + a_9 \cdot {\theta_{Moon}}^3 \ , \end{aligned} \tag{5.30}$$

where a_i are polynomial coefficients. For example, Table 5.1 provides ViaSat polynomial coefficients for calculation of $K_{2uniform_{poly}}$ for different antenna reflector diameter sizes.

Table 5.1: ViaSat K_2 polynomial coefficients

Coefficients	$d = 5.4m$	$d = 7.3m$	$d = 9.1m$	$d = 10.26m$	$d = 11.28m$
a_0	0.22124	-3.22454	0.4137	0.5541	0.7434
a_1	-0.00975	0.13412	-1.2490	-2.9581	-0.3145
a_2	0.16554	-2.12968	31.6666	75.1404	7.6079
a_3	-0.57331	8.21186	-269.3682	-637.2681	-60.4003
a_4	-4.52011	50.88899	1.0325	-0.6066	-12.6905
a_5	1.64387	4.04585	-5.8184	-7.3650	0.9865
a_6	-0.21724	3.08215	776.2878	1808.7976	153.4486
a_7	23.47034	-201.17202	-80.5964	-65.4370	66.2610
a_8	-15.20528	-30.70381	142.7291	156.7675	12.4544
a_9	4.70339	4.38388	-50.1728	-60.9194	-17.1503

Another K_2 approximation method usually found in literature is expressed using the Bessel functions of first and second order:

$$K_{2uniform_{Bessel}} = \frac{(1.6162\frac{\theta_{Moon}}{\theta_{HPBW}})^2}{4[1 - {J_1}^2(1.6162\frac{\theta_{Moon}}{\theta_{HPBW}}) - {J_0}^2(1.6162\frac{\theta_{Moon}}{\theta_{HPBW}})]} , \tag{5.31}$$

which derives from the approximation of the normalized radiation pattern given with the Bessel function of the first kind and assuming $sin(\theta) = \theta$:

$$g(\theta, \phi) = \left[\frac{2J_1(1.6162\frac{\theta}{\theta_{HPBW}})}{1.6162\frac{\theta}{\theta_{HPBW}}}\right]^2 . \tag{5.32}$$

In order to select the best method for K_2 estimation, using GRASP, I calculated the radiation patterns for the Cassegrain antennas of reflector diameter sizes d = 5.4m, d = 7.3m, d = 9.1m, d = 10.26m and d = 11.28m. Then,

the extended source correction factor K_2 was calculated by (5.25) for all radiation patterns and different Moon subtended solid angles ($\theta_{Moon} = 0.45°$, $\theta_{Moon} = 0.49°$, $\theta_{Moon} = 0.5°$, $\theta_{Moon} = 0.53°$, $\theta_{Moon} = 0.56°$). The obtained results were taken as a reference in comparison of different estimation methods ($K_{2uniform_{poly}}$, $K_{2uniform_{Gauss}}@k = 70$, $K_{2uniform_{Gauss}}@k = 58.96(1 + 0.0107 \cdot T_e)$ and $K_{2uniform_{Bessel}}$).

The reference antenna radiation patterns were calculated for Cassegrain and Front-Fed antennas of given reflector diameter sizes for frequency of $f_{\text{GHz}} = 8.25\text{GHz}$, including blockage effect, with edge tapering of both $T_e = -10dB$ and $T_e = -15dB$, and with $\frac{f}{d}_{(Cas)} = 0.3$ and $\frac{f}{d}_{(FF)} = 1.5$ respectively. The goal of this comparison was to observe the approximation methods fitting to the reference for different tapering and antenna geometry settings.

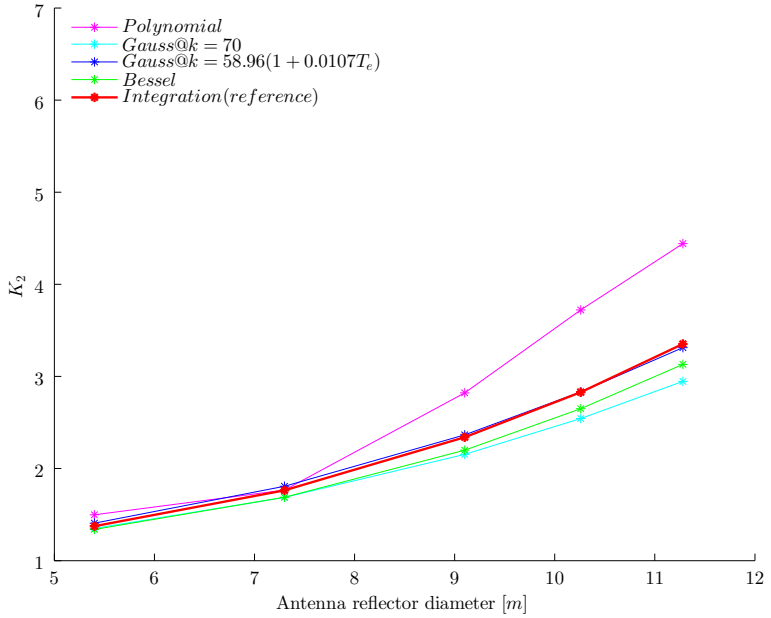

Figure 5.10: K_2 approximation methods comparison for Cassegrain antenna with $T_e = -10dB$, and for $\theta_{Moon} = 0.45°$

From the given figures (Figure 5.10 - Figure 5.17) it can be observed that the polynomial approximation method, given by the vendor, for the reflector diameters larger than $7m$ diverges by the largest factor from the reference level

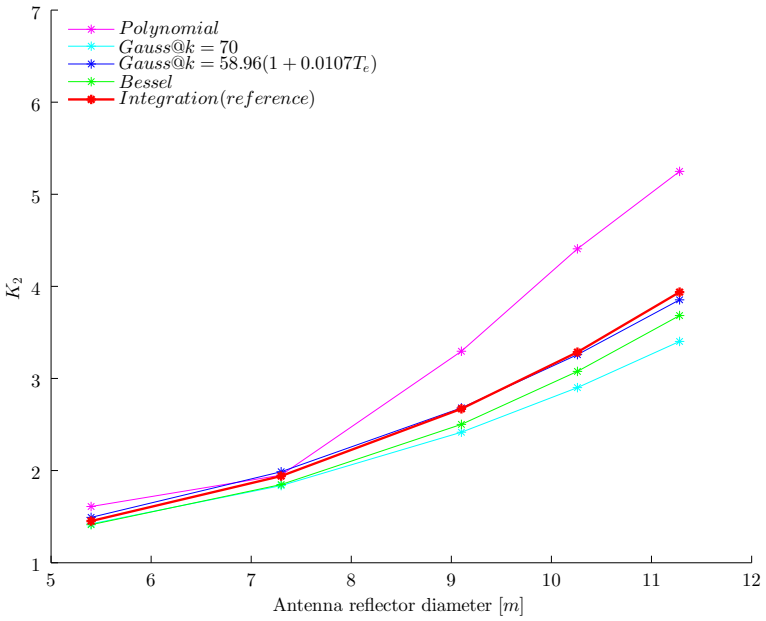

Figure 5.11: K_2 approximation methods comparison for Cassegrain antenna with $T_e = -10dB$, and for $\theta_{Moon} = 0.49°$

(integration of simulated radiation pattern). The divergence of the polynomial approximation method is assumed to be due to double-shaping of reflectors using the reflector synthesis. However, due to complexity and specificities of double-shaping, the validation of polynomial method for the double-shaped antennas was left out in this thesis. To estimate beamwidth factor in order to use Gaussian approximation for double-shaped antennas, the value of uniform illuminated aperture $k = 58.96$ is given as a possible value of the rough estimation.

Another information that can be observed is that the best fitting to the reference values is obtained using the Gaussian approximation when the beamwidth factor is given as $k = 58.96(1 + 0.0107 \cdot T_e)$. Also, it can be seen that the Gaussian approximation when beamwidth factor is given as $k = 70$ yields significantly lower values than the reference, and is probably suitable just for one specific edge tapering.

It can be seen that higher values of edge taper T_e result in lower values of extended source size correction factor K_2 and hence in smaller gradient of K_2 curve.

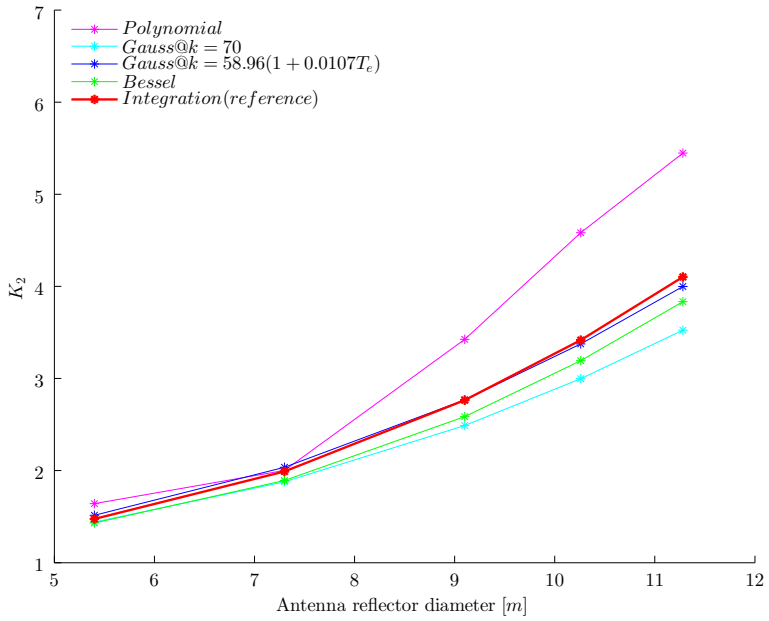

Figure 5.12: K_2 approximation methods comparison for Cassegrain antenna with $T_e = -10dB$, and for $\theta_{Moon} = 0.50°$

Also, the Gaussian approximation using $k = 58.96(1 + 0.0107 \cdot T_e)$ beamwidth factor does not show significant differences when used with Front-Fed antennas instead of Cassegrain antennas.

However, it must be noted that the most recommended method for extended source size correction factor calculation is using the integration of the real measured radiation pattern according to the Equation (5.24).

Measurement and calculation of the antenna radiation pattern and calculation of the extended source size correction factor using the integration of the real measured radiation pattern is necessary in case that the measured G/T quality factor is lower than usual. It is done according to the Equation (5.24).

5.2.1.3 Other correction factors

In addition to extended source size correction factor K_2, the atmospheric attenuation correction factor K_1 has to taken in consideration as well as polarization

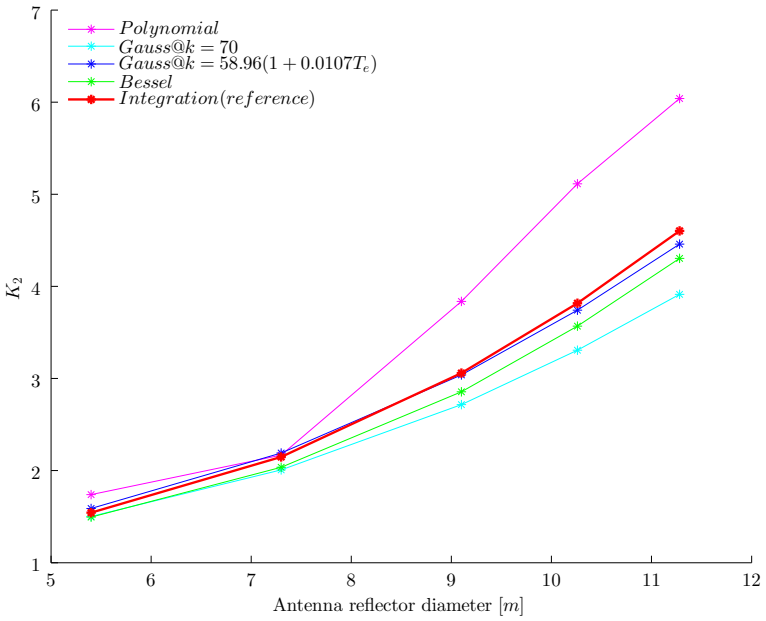

Figure 5.13: K_2 approximation methods comparison for Cassegrain antenna with $T_e = -10dB$, and for $\theta_{Moon} = 0.53°$

correction factor K_3 if needed.

Atmospheric attenuation correction factor calculation procedure is given in section (2.3.2), and has to be given in linear scale.

Polarization correction factor, however, is applied just for the sources with specified polarization, like elliptical, or partial polarization. Typical example of partial elliptically polarized source is Taurus A, with value of $K_3 = 0.998$ [45]. K_3 correction factor is given in range from 0 to 1, with 1 being the default value for randomly polarized sources like Moon.

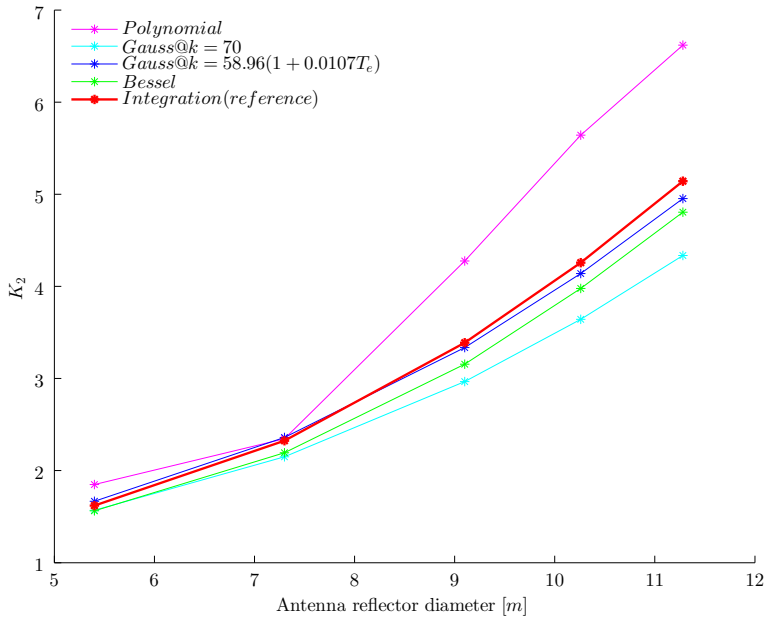

Figure 5.14: K_2 approximation methods comparison for Cassegrain antenna with $T_e = -10dB$, and for $\theta_{Moon} = 0.56°$

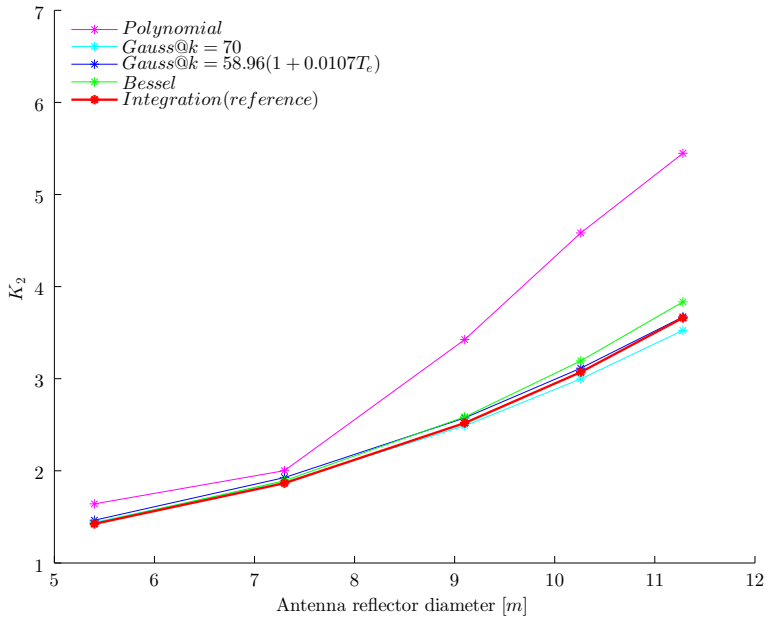

Figure 5.15: K_2 approximation methods comparison for Cassegrain antenna with $T_e = -15dB$, and for $\theta_{Moon} = 0.50°$

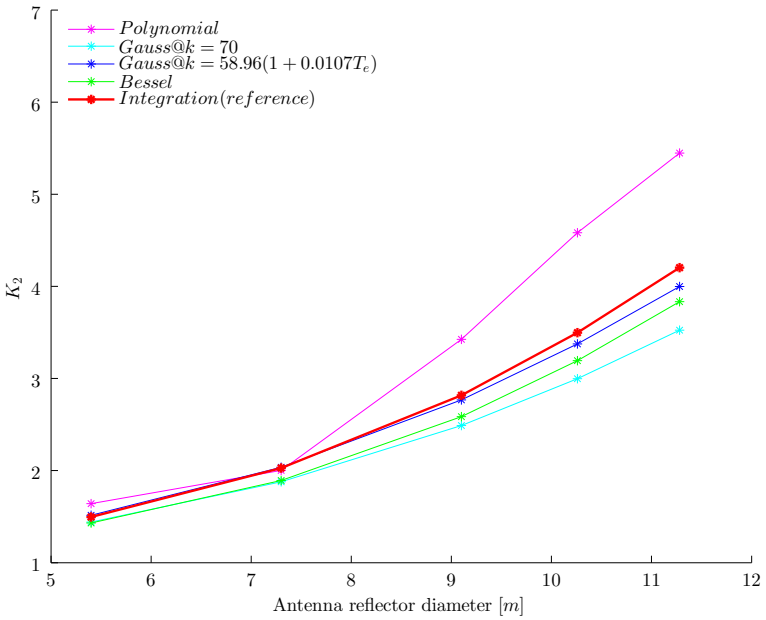

Figure 5.16: K_2 approximation methods comparison for Front-Fed antenna with $T_e = -10dB$, and for $\theta_{Moon} = 0.50°$

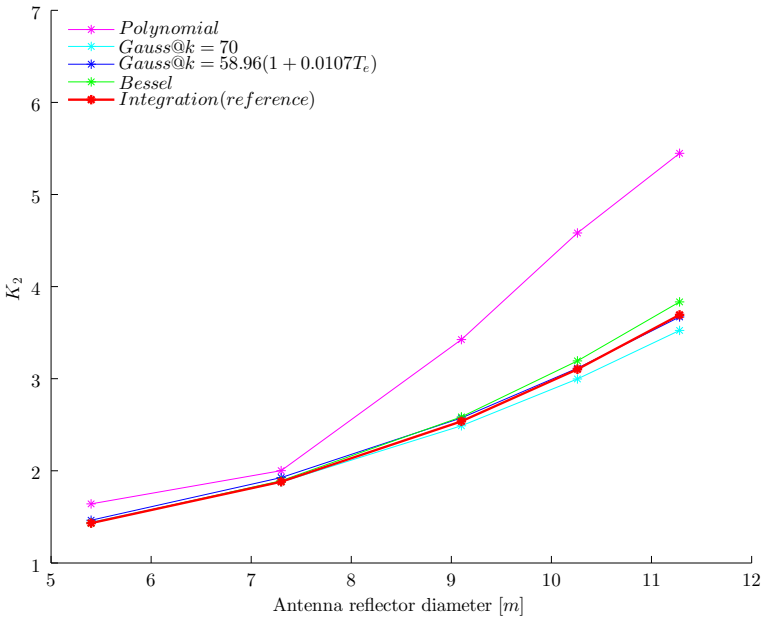

Figure 5.17: K_2 approximation methods comparison for Front-Fed antenna with $T_e = -15dB$, and for $\theta_{Moon} = 0.50°$

6 Measurements

This chapter provides the measurement procedure according to the direct method for G/T measurement using the Moon as radio frequency source. Also, it provides the performed measurements, calculations and deductions using the double-shaped Cassegrain antenna with main reflector diameter size of $d = 11.28$m, used as receiving antenna of remote sensing LEO satellites.

Measurement procedure is result of detailed study and analysis, while the proposed settings for the spectrum analyser have been traded-off and selected in order to provide the best compromise between stability and measurement error.

6.1 Measurement Procedure

Due to the low power level of received signal using the Moon as a radio source, the measurement tool, Spectrum Analyser, has to be mounted as close as possible to the LNA output. As the antenna is moveable, it is advised to perform the measurements at the input of the FO converter in the antenna basement.

6.1.1 Measurement conditions with Moon as a source

The measurements should be done in days between waxing Moon phase and waning Moon phase, to ensure we have full Moon or almost-full Moon while performing the measurements with narrow beam antenna, considering as reference values the data available at the NASA website [29].

Also, the measurements should be performed, if possible, during the night to minimize the influence of solar radiation and thermal radiation of the atmosphere.

It is advised to perform the measurements when the Moon's elevation is higher than 30° and should be verified that no other RF source is in the approximately 10° angular distance in azimuth and 5° angular distance in elevation.

6.1.2 Measurement setup

In order to efficiently obtain stable measurement results, the following spectrum analyser setting has been obtained:

1. Center frequency: Intermediate Frequency (typically 750 MHz)
2. Frequency span: 0 Hz
3. dB/div: 1
4. RBW: 100 kHz
5. VBW: 10 Hz
6. Marker: ON
7. Sweep Time: 100 ms
8. Average: 10

Because we are interested just in the signal power coming from one direction at exact frequency, the span is set to 0 Hz, also in order to achieve greater velocity of measurement. Video bandwidth is set to low value in order to reduce the spikes created by the noisy signal, and Resolution bandwidth is set to 100kHz to enlarge the Fast Fourier Transform bit size and frequency precision in measurement. Low RBW, however, requires higher acquisition time.

Average in this method was set to 10, in order to further stabilize the measurement reading, and to not introduce too large acquisition time.

In case that the Spectrum Analyser allows, it is possible to set the sweep time and dB/div display representation to lower values.

6.1.3 Spectrum Analyser readings

Ground stations that have implemented ACU, with tracking enabled, it is recommended to use tracking in order avoid miss-pointing.

Each single measurement consist of three different values:

- On-source: received power while pointing at the Moon
- Off-source: received power while pointing at the cold sky, at the same elevation as the On-source measurement, but with 5° tilt in azimuth with reference to the Moon.
- 5°elevation: received power while pointing at the cold sky at the elevation of 5° relative to the horizon.

The measurements should be done with a frequency of three to five minutes, that is sufficient time for the acquisition of desired three values. Five minute frequency of measurements will allow the collection of six measurements in 30 minutes.

Finally, the calculation procedure is given as follows:

1. Obtain a set of 6 values of Y-factor (5.1) by the On-source [W] and Off-source [W] measurement ratio.

2. Obtain a set of 6 values of ΔCEL by the Off-source [W] and 5°elevation [W] measurement ratio.

3. Obtain final Y-factor value as the average of set of 6 Y-factor measurements.

4. Obtain final ΔCEL value as the average of set of 6 ΔCEL measurements.

5. The estimated value of Y-factor is used to obtain G/T value at the Moon's elevation angle (5.19).

6. The estimated values of Y-factor and ΔCEL are used to obtain the G/T value at the 5° elevation angle relative to horizon (5.23).

6.2 Antenna characteristics

The measurements were performed on operational receiving antenna of low-earth-orbit satellites for remote sensing, situated in Matera, Italy (Figure 6.1). The antenna is Cassegrain type with main reflector diameter $d = 11.28$m. Also, the antenna is double-shaped with two reflector synthesis for the given operational frequency, in order to achieve very high efficiency ($\eta \approx 90\%$) and almost uniform illumination.

Figure 6.1: X-band ground station with $d = 11.28$ m

The antenna under measurement has full rotational coverage without key-holes. Pointing accuracy is better than 0.1°, and tracking accuracy in autotrack mode is better than 0.05°. Visibility mask is lower than 4° for any azimuth angle. Antenna's intermediate frequency is 750 MHz and its polarization is circular

RHCP/LHCP. Antenna basic properties are given in Table 6.1.

Table 6.1: Antenna under measurement information

Type	Cassegrain
Frequency	$f = 8.1775$ GHz
Reflector diameter	$d = 11.28$ m
Approx. Gain	$G \approx 57.5$ dBi
Approx. T_{rec}	$T_{rec} \approx 56$ K
Approx. Antenna ohmic loss	$L_{dB} \approx 0.5$ dB

Controlling of the antenna was performed remotely from the control room using the specific software made by antenna vendor to efficiently operate with antenna movement and source tracking. Remote controlling software is presented on the Figure 6.2.

Figure 6.2: Software for antenna remote control

The measurements were performed using the direct G/T method, with Moon as a source, following the procedure described in the section 6.1.

6.3 Performed measurements and G/T calculation with Moon as a source

Measurement readings were obtained with the spectrum analyser *Advantest R3131A* connected to the input of the FO converter. The weather information was gathered from the local weather station located next to the ground station and is presented in Table 6.2.

Table 6.2: Local weather information - Moon

Weather	Cloudy
Local Temperature	14.9°C
Local Humidity	91%
Local Pressure	960.9 hPa
Date	13.10.2016

Table 6.3 contains six sets of measurements according to the measurement procedure. It must be noted that the time of the measurement is expressed in Coordinated Universal Time (UTC). The spectrum analyser setup, and the first set of measurement readings *set 1* are presented in Figure 6.3.

Table 6.3: Measurement results with Moon as a source

	Time (UTC) [hh:mm]	Elevation [°]	On-source [dBm]	Off-source [dBm]	5°elevation [dBm]
set 1	19 : 23	40.30	−79.26	−82.87	−81.48
set 2	19 : 28	40.66	−79.38	−82.9	−81.50
set 3	19 : 31	40.75	−79.28	−82.87	−81.48
set 4	19 : 33	40.91	−79.38	−82.9	−81.50
set 5	19 : 36	40.98	−79.34	−82.87	−81.59
set 6	19 : 38	41.04	−79.30	−82.85	−81.60

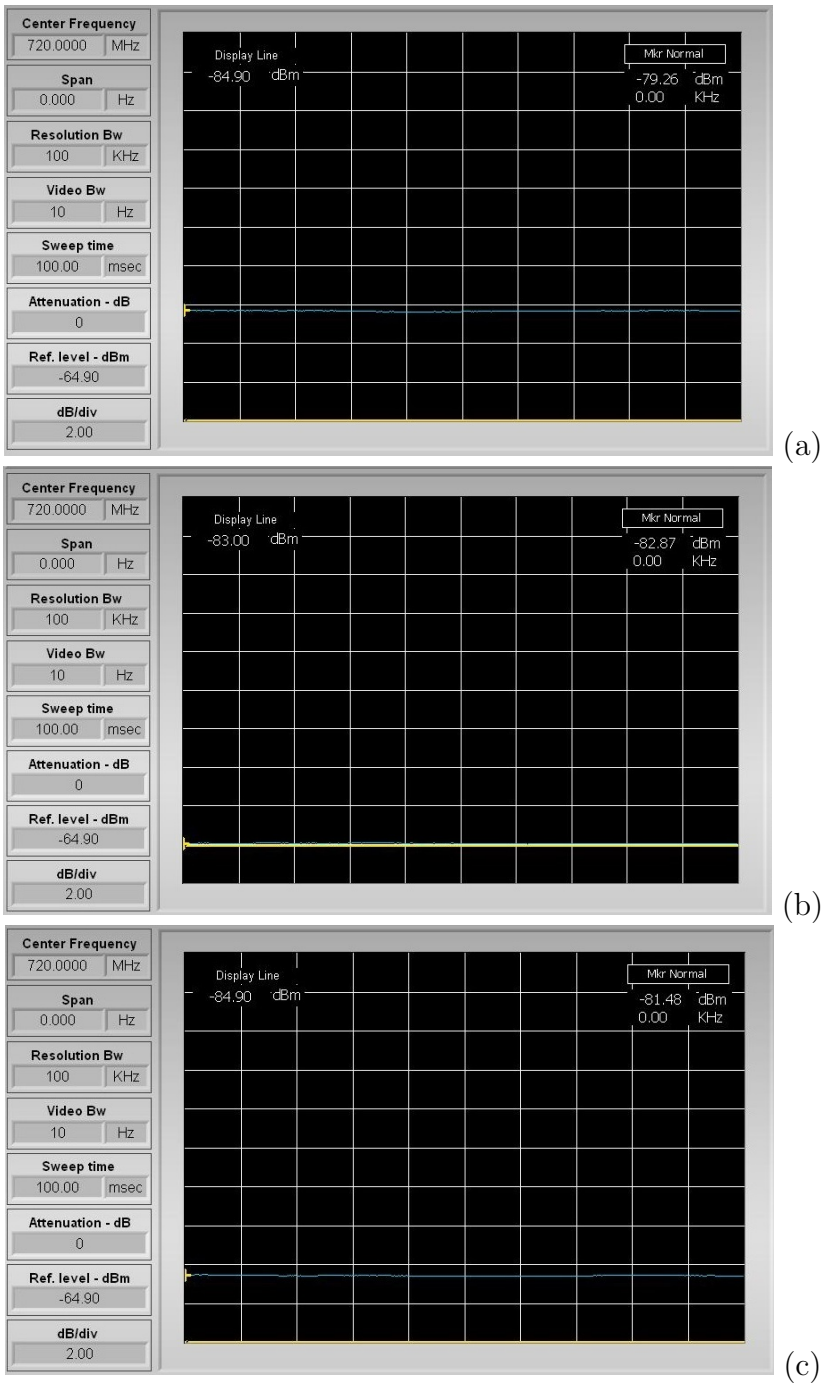

Figure 6.3: Spectrum analyser readings: (a) *On-source* reading, (b) *Off-source* reading and (c) 5°*elevation* received power reading.

6.3.1 G/T calculation

Using the measurement data provided in Table 6.3, the final Y-factor and ΔCEL values were obtained by averaging of Y-factor and ΔCEL for each set of measurements.

Lunar diameter and phase cycle, for the date and time of measurements, were obtained from [29], and are presented in Figure 6.4, where lunar angular diameter (highlighted) is expressed in arcseconds, and the lunar phase angle (S-O-T) is expressed in degrees.

```
*******************************************************************************************************************************
 Date__(UT)__HR:MN     R.A._(ICRF/J2000.0)_DEC  APmag  S-brt Ang-diam           delta      deldot    S-O-T /r    S-T-O
*******************************************************************************************************************************
$$SOE
 2016-Oct-13 19:20  m  23 16 46.66 -06 02 14.9 -11.99   4.14 1975.582 0.00242513612307  -0.1800073 147.0394 /T  32.8848
 2016-Oct-13 19:21  m  23 16 48.23 -06 02 04.2 -11.99   4.14 1975.641 0.00242506419578  -0.1786447 147.0459 /T  32.8783
 2016-Oct-13 19:22  m  23 16 49.80 -06 01 53.4 -11.99   4.14 1975.699 0.00242499281547  -0.1772799 147.0524 /T  32.8719
 2016-Oct-13 19:23  m  23 16 51.37 -06 01 42.6 -11.99   4.14 1975.757 0.00242492198298  -0.1759130 147.0588 /T  32.8654
 2016-Oct-13 19:24  m  23 16 52.93 -06 01 31.9 -11.99   4.14 1975.814 0.00242485169916  -0.1745441 147.0653 /T  32.8590
 2016-Oct-13 19:25  m  23 16 54.50 -06 01 21.1 -11.99   4.14 1975.871 0.00242478196481  -0.1731731 147.0718 /T  32.8525
 2016-Oct-13 19:26  m  23 16 56.07 -06 01 10.3 -11.99   4.14 1975.927 0.00242471278077  -0.1718002 147.0782 /T  32.8461
 2016-Oct-13 19:27  m  23 16 57.63 -06 00 59.5 -11.99   4.14 1975.983 0.00242464414782  -0.1704252 147.0847 /T  32.8397
 2016-Oct-13 19:28  m  23 16 59.19 -06 00 48.7 -11.99   4.14 1976.038 0.00242457606678  -0.1690482 147.0911 /T  32.8332
 2016-Oct-13 19:29  m  23 17 00.76 -06 00 37.9 -11.99   4.14 1976.093 0.00242450853841  -0.1676693 147.0976 /T  32.8268
 2016-Oct-13 19:30  m  23 17 02.32 -06 00 27.1 -11.99   4.14 1976.148 0.00242444156350  -0.1662885 147.1040 /T  32.8204
 2016-Oct-13 19:31  m  23 17 03.88 -06 00 16.3 -11.99   4.14 1976.202 0.00242437514281  -0.1649058 147.1104 /T  32.8139
 2016-Oct-13 19:32  m  23 17 05.44 -06 00 05.5 -11.99   4.14 1976.256 0.00242430927710  -0.1635213 147.1169 /T  32.8075
 2016-Oct-13 19:33  m  23 17 07.00 -05 59 54.7 -11.99   4.14 1976.309 0.00242424396710  -0.1621349 147.1233 /T  32.8011
 2016-Oct-13 19:34  m  23 17 08.56 -05 59 43.9 -11.99   4.14 1976.362 0.00242417921355  -0.1607466 147.1297 /T  32.7947
 2016-Oct-13 19:35  m  23 17 10.11 -05 59 33.0 -11.99   4.14 1976.414 0.00242411501717  -0.1593566 147.1362 /T  32.7883
 2016-Oct-13 19:36  m  23 17 11.67 -05 59 22.2 -11.99   4.14 1976.466 0.00242405137869  -0.1579648 147.1426 /T  32.7819
 2016-Oct-13 19:37  m  23 17 13.22 -05 59 11.4 -11.99   4.14 1976.518 0.00242398829879  -0.1565713 147.1490 /T  32.7755
 2016-Oct-13 19:38  m  23 17 14.78 -05 59 00.5 -11.99   4.14 1976.569 0.00242392577819  -0.1551761 147.1554 /T  32.7691
 2016-Oct-13 19:39  m  23 17 16.33 -05 58 49.6 -11.99   4.14 1976.619 0.00242386381755  -0.1537791 147.1618 /T  32.7627
 2016-Oct-13 19:40  m  23 17 17.88 -05 58 38.8 -11.99   4.14 1976.669 0.00242380241755  -0.1523805 147.1683 /T  32.7563
$$EOE
*******************************************************************************************************************************
```

Figure 6.4: Moon's ephemeris - HORIZON

In order to calculate the G/T quality factor, it is necessary to estimate the Moon's flux density S_{Moon}. The values of $\overline{T_0}$, $\frac{\overline{T_1}}{\overline{T_0}}$, ψ and $\overline{T_{Moon}}$ were calculated following the equations in the section 4.4, and are presented in Table 6.4, together with measured final Y-factor and ΔCEL given in linear scale. Also, lunar angular ephemeris are converted to degrees and their averaged value is added to Table 6.4.

Lunar flux density can now be estimated using the calculated values from Table 6.4 according to the Equation (4.13):

$$S_{Moon} = \frac{2k_B\pi^3}{4 \cdot 180^2 {c_0}^2} \cdot f^2 \cdot \overline{T_{Moon}} \cdot {\theta_{Moon}}^2 = 3.17 \cdot 10^{-22} \ \left[\mathrm{W\,m^{-2}\,Hz^{-1}}\right] \ . \quad (6.1)$$

Table 6.4: Calculated values for lunar flux density estimation

Parameter	Value
Y-factor	2.266
ΔCEL	0.733
$\overline{T_0}$	210.687 K
$\frac{\overline{T_1}}{\overline{T_0}}$	0.05515
$\overline{T_{Moon}}$	214.0622 K
ψ (lunar phase leg)	40.243°
$\overline{\phi}$ (lunar phase angle)	147.114°
Lunar phase angle cycle	increasing
$\overline{\theta_{Moon}}$ (lunar angular diameter)	0.549°

Atmospheric attenuation correction factor K_1, given in both linear and logarithmic scale, is calculated using the section 2.3.2, considering both gaseous and cloud attenuation, for the averaged antenna elevation of 40.77° measured from horizon:

$$\begin{aligned} [K_1]_{dB} &= A_T = 0.14 \text{ [dB]} \\ K_1 &= 10^{\frac{A_T}{10}} = 1.033 \ . \end{aligned} \tag{6.2}$$

Extended source size correction factor K_2, is calculated using the proposed calculation method with Equation (5.29) and Equation (5.27), instead of using the integration method given in Equation (5.25), because no received signal degradation level was noticed while receiving satellite data with the antenna under test. Therefore, it is assumed that the antenna obtained its optimal geometry and that the approximation method can be used to calculate the extended source size correction factor. Correction factor was calculated assuming the uniform illumination and the edge tapering of $T_e = 0$ dB, because the antenna under

measurement is double-shaped.

$$\begin{aligned} \theta_{HPBW} &= 58.96(1 + 0.0107 \cdot Te) \cdot \frac{\lambda}{d} = 0.1916^\circ \\ K_2 &= \frac{\ln(2) \cdot (\frac{\theta_{Moon}}{\theta_{HPBW}})^2}{1 - e^{-\ln(2) \cdot (\frac{\theta_{Moon}}{\theta_{HPBW}})^2}} = 5.71 \ . \end{aligned} \tag{6.3}$$

Having obtained the flux density value, Y-factor, and correction factors values it is possible to estimate the G/T quality factor given with the Equation (5.19), for the averaged antenna elevation of 40.77° measured from horizon, both in linear and logarithmic scale:

$$\begin{aligned} \frac{G}{T}@(40.77^\circ) &= \frac{8\pi \cdot k_B \cdot (Y-1)}{\lambda^2 \cdot S} \cdot K_1 \cdot K_2 = 6080 \\ \left[\frac{G}{T}\right]_{dB}@(40.77^\circ) &= 10 \cdot \log_{10}\left(\frac{G}{T}\right) = 37.84 \ [\mathrm{dB\,K^{-1}}] \ . \end{aligned} \tag{6.4}$$

Finally, the G/T quality factor value using the direct method and Moon as a source, given at the minimum elevation of 5° measured from horizon is calculated:

$$\left[\frac{G}{T}\right]_{dB} = \left[\frac{G}{T}(40.77^\circ)\right]_{dB} + [\Delta CEL]_{dB} = 36.49 \ [\mathrm{dB\,K^{-1}}] \ . \tag{6.5}$$

6.3.1.1 Comparison with vendor-provided K_2 correction factor value

Vendor provided extended source size correction factor is given in polynomial form expressed with Equation (5.30), with the polynomial coefficients presented in Table 5.1 for the antenna of reflector diameter $d = 11.28$m.

Polynomial expression for K_2 correction factor depends only on frequency and Moon's angular diameter. For the given parameters at the time of measurement polynomial estimation of correction factor yields:

$$K_{2_{polynomial}} = 6.3385 \ . \tag{6.6}$$

Obtained $K_{2_{polynomial}}$ value provided by the vendor results in significantly higher value of K_2 which consequently corresponds to the higher value of G/T quality factor for 0.454dB.

6.4 Performed measurements and G/T calculation with Cassiopeia A as a source

Measurements using Cassiopeia A as a source were performed following the same measurement procedure given in Section 6.1 with the same spectrum analyser *Advantest R3131A* connected to the input of the FO converter.

Using Cassiopeia A as a source, the K_2 correction factor becomes very small with almost negligible uncertainty, but the higher uncertainty caused by low Y-factor value is introduced. However, Cassiopeia A has very-well defined flux density and decay factor described in [26, 46].

The intention of this subsection is to provide an insight whether the definition of Moon's flux density and correction factors lead to the G/T quality factor values comparable to the G/T values obtained using Cassiopeia as a source within few tenths of decibel.

Following Table 6.5 and Table 6.6 are presenting measurement readings and weather conditions at the time of measurements:

Table 6.5: Measurement results with Cassiopeia A as a source

	Time (UTC) [hh:mm]	Elevation [°]	On-source [dBm]	Off-source [dBm]	5°elevation [dBm]
set 1	17 : 28	57.3	−83.25	−83.63	−82.75
set 2	17 : 31	57.6	−83.32	−83.66	−82.76
set 3	17 : 33	57.9	−83.29	−83.65	−82.74
set 4	17 : 36	58.3	−83.28	−83.64	−82.71
set 5	17 : 38	58.6	−83.26	−83.61	−82.69
set 6	17 : 42	58.9	−83.28	−83.64	−82.71

Averaging Y-factor, ΔCEL, and elevation angle values it is possible to obtain

Table 6.6: Local weather information - Cassiopeia A

Weather	Clear
Local Temperature	14°C
Local Humidity	90%
Local Pressure	960 hPa
Date	19.10.2016

following:

$$\begin{aligned} Y\text{-factor} &= 1.086 \\ \Delta\text{CEL} &= 0.811 \\ [\Delta CEL]_{dB} &= -0.91 \ . \end{aligned} \tag{6.7}$$

Atmospheric attenuation correction factor K_1, given in both linear and logarithmic scale, is calculated using the Section 2.3.2, considering just gaseous attenuation due to clear weather conditions, for the averaged antenna elevation of 58.1° measured from horizon:

$$\begin{aligned} [K_1]_{dB} &= A_T = 0.051 \text{ [dB]} \\ K_1 &= 10^{\frac{A_T}{10}} = 1.012 \ . \end{aligned} \tag{6.8}$$

Extended source size correction factor K_2, is calculated following the same procedure like when using Moon as a source, assuming the uniform illumination and the edge tapering of $T_e = 0$[dB], with the Cassiopeia A angular diameter elaborated in [47] ($\theta_{CasA} = 0.0767°$):

$$K_{2CasA} = 1.0565 \ . \tag{6.9}$$

The Cassiopeia A flux density is calculated using the equations provided in Table 4.1, considering the decay rate for the date of measurement provided with Equation (4.10).

$$S_{CasA} = 401.564 \cdot 10^{-26} \ \left[\mathrm{W\,m^{-2}\,Hz^{-1}}\right] \ . \tag{6.10}$$

Finally it is possible to estimate the G/T quality factor given with the Equation (5.19) and corrected to the minimum elevation angle:

$$\begin{aligned}
&\frac{G}{T}@(58.1^\circ) = \frac{8\pi \cdot k_B \cdot (Y-1)}{\lambda^2 \cdot S_{CasA}} \cdot K_1 \cdot K_{2CasA} = 5911 \\
&\left[\frac{G}{T}\right]_{dB} @(58.1^\circ) = 10 \cdot \log_{10}\left(\frac{G}{T}\right) = 37.71 \qquad [\mathrm{dB\,K^{-1}}] \\
&\left[\frac{G}{T}\right]_{dB} = \left[\frac{G}{T}(58.1^\circ)\right]_{dB} + [\Delta CEL]_{dB} = 36.81 \qquad [\mathrm{dB\,K^{-1}}]
\end{aligned} \tag{6.11}$$

Estimation of G/T quality factor value using Cassiopeia A as a source, provides G/T value higher than when using the Moon as a source for 0.32 dB. However, also the uncertainty of G/T calculated value is much higher than when using a Moon as a source.

6.5 G/T estimation using MATLAB antenna noise temperature code, GRASP simulated pattern, and receiver component characteristics

This section provides an estimation of G/T quality factor using the antenna radiation pattern to simulate the antenna noise temperature implemented within MATLAB code. Because of complexity of entire radiation pattern measurement, and because the specification of double-shaped antenna is proprietary data, in order to simulate the radiation pattern, the antenna under measurement was designed and simulated as a rotationally symmetric Cassegrain antenna with edge tapering $T_e = 10$dB and RHCP polarization.

In order to estimate G/T quality factor, firstly radiation pattern was simulated using the GRASP software. Radiation pattern is given in Theta Phi coordinates (θ, ϕ) and is presented in Figure (6.6). Then, the radiation pattern was imported in the MATLAB code for calculating the antenna noise temperature according to the local weather conditions at the moment of measurement and antenna elevation, in order to estimate the antenna noise temperature. Receiver

noise temperature was estimated calculating the cascade noise temperature of the elements in the receiver.

The receiver is composed of the following elements with their gains and noise temperatures given in Table 6.7.

Table 6.7: Receiver element rough approximate cascade gains and noise temperatures

Element	Gain in [dB]	Noise temperature [K]
LNA	43	53 K
Signal path to DC	-7	1163.4 K
Down converter	23	11255.1 K
Cables and losses	-15	8880.6 K

Calculating the cascade it is possible to obtain the approximate value of receiver noise temperature $T_{rec} \approx 56$K. The antenna ohmic losses and waveguide losses to the LNA are consistent of feed loss, waveguide loss, coupler loss and switch loss, together approximated to $L \approx 0.4$dB.

Values of approximate receiver noise temperature T_{rec} and losses L, are given as an input to the MATLAB code (Appendix B) in order to provide the estimation of G/T quality factor:

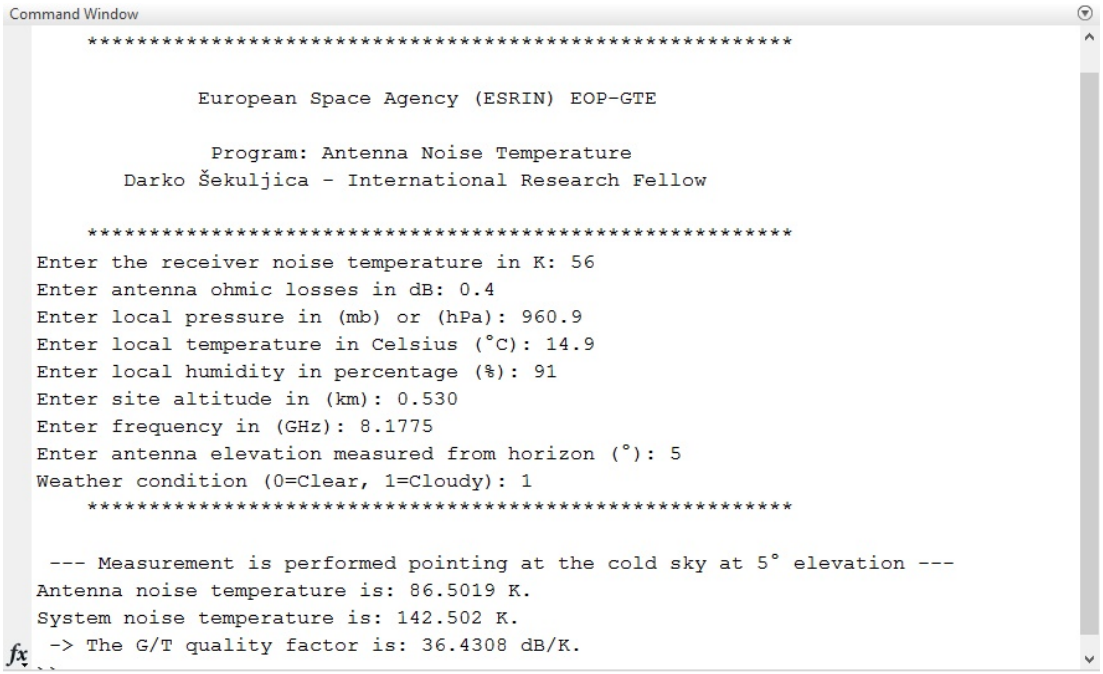

Figure 6.5: MATLAB code input and output values

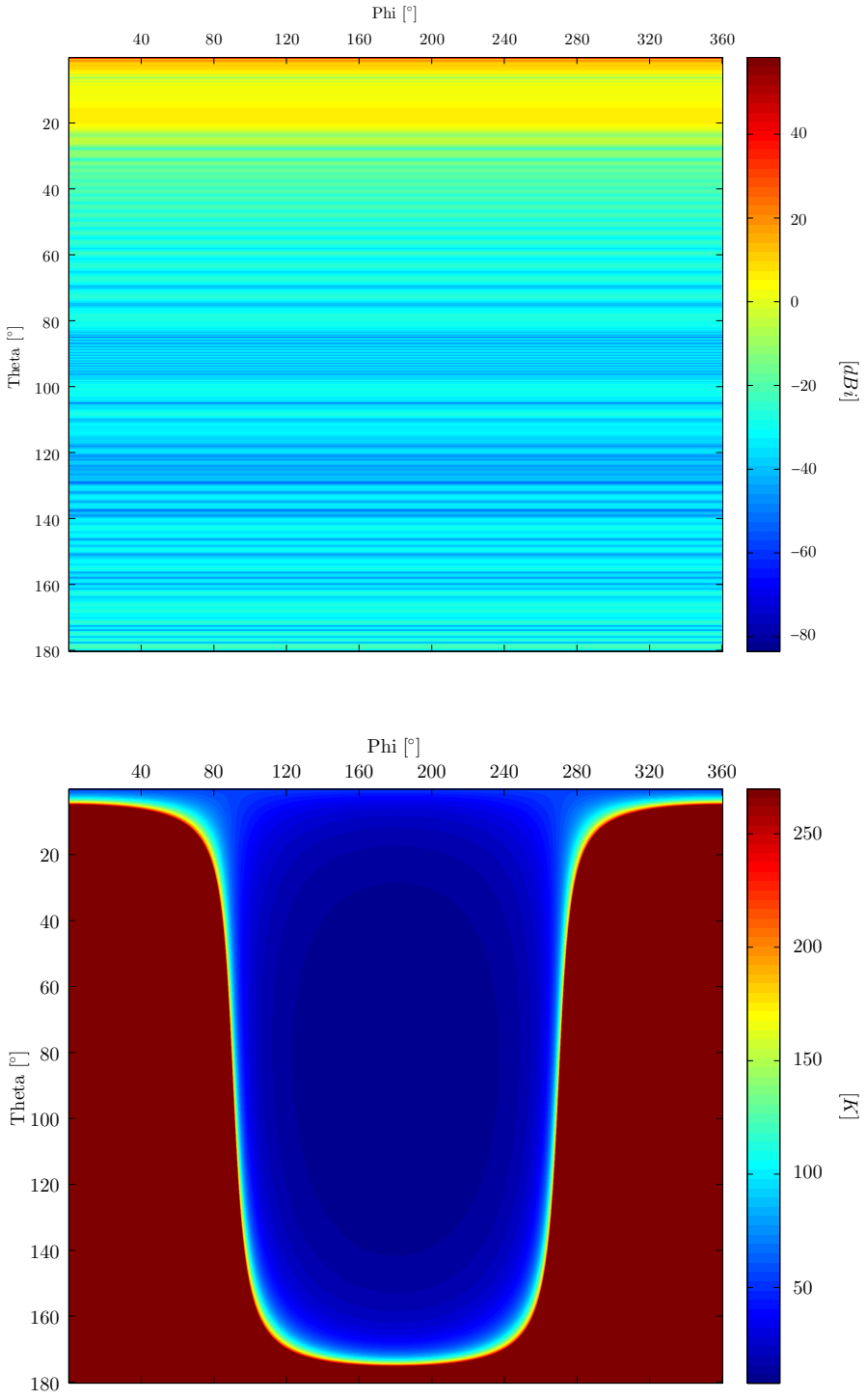

Figure 6.6: Antenna radiation pattern (uppermost) and surrounding brightness temperature matrix (downmost) at 5° elevation in Theta Phi coordinates

7 Summary and Conclusions

The motivation of this thesis was to analyse and to consolidate an accurate and efficient method to estimate the G/T quality factor. This factor is needed for the operational ground stations that work on a tight schedule and that need frequent performance verifications. This kind of measurement method becomes especially of great importance for establishments with several constantly operating ground stations because indirect methods for verifying each individual ground station in terms of its G/T factor would become time consuming and could produce overhead.

The atmospheric attenuation, which is an important component in G/T factor estimation, is specified by the latest ITU-R recommendations, and it is presented both **i)** for high elevation angles considering the flat Earth model, and **ii)** for low elevation angles considering the effect of the Earth's curvature.

Analysis of possible RF sources and their flux densities needed an overview of numerous scientific papers describing the behaviour of RF sources for different frequencies. Taking into consideration the most appropriate RF sources, the Moon was proposed as a source because of its high radiation flux density and stability if a uniformly bright disk is considered. The Moon's radiation was modelled as the radiation of a black-body. The flux density was given for the selected frequency bandwidth in dependence of a black-body's average surface temperature, lunar phase and the Moon's angular diameter at the time of measurement. This was found to sufficiently represent the Moon-Earth geometry. The average surface temperature has been obtained by extrapolating the measured values for

the frequency of interest.

The important task was also to analyse the methods to approximate extended source size correction factor. This is because a small error in the correction factor can result in an error of several tenths of a decibel in the final G/T value. Using numerous simulated radiation patterns of X-band antennas with different reflector diameters a best-fit method for the extended source size correction factor estimation was obtained. This considered also the feed edge taper. Each antenna design and radiation pattern simulation were produced using the GRASP antenna design software, with which simulation settings to address all the effects such as spill-over and blockage were considered.

In the case the antenna reflector surface changed, or the feed gets out of focus, the measured G/T value will be lower compared to the G/T value before the change. Using the method proposed in this thesis and using the obtained method for extended source size correction factor estimation, the lower G/T value can be obtained. Because such value is not real and is too optimistic, the mentioned method provides good indication of changes of the antenna. Hence, the obtained G/T estimate value should not be used and the antenna radiation pattern has to be newly determined. This is because the extended source size correction factor, in that case, has to be recalculated by employing the integral equation described in Section 5.2.

The measurement procedure was a subject of the detailed analysis and proposed settings for the spectrum analyser have been traded-off and selected in order to provide the best compromise between measurement stability and measurement error. Spectrum analyser settings can vary slightly according to the quality of the measurement equipment. The measurements were successfully performed with the spectrum analyser *Advantest R3131A*, on a tight schedule following the given procedure. This was done on the operational X-band Cassegrain antenna which is used for receiving data from LEO satellites and which is located at the e-GEOS station in Matera in Southern Italy.

The measurements of the G/T quality factor carried out with our direct method using the Moon with the antenna in Matera are consistent and in line with the expectations obtained using the simulated radiation pattern and the developed MATLAB code. They also agree well with other parallel direct measurements made in the same occasion using a star (Cassiopeia A) as the source, with G/T value deviations within 0.35 dB.

Comparing the test results with the values given by the vendor for the extended source correction factor it turned out that provided values are often too optimistic. The method employing the Gaussian pattern as a function of edge taper proposed in this thesis, as shown in Section 6.3.1, gives more realistic values.

Based on the obtained results of the study, ESA has consolidated the method described in this thesis as its standard approach for the periodic G/T factor verification of X-band antennas, which are used for the data acquisition from ESA's Earth Observation satellites. A specific ESA document, which is part of the requirements of all the contracts for acquisition services, has been released.

Bibliography

[1] K. Rohlfs in T. Wilson, *Tools of radio astronomy*. Springer Science & Business Media, 2013.

[2] B. R. Elbert, *Introduction to satellite communication*. Artech house, 2008.

[3] D. M. Pozar, *Microwave engineering*. John Wiley & Sons, 2009.

[4] ITU-R recommendation, "Attenuation by atmospheric gases," *ITU-R P. 676*, vol. 10, 2013.

[5] L. J. Ippolito, *Radiowave propagation in satellite communications*. Springer Science & Business Media, 2012.

[6] ITU-R recommendation, "Reference Standard Atmospheres," *ITU-R P. 835*, vol. 5, 2012.

[7] ITU-R recommendation, "Attenuation due to clouds and fog," *ITU-R P. 840*, vol. 6, 2013.

[8] ITU-R recommendation, "Propagation data and prediction methods required for the design of Earth-space telecommunication systems," *ITU-R P. 618*, vol. 12, 2015.

[9] L. C. Godara, *Handbook of antennas in wireless communications*, vol. 4. CRC press, 2001.

[10] B. Batagelj, "Satelitske komunikacije." Available at: http://antena.fe.uni-lj.si/studij/skn/gradivo/satelitske_komunikacije_Batagelj.pdf. [Accessed: 02. 11. 2016].

[11] P. Patel, "Inexpensive multi-mode satellite tracking feed antenna," v *IEE Proceedings H-Microwaves, Antennas and Propagation, volume=35, number=6, pages=381–386, year=1988, organization=IET.*

[12] J. D. Kraus, "Antennas," 1988.

[13] T. A. Milligan, *Modern antenna design.* John Wiley & Sons, 2005.

[14] TICRA, "GRASP official web-page." Available at: http://www.ticra.com/products/software/grasp. [Accessed: 26. 10. 2016].

[15] W. C. Gibson, *The method of moments in electromagnetics.* CRC press, 2014.

[16] M. Vidmar, "Antene in razširjanje valov." Available at: http://antena.fe.uni-lj.si/literatura/ar.zap.pdf. [Accessed: 02. 11. 2016].

[17] S. J. Orfanidis, *Electromagnetic waves and antennas.* Rutgers University New Brunswick, NJ, 2002.

[18] T. Wilson, "Tools of Radio Astronomy, ed. TL Wilson, K. Rohlfs, & S. Hüttemeister," 2009.

[19] W. C. Daywitt, "An error analysis for the use of presently available lunar radio flux data in broadbeam antenna-system measurements," *Error analysis for the use of presently available lunar radio flux data in broadbeam antenna-system measurements.. Report NBS-TN-1073, Natl. Bur. Stand., Washington, DC, USA, 30 pp.*, vol. 1, 1984.

[20] Z. Kopal, *Advances in astronomy and astrophysics*, vol. 3. Academic Press, 2013.

[21] D. Guidice in J. Castelli, "The use of extraterrestrial radio sources in the measurement of antenna parameters," *IEEE Transactions on Aerospace and Electronic Systems*, no. 2, str. 226–234, 1971.

[22] NOAA, "Solar Radio Data." Available at: http://legacy-www.swpc.noaa.gov/ftpdir/lists/radio/7day_rad.txt. [Accessed: 24. 10. 2016].

[23] W. C. Daywitt, "On 10-60 GHz G/T measurements using the Sun as a source: A preliminary study," *Report, 1985-1986 National Bureau of Standards, Boulder, CO. Electromagnetic Fields Div.*, vol. 1, str. 1985–1986, 1986.

[24] ITU-R recommendation, "Determination of the G/T ratio for Earth stations operating in the fixed-satellite service," *ITU-R S. 733*, vol. 2, 2000.

[25] D. E. Reichart in A. W. Stephens, "The Fading of Supernova Remnant Cassiopeia A from 38 MHz to 16.5 GHz from 1949 to 1999 with New Observations at 1405 MHzThe data presented here were obtained by participants of Educational Research in Radio Astronomy (ERIRA) 1992-1999, an outreach program that has received support from the National Radio Astronomy Observatory, the Ohio State University, the Pennsylvania State University, and the University of Pittsburgh at Bradford.," *The Astrophysical Journal*, vol. 537, no. 2, str. 904, 2000.

[26] E. Ekelman in C. Abler, "Antenna gain measurements using improved radio star flux density expressions," v *Antennas and Propagation Society International Symposium, 1996. AP-S. Digest, volume=1, pages=172–175, year=1996, organization=IEEE.*

[27] A. Kuzmin, *Radioastronomical methods of antenna measurements.*

[28] J. L. Linsky, "The Moon as a proposed radiometric standard for microwave and infrared observations of extended sources," *The Astrophysical Journal*

Supplement Series, vol. 25, str. 163, 1973.

[29] JPL-NASA, "HORIZONS Web-Interface." Available at: http://ssd.jpl.nasa.gov/horizons.cgi. [Accessed: 24. 10. 2016].

[30] D. F. Wait, M. Kanda, W. Daywitt in C. Miller, "A study of the measurement of G/T using Cassiopeia A," tech. rep., DTIC Document, 1974.

[31] K. G. Johannsen in A. Koury, "The moon as source for G/T measurements," *IEEE Transactions on Aerospace and Electronic Systems*, no. 5, str. 718–727, 1974.

[32] J. S. Hollis, T. Lyon in L. Clayton, *Microwave antenna measurements*. Scientific-Atlanta, 1970.

[33] ITU-R recommendation, "Radio noise," *ITU-R P. 372*, vol. 12, 2015.

[34] C. Ho, A. Kantak, S. Slobin in D. Morabito, "Link analysis of a telecommunication system on earth, in geostationary orbit, and at the Moon: Atmospheric attenuation and noise temperature effects," *IPN Progress Report*, str. 42–168, 2007.

[35] Y. Han in E. R. Westwater, "Analysis and improvement of tipping calibration for ground-based microwave radiometers," *IEEE Transactions on Geoscience and Remote Sensing*, vol. 38, no. 3, str. 1260–1276, 2000.

[36] J. Waters, "2.3. Absorption and Emission by Atmospheric Gases," *Methods in Experimental Physics*, vol. 12, str. 142–176, 1976.

[37] H. Stephen, S. Ahmad in T. C. Piechota, "Land surface brightness temperature modeling using solar insolation," *IEEE Transactions on Geoscience and Remote Sensing*, vol. 48, no. 1, str. 491–498, 2010.

[38] D. H. Menzel, *Fundamental formulas of physics*, vol. 2. Courier Corporation, 1960.

[39] W. Welch in D. DeBoer, "Expected properties of the ATA antennas," *ATA Memo Series*, vol. 66, 2004.

[40] A. Solovey in R. Mittra, "Extended source size correction factor in antenna gain measurements," v *Microwave Conference, 2008. EuMC 2008. 38th European, pages=983–986, year=2008, organization=IEEE.*

[41] H. Ko, "On the determination of the disk temperature and the flux density of a radio source using high-gain antennas," *IRE Transactions on Antennas and Propagation*, vol. 9, no. 5, str. 500–501, 1961.

[42] T. Pratt in C. W. Bostian, *Satellite communications.* John Wiley & Sons, 1986.

[43] R. A. Nelson, "Antennas: the interface with space," *Via Satellite, Sep*, 1999.

[44] ITU, *Handbook on Satellite Communications (FSS).* International telecommunication union, 2002.

[45] R. Allen in A. Barrett, "Absolute measurements of the radio flux from Cassiopeia A and Taurus A at 3.64 and 1.94 cm," *The Astrophysical Journal*, vol. 149, str. 1, 1967.

[46] J. Baars, P. Mezger in H. Wendker, "The Spectra of the Strongest Non-Thermal Radio Sources in the Centimeter Wavelength Range.," *The Astrophysical Journal*, vol. 142, str. 122, 1965.

[47] M. Kanda, "An error analysis for absolute flux density measurements of Cassiopeia A," *IEEE Transactions on Instrumentation Measurement*, vol. 25, str. 173–182, 1976.

Appendices

A Extended source size correction factor computed from Gaussian approximation of radiation pattern

The normalized Gaussian approximation of radiation pattern is given by the Equation (5.26) and its corresponding extended noise correction factor is given by the Equation (5.27) that considers the uniform brightness disk. In following, the intermediate steps between two equations are given:

Assume the rotationally symmetric pattern and express the Gaussian approximation in following way, where p is a constant.

$$g(\theta, \phi) = e^{-(p\theta)^2} \tag{A.1}$$

Now, if θ_{HPBW} is the angle between the half-power points of the antenna main lobe, the equation can be written:

$$\begin{aligned} \theta_H &= \frac{\theta_{HPBW}}{2} \\ g(\theta_H, \phi) &= \frac{1}{2} \\ \frac{1}{2} &= e^{-p^2{\theta_H}^2} \\ -\ln(2) &= -p^2{\theta_H}^2 \\ p &= \frac{\sqrt{\ln(2)}}{\theta_H} \end{aligned} \tag{A.2}$$

From the determination of the constant p it is possible to obtain the Gaussian

approximation for the antenna with given θ_{HPBW}:

$$g(\theta, \phi) = e^{-\ln(2)\cdot\left(\frac{\theta}{\theta_H}\right)^2} \tag{A.3}$$

The remaining part is to calculate the K_2 correction factor given in dependence of θ_S, where $\theta_S = \frac{\theta_{Source}}{2}$:

$$K_2 = \frac{\int_0^{2\pi}\int_0^{\theta_S} \sin(\theta)\, d\theta\, d\phi}{\int_0^{2\pi}\int_0^{\theta_S} g(\theta, \phi)\sin(\theta)\, d\theta\, d\phi} = \frac{I1}{I2} \tag{A.4}$$

assuming that $\sin(\theta) \approx \theta$ for small angles of θ where,

$$I1 = \int_0^{2\pi}\int_0^{\theta_S} \sin(\theta)\, d\theta\, d\phi = \int_0^{2\pi}\int_0^{\theta_S} \theta\, d\theta\, d\phi = \pi {\theta_S}^2 \tag{A.5}$$

and

$$\begin{aligned} I2 &= \int_0^{2\pi}\int_0^{\theta_S} g(\theta, \phi)\sin(\theta)\, d\theta\, d\phi \\ &= \int_0^{2\pi}\int_0^{\theta_S} e^{-(p\theta)^2}\sin(\theta)\, d\theta\, d\phi \\ &= -2\pi\left(\frac{e^{-(p\theta)^2}}{2p^2}\right)\Bigg|_0^{\theta_S} \\ &= -\frac{\pi}{p^2}\left(e^{-(p\theta_S)^2} - 1\right) \\ &= \frac{\pi}{p^2}\left(1 - e^{-(p\theta_S)^2}\right) \end{aligned} \tag{A.6}$$

Finally K_2 can be expressed as:

$$\begin{aligned} K_2 &= \frac{\pi {\theta_S}^2}{\frac{\pi}{p^2}\left(1 - e^{-(p\theta_S)^2}\right)} \\ &= \frac{p^2 {\theta_S}^2}{1 - e^{-(p\theta_S)^2}} \\ &= \frac{\ln(2)\cdot\left(\frac{\theta_S}{\theta_H}\right)^2}{1 - e^{-\ln(2)\cdot\left(\frac{\theta_S}{\theta_H}\right)^2}} \\ &= \frac{\ln(2)\cdot\left(\frac{\theta_{Moon}}{\theta_{HPBW}}\right)^2}{1 - e^{-\ln(2)\cdot\left(\frac{\theta_{Moon}}{\theta_{HPBW}}\right)^2}} \end{aligned} \tag{A.7}$$

B MATLAB code - antenna noise temperature and G/T estimation

```
%*************************************************************************%
%******** PROGRAM: ANTENNA NOISE TEMPERATURE AND G/T ESTIMATION **********%
%*************************************************************************%

% DESCRIPTION:
% * This script computes the antenna noise temperature in Kelvins by
%   simple integration and estimates the G/T quality factor.
% * The radiation pattern is generated in GRASP10, and the output is given
%   in a theta - phi grid (see GRASP manual).
% * The brightness temperature matrix is generated taking in consideration
%   the atmospheric attenuation and antenna elevation angle.
% * The receiver noise temperature and antenna ohmic losses are provided as
%   input for the system noise temperature calculation.
% END

% TITLE:
fprintf('    ********************************************************\n');
fprintf('                                                            \n');
fprintf('             European Space Agency (ESRIN) EOP-GTE          \n');
fprintf('                                                            \n');
fprintf('              Program: Antenna Noise Temperature            \n');
fprintf('       Darko Šekuljica - International Research Fellow\n');
fprintf('                                                            \n');
fprintf('    ********************************************************\n');


clear all;
format long;
%%
%************************** INPUT DATA ***********************************%

% Receiver noise temperature and antenna ohmic losses:
```

```
33 Treceiver = input('Enter the receiver noise temperature in K: ');
34 L_ohmic_dB = input('Enter antenna ohmic losses in dB: ');
35
36 % Local weather conditions
37 P = input('Enter local pressure in (mb) or (hPa): ');
38 t = input('Enter local temperature in Celsius (°C): ');
39 H = input('Enter local humidity in percentage (%): ');
40 site_alt = input('Enter site altitude in (km): ');
41 f = input('Enter frequency in (GHz): ');
42 elevation = input('Enter antenna elevation measured from horizon (°): ');
43 cloud_flag = input('Weather condition (0=Clear, 1=Cloudy): ');
44
45 %P = 960.9;              % local pressure in (mb) or (hPa)
46 %t = 14.9;               % local temperature in Celsius (°C)
47 %H = 91;                 % local humidity in percentage (%)
48 %site_alt = 0.530;       % site altitude expressed in (km)
49 %f = 8.1775;             % frequency in (GHz)
50 %elevation = 5;          % antenna elevation measured from horizon (°)
51 %cloud_flag = 1;              % include the attenuation due to clouds
52 R = 8500;               % 4/3 Earth Radius (effective radius) in (km)
53 inclined_path_flag = 1;      % calculate using the antenna location height
54 L_red = 1;                   % (kg/m^2) - for gasses
55
56 %%
57 %********************** ATMOSPHERIC ATTENUATION ************************%
58 %***************************** OXYGEN **********************************%
59 % DESC:
60 % Atmospheric attenuation for the angles > 5° is calculated according
61 % to the specifications in ITU-R P.676-10.
62 %
63 % Atmospheric attenuation for the angles < 5° is calculated according
64 % to the L.J.Ippolito: Radiowave Propagation in Satellite Communications.
65 %
66 % Atmospheric attenuation due to clouds is calculated according to the
67 % ITU-R P.840-6 specifications.
68
69
70 rp = P/1013;
71 rt = 288/(273+t);
72
73 eps1 = rp^(0.0717) * rt^(-1.8132) * exp(0.0156*(1-rp)-1.6515*(1-rt));
74 eps2 = rp^(0.5146) * rt^(-4.6368) * exp(-0.1921*(1-rp)-5.7416*(1-rt));
75 eps3 = rp^(0.3414) * rt^(-6.5851) * exp(0.2130*(1-rp)-8.5854*(1-rt));
76
77 gamma0 = ((7.2*rt^(2.8))/(f^2 + 0.34*rp^2 * rt^(1.6)) +...
78     (0.62*eps3)/((54-f)^(1.16*eps1)+0.83*eps2))*f^2 * rp^2 * 10^(-3);
```

```
79
80  t1 = (4.64/(1+0.066*rp^(-2.3)))*exp(-((f-59.7)/...
81      (2.87+12.4*exp(-7.9*rp)))^2);
82  t2 = (0.14*exp(2.12*rp))/( (f-118.75)^2 + 0.031*exp(2.2*rp) );
83  t3 = (0.0114/(1+0.014*rp^(-2.6)))*f*( (-0.0247+0.0001*f+1.61*f^2 *...
84      10^(-6))/(1-0.0169*f+4.1*f^2*10^(-5)+3.2*f^3*10^(-7)) );
85
86  h0 = (6.1/(1+0.17 * rp^(-1.1))) * (1+t1+t2+t3);
87  if inclined_path_flag == 1
88      h0 = h0*exp(-site_alt/h0);
89  end
90  %************************** WATER VAPOUR ******************************%
91
92  rho = (216.7/(t+273.7)) * (H/100) * (1+10^(-4)*(7.2+P*(0.0032+5.9*t^2*...
93      10^(-7)))) *6.1121*exp( ((18.678-(t/234.5))*t)/(t+257.14) );
94  if inclined_path_flag == 1
95      rho = rho * exp(site_alt/2);
96  end
97  eta1 = 0.955*rp*rt^(0.68) + 0.006*rho;
98  eta2 = 0.735*rp*rt^(0.5) + 0.0353*rt^4 * rho;
99
100 part1 = ((3.98*eta1*exp(2.23*(1-rt))) / ((f-22.235)^2 + 9.42*eta1^2))...
101     * (1+((f-22)/(f+22))^2);
102 part2 = ((11.96*eta1*exp(0.7*(1-rt))) / ((f-183.31)^2 + 11.14*eta1^2)) +...
103     ((0.081*eta1*exp(6.44*(1-rt))) / ((f-321.226)^2 + 6.29*eta1^2));
104 part3 = ((3.66*eta1*exp(1.6*(1-rt))) / ((f-325.153)^2 + 9.22*eta1^2)) +...
105     ((25.37*eta1*exp(1.09*(1-rt))) / ((f-380)^2));
106 part4 = ((17.6*eta1*exp(1.46*(1-rt))) / ((f-448)^2)) +...
107     ((844.6*eta1*exp(0.17*(1-rt))) / ((f-557)^2)) * (1+((f-557)/(f+557))^2);
108 part5 = ((290*eta1*exp(0.41*(1-rt))) / ((f-752)^2)) *...
109     (1+((f-752)/(f+752))^2);
110 part6 = ((8.3328*10^4 *eta2*exp(0.99*(1-rt))) /...
111     ((f-1780)^2)) * (1+((f-1780)/(f+1780))^2);
112 part7 = f^2 * rt^(2.5) * rho * 10^(-4);
113
114 gammaW = (part1 + part2 + part3 + part4 + part5 + part6)*part7;
115
116
117 sigmaW = 1.013/(1+exp(-8.6*(rp^(-0.57))));
118 hW = 1.66*(1+ ((1.39*sigmaW)/((f-22.235)^2+2.56*sigmaW)) +...
119     ((3.37*sigmaW)/((f-183.31)^2+4.69*sigmaW)) + ((1.58*sigmaW)/...
120     ((f-325.1)^2+2.89*sigmaW)));
121 if inclined_path_flag == 1
122     hW = hW*exp(-site_alt/hW);
123 end
124
```

```
125 %********************** GASEOUS ATTENUATION ****************************%
126 A_zenith = gamma0*h0 + gammaW*hW;        % Zenith attenuation in dB
127
128 %********************** CLOUD ATTENUATION ****************************%
129 if cloud_flag == 1
130     theta = 300/(t+273);
131     e0 = 77.66 + 103.3*(theta-1);
132     e1 = 0.0671*e0;
133     e2 = 3.52;
134     % principal relaxation frequency in GHz
135     fp = 20.20-146*(theta-1)+316*(theta-1)^2;
136     % secondary relaxation frequency in GHz
137     fs = 39.8*fp;
138
139     ee2 = (f*(e0-e1))/(fp*(1+(f/fp)^2)) + (f*(e1-e2))/(fs*(1+(f/fs)^2));
140     ee1 = (((e0-e1))/((1+(f/fp)^2))) + (((e1-e2))/((1+(f/fs)^2))) + e2;
141
142     eeta = (2+ee1)/ee2;
143
144     K_l = (0.819*f)/(ee2*(1+eeta^2));   % (dB/km) / (g/m^3)
145     A_cloud = (L_red * K_l)/sind(elevation);
146 else
147     K_l = 0;
148 end
149 %***************************** END ***********************************%
150 %%
151 %***************** SURROUNDING BRIGHTNESS TEMPERATURES ******************%
152 % DESC:
153 % This part of the script creates the surrounding brightness temperature
154 % matrix taking into the account the antenna elevation and atmospheric
155 % attenuations.
156 %
157 % Brightness temperature matrix is given in Theta-Phi corrdinates and is
158 % generated using the spherical law of cosines.
159
160
161 % Apparent temperature of sourroundings
162 Earth_emissivity = 0.93;            % in percentage (%)
163 Tsky = 3;                           % Cold sky brightness temp in (K)
164 Tearth = 290 * Earth_emissivity;    % Earth brightness temp in (K)
165 T0 = 290;                           % Conventional temperature -
166                                     % average surface physical temperature
167 Tmpt = 270;                         % Brightness temperature of the
168                                     % atmosphere
169
170 % The step size for generating the matrix
```

```
171 m = 0.2;        % distance between two samples in Theta or Phi angle in (°)
172
173 % Matrix size information
174 rows = 1:m:181;
175 columns = 1:m:361;
176 matrix = zeros(length(rows),length(columns));
177 matsize = size(matrix);
178
179 % Generating the matrix:
180 % Matrix marks the earth-sky boundary according to antenna elevation.
181 flag = 0;
182 iter = 1;
183 h1 = waitbar(0,'[1/2]  Generating brightness temperature matrix');
184 for j = 1:matsize(2);
185     phi1 = (180+m) - j*m;
186     flag = 0;
187     for i = 1:matsize(1)
188         if (flag == 0)
189             elev = 90-elevation;
190             corrangle = acosd((cosd(i*m-m)*cosd(elev))+(sind(i*m-m)*...
191                 sind(elev)*cosd(phi1)));
192             if (round(corrangle) == 90)
193                 matrix(1:i+1,j) = 1;
194                 iter = iter + 1;
195                 flag = 1;
196             end
197         end
198     end
199     waitbar(j/matsize(2),h1)
200 end
201 close(h1);
202 matrix(matrix==1) = Tsky;
203 matrix(matrix==0) = Tearth;
204
205
206 % Correcting the matrix:
207 % Brightness temperatures of the cold sky are corrected for the atmospheric
208 % attenuations calculated earlier in the script. For the correction
209 % spherical law of cosines is used:
210 h2 = waitbar(0,'[2/2]   Correcting for the atmospheric attenuation');
211 for j = 1:matsize(2);
212     phi1 = (180+m) - j*m;
213     for i = 1:matsize(1)
214         elev = 90-elevation;
215         corrangle = acosd((cosd(i*m-m)*cosd(elev))+(sind(i*m-m)*...
216             sind(elev)*cosd(phi1)));
```

```
217         if(matrix(i,j) == Tsky)
218             if (corrangle > 80);
219                 curvature_factor = (( (2*gamma0*h0)/(sqrt(sind(90-...
220                     corrangle)^2 + (2*h0/R))+sind(90-corrangle)) ) +...
221                     ( (2*gammaW*hW)/(sqrt(sind(90-corrangle)^2 +...
222                     (2*hW/R))+sind(90-corrangle)) ) /  (A_zenith *...
223                     (1/sind(90-corrangle)));
224                 Attenuation_i_j = ( (2*gamma0*h0)/...
225                     (sqrt(sind(90-corrangle)^2 + (2*h0/R))+...
226                     sind(90-corrangle)) ) + ( (2*gammaW*hW)/...
227                     (sqrt(sind(90-corrangle)^2 + (2*hW/R))+...
228                     sind(90-corrangle)) ) + curvature_factor*...
229                     ((L_red * K_l)/sind(90-corrangle));
230                 matrix(i,j) = Tmpt - (Tmpt-Tsky)/(10^(0.1*Attenuation_i_j));
231             else
232                 Attenuation_i_j = A_zenith * (1/sind(90-corrangle)) +...
233                     (L_red * K_l)/sind(90-corrangle);
234                 matrix(i,j) = Tmpt - (Tmpt-Tsky)/(10^(0.1*Attenuation_i_j));
235             end
236         end
237         if(matrix(i,j)==Tearth)
238             if(corrangle < 95)
239                 matrix(i,j) = Tearth;
240             end
241         end
242     end
243     waitbar(j/matsize(2),h2)
244 end
245 close(h2);
246 %****************************** END ***********************************%
247 %%
248 %********************** RADIATION PATTERN ******************************%
249 % DESC:
250 % This part of the script reads the electric-field radiation pattern
251 % produced in GRASP10 software, and given in Theta-Phi coordinates.
252 %
253 % Radiation pattern is given in two columns and has to be properly
254 % reshaped.
255
256 % Define radiation pattern matrix size:
257 Nphi = size(matrix, 2);          % number of columns
258 Ntheta = size(matrix, 1);        % number of lines
259 delta_angle = 180/(Ntheta-1);    % sample distance in Theta or Phi (°)
260
261 % Load data radiation pattern data:
262 load ELPAT;
```

```
263
264 elfield = elpat(:,1).^2 + elpat(:,2).^2;
265 power = reshape(elfield, Nphi, Ntheta);
266 power = power';                    % antenna's power pattern (directivity)
267 clear a elfield;
268
269 %****************************** END ***********************************%
270 %%
271 %********************** ANTENNA NOISE TEMPERATURE **********************%
272 % DESC:
273 % In order to calculate the antenna noise temperature, it is neccesary to
274 % calculate corresponding integration surface areas. The areas are
275 % calculated using the MATLAB built-in function >>areaquad<<
276 %
277 % Integration is simplified, and performed summing the output of
278 % element-wise multiplication of brightness temperature matrix, antenna
279 % radiation pattern and corresponding surface area matrix.
280
281 for i = 1:(Ntheta-1)
282     area(i) = areaquad(-90+i*delta_angle-(delta_angle/2),0,-90+...
283         i*delta_angle+(delta_angle/2),(0+delta_angle)) .* (4*pi);
284 end
285 area = [areaquad(-90,0,-90+(delta_angle/2),(0+delta_angle))*(4*pi) area];
286 area_matrix = repmat(area',1,Nphi);
287
288 Tant = sum(sum(power.*area_matrix.*matrix)) / sum(sum(power.*area_matrix));
289 %****************************** END ***********************************%
290 %%
291 %************************** G/T calculation ****************************%
292 % DESC:
293 % Antenna noise temperature is re-calculated as cascade of antenna noise
294 % temperature caused by external noise sources and internal noise due to
295 % antenna ohmic losses.
296 %
297 % Receiver noise temperature is provided as input to the script.
298 %
299 % System noise temperature is sum of re-calculated antenna noise
300 % temperature and receiver noise temperature.
301
302
303 %Treceiver = 56;              % receiver noise temperature in (K)
304 %L_ohmic_dB = 0.4;              % antenna ohmic losses in decibels (dB)
305 Lfeed = 10^(L_ohmic_dB*0.1);
306 gain = 10^(0.1*(10*log10(max(max(power)))-L_ohmic_dB));
307
308 Tantenna1 = (Tant/Lfeed)+(T0/Lfeed)*(Lfeed-1);
```

```
309 Tsys = Tantenna1 + Treceiver;
310 GT = 10.*log10(gain/Tsys);
311 %****************************** END ***********************************%
312 %%
313 %****************************** OUTPUT ********************************%
314 % Final output:
315 fprintf('    ************************************************************\n');
316 fprintf(['\n --- Measurement is performed pointing at the cold sky'...
317     ' at %g° elevation ---\n'],elevation);
318 fprintf('Antenna noise temperature is: %g K.\n',Tantenna1);
319 fprintf('System noise temperature is: %g K.\n',Tsys);
320 fprintf(' -> The G/T quality factor is: %g dB/K.\n',GT);
```